Stable isotope geothermometry applied to selected vein type ore deposits of the Eastern Alps

Dissertation

DI Thomas Unterweissacher

Montanuniversität Leoben

Department of Applied Geosciences and Geophysics

Chair of Geology and Economic Geology

Supervisor

em. O.Univ.-Prof. Dr. phil. Fritz Ebner

Referees

em. O.Univ.-Prof. Dr. phil. Fritz Ebner

Ao.Univ.-Prof. Mag.rer.nat. Dr. mont. Thomas Meisel

January 2013

Affidavit

I declare in lieu of oath, that I wrote this thesis and performed the associated research myself, using only the literature cited in this volume.

Thomas UNTERWEISSACHER

The man who moved the mountain, was the man who started to take away small rocks.

after Confucius, *551-479 BCE.*

Abstract

Quartz and various carbonate minerals often form gangue minerals within hydrothermal ore deposits. This thesis deals with the applicability of carbonate-quartz gangue as geothermometer. The results are comparable with „classical" geothermometers like microthermometry and cation exchange geothermometers. The temperature range is crosschecked with results of arsenopyrite and solid solution geothermometry. The applicability of stable isotope geothermometry is limited by the grade of isotopic equilibrium between quartz and carbonate and possible younger alteration by migrating fluids.

Vein deposits with great vertical extent within the Austroalpine and Sub-Penninic parts of the Eastern Alps were the objects of study. The individual deposits of Erzwies-Siglitz (Pb-Zn), Mitterberg-Buchberg (Cu), Radmer (Cu), Zinkwand (Ni-Co-Bi), Tösens (Pb-Zn) and Kraubath (magnesite) are discussed in detail.

The reconstruction of the mineralising fluids results in similar mineralising processes during during Eo-Alpine and Neogene times. The main motor of metallogenesis within the worked deposits are metamorphic waters driven by orogenic induced fluid flow. The formation of the Erzwies-Siglitz, Mitterberg-Buchberg, Radmer, Tösens and Zinkwand deposits is related to such metamorphogenous fluids. Although formation ages, mineralogy and host rocks are different the mineralising fluids are dominated by fluids enriched in $\delta^{18}O$ (7 bis 18 ‰ VSMOW) and depleted in $\delta^{13}C$ (-6 bis -14 ‰ VPDB). Metasediments and metacarbonates represent the main source rocks for this kind of metamorphogenic fluids.

The investigated metamorphogenous deposits are the product of a multiphase genesis. Primary fine dispersed metals or transition metals or enrichments thereof were mobilised by metamorphogenous fluids during Variscan and Alpine orogenesis. The declining orogenesis with subsequent extensional tectonics lead to the formation of vein type deposits.

Another important mineralisation process is represented by the formation of magnesite close to the palaeosurface. The cryptocrystalline magnesite deposit of Kraubath is bound to shallow extensional tectonic structures in form of veins. Subsidiary sedimentary magnesite occurs within hangingwall Miocene sediments. In this case, the mineralising low tempered hydrothermal fluid system is strongly influenced by meteoric waters.

Suggestions for the application of quartz-carbonate mineral pairs as geothermometer and for the reconstruction of mineralising fluid systems at a regional scale conclude this work.

Zusammenfassung

Quarz und verschiedene Karbonatminerale (Kalzit, Ankerit, Siderit) stellen häufig Gangarten in hydrothermalen Lagerstätten dar. Die Anwendbarkeit von Quarz-Karbonat Mineralpaaren als Geothermometer wurde untersucht und hinsichtlich ihrer diesbezüglichen Eignung diskutiert. Der Vergleich mit klassischen Geothermometern wie Mikrothermometrie, Kationenaustauschgeothermometrie ergibt eine gute Anwendbarkeit der Isotopengeothermometer. Einschränkungen ergeben sich aus einem Isotopenungleichgewicht zwischen Karbonat und Quarz sowie durch mögliche jüngere Fluidalteration.

Verschiedene gangförmige Erzlagerstätten in unterschiedlichen geologischen Einheiten der Ostalpen wurden untersucht. Im Detail wurden das Pb-Zn Vorkommen Erzwies-Siglitz im Sub-Penninikum, die Kupfervererzung im Bereich Mitterberg-Buchberg und die Vererzung des Paradeistollens in der Radmer innerhalb der Grauwackenzone, die Ni-Co-Bi Vererzung der Zinkwand und der kryptokristalline Magnesit von Kraubath im Silvretta-Seckau Deckensystem sowie das ehemalige Pb-Zn Vorkommen von Tösens im Ötztal-Stubai Komplex bearbeitet.

Der Großteil der untersuchten Vorkommen im Sub-Penninikum und im Ostalpin zeigt ähnliche lagerstättenbildende Prozesse, die intrakreatzischer (Eo-Alpidischen) und neogener Tektonik zuzuordnen sind. Die Vorkommen Erzwies-Siglitz, Mitterberg-Buchberg, Radmer, Tösens und Zinkwand sind metamorphogenen Prozessen während der Eo-Alpinen Phase und des Neogens zuzuordnen. Trotz unterschiedlichen Alters, Mineralführung und Nebengesteine sind die lagerstättenbildenden Fluide durch $\delta^{18}O$ Werte von 7 bis 18 ‰ VSMOW und durch negative $\delta^{13}C$ Werte von -6 bis -14 ‰ VPDB charakterisiert. Diese metamorphogenen Fluide sind in erster Linie durch ihre „Muttergesteine" und die Migrationsdistanz beeinflusst.

Die Entstehung der bearbeiteten metamorphogenen Lagerstätten ist eindeutig als mehrphasig anzusehen. Ein primärer dispers im Gestein verteilter Stoffbestand verschiedener Metalle und Übergangsmetalle bzw. mögliche Anreicherungen wurden im Zuge der variszischen und alpidischen Gebirgsbildung mehrmals durch metamorphogene Fluide mobilisiert und während der abklingenden Metamorphose in Form von Gängen wieder abgelagert.

Einen wichtigen lagerstättenbildenden Prozess stellt auch die oberflächennahe Bildung von kryptokristallinem Magnesit bei Kraubath dar. Hierbei ist eine starke Beeinflussung durch meteorische Wässer zu beobachten. Gegenwärtig können magmatische bzw. metamorphogene Fluide für Genese des Magnesits von Kraubath ausgeschlossen werden. Deshalb wird für die Genese des kryptokristallinen Magnesits von Kraubath eine oberflächennahe sowie zeitgleiche Bildung mit der neogenen Störungstektonik des Fohnsdorfer Beckens postuliert.

Anregungen zur Anwendung von Quarz-Karbonat Mineralpaaren als Geothermometer und zur Rekonstruktion von lagerstättenbildenden Fluiden im Regionalmaßstab runden die Arbeit ab.

Acknowledgement

Without the help and support of many people the preparation of this manuscript would not have been possible. First of all want to thank my supervisor Fritz EBNER for encouraging me to write this thesis. He was always available for discussions and was supporting me in an excellent way. Furthermore I wanted to thank all present and former staff members of the Chair of Geology and Economic Geology at the Montanuniversität Leoben: G. RANTITSCH, W. PROCHASKA , H. MALI, K. HORKEL, K. LASSING, A. WÖLFLER and S. FEUCHTER. Thanks to all of you for scientific, technical and moral assistance during uncounted coffee breaks.
Sampling at former mining districts is not possible without proper knowledge of the local conditions. I want to express my thanks to J. GRILL of the „ Schurfgemeinschaft Zinkwand", C. STRANZL (RHI AG), M. SCHRAMM (Univ. Salzburg), C. STURM and C. MAYR of the „Verein Bergwerk Platzertal", G. SCHWARZENBACHER of the Austrian Armed Forces as well as M. PFATSCHBACHER and L. GOTTSBACHER of the „Kupferschaubergwerk Radmer" for assistance during field trips and mine visits. Thanks for introducing me into the miracles of stable isotope measurements go to R. GRATZER, C. SPÖTL (Univ. Innsbruck), A. BOYCE and A. FALLICK (SUERC Glasgow).

Fruitful discussions with H. MIRNEJAD (Univ. Tehran) and V. SIMIC (Univ. Belgrade) contributed a lot to the genetical model of crystalline magnesite.
F. ZACCHARINI, H. MÜHLHANS and F. MITTERMAYR (TU Graz) offered their help during microprobe measurement campaigns.
Furthermore I want express my gratitude to my friends and colleagues who were nearly always available for discussions and talks: O. KRISCHE, S. SCHNITZER, A. SCHMID, P. KOLLEGGER, G. DOPPLER, E. HENJES-KUNST, S. NEUMEISTER, B. BUCHEGGER, D. GALLHOFER, A. KLAPF, H. PLUCH, M. K. STOCKER. DIETMAYER-KRÄUTLER, P. KROISSENBRUNNER, R. EHRREICH and G. KIENAST.
Finally my gratitude goes to Julia and my family for supporting and enduring me even under stressful conditions.

This work was supported by the Austrian Academy of Sciences in the framework of the "Kommission für Grundlagen der Mineralrohstoffforschung" as a part of the project „Sauerstoff- und Kohlenstoffisotopie ausgewählter ostalpiner Lagerstätten".

This thesis includes laboratory and field work of several co-supervised BSc theses by the author: DIETMAYER-KRÄUTLER 2013; KROISSENBRUNNER 2012. Chapter 4.4 dealing with cryptocrystalline magnesite includes also stable isotope values of magnesite samples prepared by the magnesite working group consisting of F. EBNER, H. MALI, K. HORKEL and T. UNTERWEISSACHER collected between 2006 and 2012.

Contents

Nomenclature

Acronyms

ω	mass fraction
apfu	atoms per formula unit
BSE	back scattered electron
CDT	Canyon Diablo Troilite
EMP	Electron Microprobe
lP/hT	low pressure / high temperature
Min	mineral
RL	reflected light
SEDEX	sedimentary-exhalative
SUERC	Scottish Universities Environmental Research Centre
SW	Seawater
TL	Transmitted light
VPDB	Vienna Pee Dee Belemnite
VSMOW	Vienna Standard Mean Ocean Water
XN	crossed nicols

Mineral Phases

ank	ankerite $CaFe(CO_3)_2$
apy	arsenopyrite FeAsS
bi	native bismuth
bou	boulangerite $Pb_5Sb_4S_{11}$
brn	bournonite $PbCuSbS_3$
cal	calcite $CaCO_3$
cc	chalocite Cu_2S
cpy	chalcopyrite $CuFeS_2$
gal	galena PbS
gdf	gersdorffite NiAsS
gud	gudmundite FeSbS
jam	jamesonite $Pb_4FeSb_6S_{14}$
lo	loellingite $FeAs_2$
mag	magnesite $MgCO_3$
mk	marcasite FeS_2
mt	magnetite Fe_3O_4
nic	nickeline NiAs
po	pyrrhotite $Fe_{1-x}S_{x=0\text{ to }0.2)}$
py	pyrite FeS_2
qtz	quartz SiO_2
saf	safflorite $CoAs_2$
sid	siderite $FeCO_3$
sku	skutterudite $CoAs_3$
sph	Sphalerite ZnS
ten	tennantite $(Cu,Ag,Fe,Co,Zn,Hg)_{12}As_4S_{13}$
tet	tetraedrite $(Cu,Ag,Fe,Co,Zn,Hg)_{12}Sb_4S_{13}$

Mineral acronyms are used as suggested by Kretz (1983). Quantities and units are used as suggested by Bakker (2011).

1. Introduction

Numerous authors (in alphabetical order: EBNER 1997, EBNER 1998, EBNER et al. 1999, EBNER 2002; FRIEDRICH 1968; PETRASCHECK 1926, 1963, 1975, 1976, 1986; POHL & BELOCKY 1994,1999; PROCHASKA 1993,1999; SCHULZ 1979a,b; TUFAR 1969, 1974; WEBER 1997) investigated the genesis of ore deposits within the Eastern Alps.

Since ore deposits in the Eastern Alps are investigated geologists are assuming that the ore forming processes are are associated with different processes like sedimentation, magmatism and/or metamorphosis. Fluid flow driven by orogenic processes is thought to be a main motor of metallogenesis in the Eastern Alps (POHL & BELOCKY 1993, 1999).

Fluid circulation is strongly connected to metamorphism. Fault zones in late orogenic stages provide suitable pathways for leaching, transportation and precipitation processes of hydrothermal-metamorphogenic fluids (POHL & BELOCKY, 1994, 1999). Primary, metal enriched rocks or fine dispersed sulphides are leached and redistribution of metals takes place during the different phases of orogenic processes. Ore genesis took place during Cadomian, Variscan and Alpine orogeny. Different metamorphic events mobilised and thinned out mineral occurrences. Brittle tectonics during the Neogene disaggregated older deposits and provided pathways for mineralising fluids as well.

Metamorphogenic fluids of similar isotopic compositions are precipitating ore minerals and carbonate-quartz gangue. The application of oxygen isotope geothermometry applied to quartz-carbonate mineral pairs is evaluated in this study. Suitable methods are applied at the different study areas as well as data in literature.

1.1. Methodology of the thesis

This work is intended to present the results of the comparison of different „classical" geothermometers with oxygen isotope geothermometry. It is mainly based on stable isotope investigations and data of fluid inclusion eluates. Stable isotope investigations of oxygen, carbon and sulphur are essential tools to describe ore forming processes. They provide informations about (1) the physico-chemical conditions of mineralisation processes (SKINNER, 1997), (2) the temperature of formation (HOEFS, 2009), (3) the origin of individual dissolved elements in solution like oxygen (POHL, 2011; HOEFS, 2009), carbon (SCHROLL & PROCHASKA, 1997) and sulphur (OHMOTO & RYE, 1979; LI & LIU, 2006) as well as (4) possible subsequent alteration and equilibration processes (ZHENG & HOEFS, 1993).

1.1.1. Stable isotope geothermometers

Basic principles

The following paragraph gives a summary of basic principles of stable isotope geochemistry according to HOEFS (2009) and SHARP (2007).

Fractionation of elements in compounds is based on the fact that compounds with heavy isotopes dissociate less likely than compounds with lighter isotopes. Elevated temperatures result in an incitation of the molecule to a higher potential energy band. The relation of vibrational frequency and mass can be expressed by Hooke´s law of a harmonic

oscillator (O'Neil, 1986):

$$\upsilon = \frac{1}{2\pi}\sqrt{\frac{k}{\mu}} \tag{1}$$

υ is the frequency, k represents the constant force-factor and μ is the reduced mass. The reduced mass of a 2-atom molecule is calculated using the masses m_1 and m_2 of the molecules M_1 and M_2:

$$\mu = \frac{m_1 m_2}{m_1 + m_2} = \frac{1}{\frac{1}{m_1} + \frac{1}{m_2}}$$

The relation of the harmonic oscillator (equation 1) results in the fact that smaller masses have higher vibrational frequencies than heavier compounds. Therefore lighter compounds dissociate more easily. Similar to equilibrium constant in chemical reactions the fractionation factor α between two mineral phases A and B can be expressed:

$$\alpha = \frac{R_A}{R_B} \tag{2}$$

R stands for the ratio of the heavy and the lighter isotope (e.g. $\frac{^{18}O}{^{16}O}$). The determination of absolute frequencies is difficult therefore the relation of individual isotopes compared to international standards (cf. Paragraph 2.2) is introduced:

$$\delta_x = \frac{R_x - R_{standard}}{R_{standard}} \,.\, 1000\,[‰]$$

Isotope fractionation is in direct relation with the temperature and can be described in the following equation using the coefficients A, B, C, D, E and F:

$$10^3 \ln\alpha = A\frac{10^{18}}{T^6} + B\frac{10^{12}}{T^4} + C\frac{10^9}{T^3} + D\frac{10^6}{T^2} + E\frac{10^3}{T} + F \tag{3}$$

or simplified to a quadratic expression and reducing to two coefficients (D, F):

$$10^3 \ln\alpha = D\frac{10^6}{T^2} + F \tag{4}$$

Using a polynomial of a higher degree makes only sense in a few cases when the fractionation equation is of higher degree itself (see Figure 1).

Taking the logarithm of equation 2:

$$\ln\alpha_{AB} = \ln(10^{-3}\delta_A + 1) - \ln(10^{-3}\delta_B + 1)$$

δ-values of minerals involved in natural rock systems result in maximum of several 10 ‰. Therefore the following approximation is applicable:

$$\ln(10^{-3}\delta + 1) \approx 10^{-3}\delta$$

or

$$\Delta_{AB} \equiv \delta_A - \delta_B \approx 10^3 \ln\alpha_{AB} \tag{5}$$

Solving the simplified fractionation equation 4 after T gives the precipitation temperature (in Kelvin) of the mineral pair in equilibrium:

$$T \approx \sqrt{\frac{D}{\Delta_{AB} - F}} \tag{6}$$

If two mineral phases have equilibrated oxygen with a reservoir (e.g. hydrothermal fluid) the difference of the individual $\delta^{18}O$ values is a function of temperature. The calculation of temperature is possible with known $\delta^{18}O_{mineral\ A}$ and $\delta^{18}O_{mineral\ B}$ due to the temperature dependency of α_{AB}. Some frequently used coefficients to determine the oxygen and carbon exchange between different species and H_2O or CO_2 are summarized in Table 1. A good source for calculation of isotope fractionation or equilibrium temperatures is the *AlphaDelta* web page of G. Beaudoin and P. Therrien at Université Laval who collected 1131 different equations[1]. The temperature dependency of the fractionation factor α_{AB} with the values of Table 1 is shown in Figures 1 and 2. The application of a suitable fractionation equation is evident. It is important to know the present carbonate phase and the approximate precipitation temperature. Choosing an inappropriate equation can result in discrepancies of several per mill for $10^3 \ln \alpha_{mineral-H_2O}$ and therefore wrong temperature estimations.

Slowly cooling down of precipitated minerals from a equilibrated solution is steadily exchanging oxygen isotopes between the different mineral phases. Calculated precipitation temperatures should be interpreted with caution. Calculated temperatures can only be used as crystallisation temperature when the mineral phases are in equilibrium with each other. The determination of isotopic equilibrium is therefore the main prerequisite to the application of stable isotopes as a geothermometer. The exchange of isotopes should have happened in a closed system. The fact of $\delta_1 - \delta_2 \equiv \triangle_{12}$ is easily transformed to $\delta_1 = \delta_2 + \triangle_{12}$. That means for a closed system at a given temperature (constant $\triangle_{12}$) that the equilibrium isotope composition for two different phases is plotting along a line.

To describe the isotopic characteristics of open fluid-rock system it is necessary to determine the characteristics of simplified fluid absent systems. In a closed system mineral assemblages have fixed modal proportions and isotopic exchange can only take place with each present phase while the bulk composition in the system remains invariant (Gregory & Criss, 1986). The two-phase closed system represented in the δ-space using simple mass balance is written

$$\delta_A = -\frac{X_A}{X_B}\delta_B + \frac{\delta_{system}}{X_A} \tag{7}$$

X_A and X_B are representing the mole fractions of the phases of the element for interest. This is a linear equation with the coordinates of δ_A and δ_B and a negative slope. The assessment of isotopic equilibrium and disequilibrium is possible by the isotherm method of Javoy et al. (1970). This graphical method is referencing the heaviest mineral in a succession to every other mineral. The determination of equilibrium or disequilibrium is therefore only possible when three or more phases are present. Only two phases oblige another attempt. Isotopic equilibrium of quartz and carbonate phases is assumed when the mineral are in textural equilibrium. Temperatures received from oxygen isotope mineral

[1] http://www2.ggl.ulaval.ca/cgi-bin/isotope/generisotope.cgi (as per June 2012)

System	A	B	C	D	E	F	T (°C)	Reference
ankerite-H_2O				4.120	-4.620	1.71	0-1200	5
calcite-H_2O				2.780		-2.89	0-500	1
calcite-H_2O				18.030		-32.42	25-350	2
dolomite-H_2O				3.260		-4.51	100-650	8
dolomite-H_2O				4.060	-4.650	1.71	0-1200	5
magnesite-H_2O				4.070	-4.640	1.72	0-1200	5
quartz-H_2O				3.340		-3.31	250-500	3
quartz-H_2O				3.380		-3.40	200-500	9
quartz-H_2O				3.306		-2.71	180-550	11
quartz-H_2O				3.650		-2.90		4
$quartz_{alpha}$-H_2O				3.550		-2.57	195-573	10
quartz-calcite				0.870				4
quartz-calcite				0.470	-0.100		0-1200	5
quartz-calcite	0.0035	0.05		0.335			>127	6
$SiO_{2\ amorphous}$-H_2O				3.520		-4.35	low T	7
siderite-HCO				4.230	-4.580	1.73	0-1200	5
dolomite-CO_2 (g)			-0.891	8.737	-18.110	8.44	<600	12
dolomite-CO_2 (g)			-0.388	5.538	-11.346	3.12	<600	13
calcite-CO_2 (g)			-0.891	8.557	-18.110	8.27	<600	12
chalcopyrite-H_2S				0.050			0-1000	14
$CaSO_4.2HO$-H_2S				5.260		6.00	200-350	12
galena-H_2S				-0.640			0-1000	14
pyrite-H_2S				0.400			200-700	12
sphalerite-H_2S				0.100			0-1000	14
S^{2-}-H_2S				-0.210	-1.23	-1.20	>25	12
SO_4^{2-}-H_2S				5.260		6.00	200-350	12

Table 1: *Coefficients used in equ. 3 and 4 for oxygen, carbon and sulphur isotope exchange.*
References: (1) Friedman & O'Neil (1977), (3) Matsuhisa *et al.* (1979), (4) Sharp & Kirschner (1994), (5) Zheng (1999), (6) Clayton & Keiffer (1991), (7) Martin *et al.* (2012) , (8) Golyshev *et al.* (1981), (9) Clayton *et al.* (1972), (10) Shiro & Sakai (1972), (11) Zhang *et al.* (1989), (12) Ohmoto & Rye (1979), (13) Sheppard & Schwarcz (1970) (14) Li & Liu (2006).

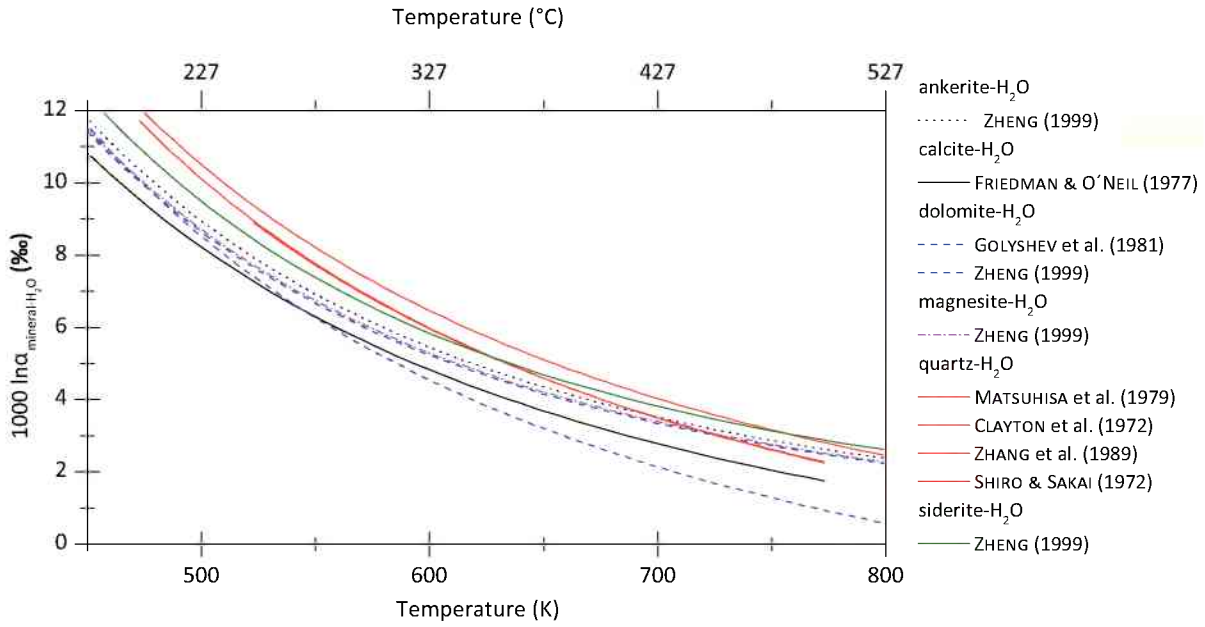

Figure 1: *Temperature dependency of equilibrium isotopic fractionation factors between carbonate minerals and H_2O. See Table 1 for corresponding equations and applicable temperature ranges .*

pairs are crosschecked with other independent geothermometers (cf. Chapters 1.1.2, 1.1.3 and 1.1.4). Deviating temperature estimations are discussed.

Uncertainty calculation

Oxygen isotope fractionation of carbonates as well as of quartz are the measured dimensions from which the formation temperature is calculated. Both values ($\delta^{18}O_{carbonate}$ and $\delta^{18}O_{quartz}$) show different relative measurement uncertainties due to different analytical methods (see Chapter 2.2). Therefore a proper calculation of accuracy is required. The simplified equation 6 shows the connection between temperature and Δ_{AB}. Table 1 shows that higher polynomials require numerical solutions. In the following an exemplary work flow for calculating the maximum absolute errors is given.

$$\Delta_{AB} = D_{AB}\,\frac{10^6}{T^2} + E_{AB}\,\frac{10^3}{T} + F_{AB} \tag{8}$$

Δ_{AB} defines the difference between $\delta^{18}O_A$ and $\delta^{18}O_B$. Solving equation 8 after T gives the solution for the formation temperature in Kelvin. The estimation of the maximum error is possible using the first derivative of equation 8 and the repeatability of oxygen measurements of minerals A and B:

$$\triangle T\,(\Delta_{AB}) := \left[\left|\frac{d}{d\Delta_{AB}} T(\Delta_{AB})\right|.\triangle_A\right] + \left[\left|\frac{d}{d\Delta_{AB}} T(\Delta_{AB})\right|.\triangle_B\right] \tag{9}$$

EXAMPLE: Using the quartz-calcite mineral pair with the fractionation equations of SHARP & KIRSCHNER (1994) and ZHENG (1999) with $D = -0.36$, $E = 4.66$, $F = -4.61$,

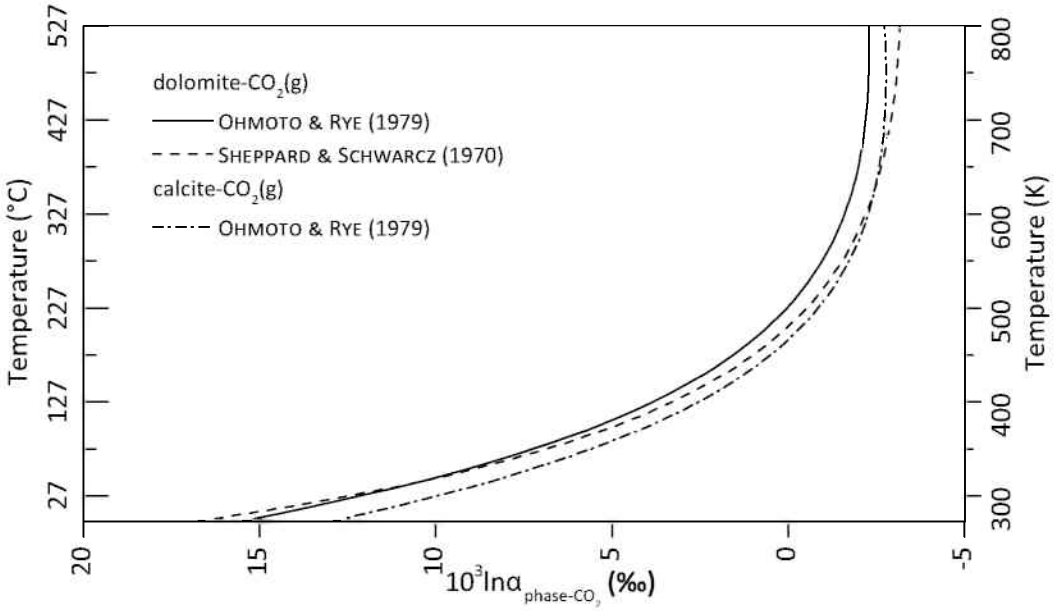

Figure 2: *Temperature dependency of equilibrium isotopic fractionation factors between calcite or dolomite and CO_2 (g). The applicable temperature lies below 600 °C. See Table 1 for references.*

$\delta^{18}O_{carbonate} = 14.01 \pm 0.07$ ‰ and $\delta^{18}O_{quartz} = 15.22 \pm 0.20$ ‰ gives a temperature estimation of 440 ± 28 °C. Due to different analytical errors the $\delta^{18}O$ measurements of quartz affect the maximum error with $(|\frac{d}{d\Delta_{quartz-calcite}} T(\Delta_{quartz-calcite})|.\triangle_{quartz}) = 21$ °C about three times higher than the $\delta^{18}O$ measurements of calcite $(|\frac{d}{d\Delta_{quartz-calcite}} T(\Delta_{quartz-calcite})|.\triangle_{calcite}) = 7.3$ °C.

1.1.2. Arsenopyrite geothermometer

The As/S ratio of arsenopyrite coexisting with other phases in the system Fe-As-S is a widely used, experimentally calibrated geothermometer (e.g. Kerestedjian 1997; Kretschmar & Scott 1976; Sharp et al. 1985). The application is valid for deposits metamorphosed under greenschist and lower amphibolite facies. For upper amphibolite and granulite facies deposits it yields too low temperatures. For low temperature hydrothermal deposits inconsistent temperatures are calculated (Sharp et al. 1985).

1.1.3. Solid solution geothermometry in the system FeAsS-NiAsS-CoAsS

Klemm (1965) proposed a geothermometer based on solid solution stability fields of sulfarsenides and diarsenides. Misra & Fleet (1975) pointed out that Klemm (1965) did not take the As for S substitution into account. Following the remarks of Fanlo et al. (2004) the sulfarsenide compositions with an As/S ratio greater than 1 are left out.

1.1.4. Fluid inclusion chemistry and cation geothermometry

The characterization of Total Dissolved Solids (TDS) provides information about the source of solutes in ore-precipitating brines and mixing processes of different fluids. The

crush-leach method is described on page 34. With this technique the I/Cl, Br/Cl, K/Na, Li/Na ion ratios are calculated. The charge balance of the solution is determined in order to trace influences caused by dissolved species that have not been analysed, or contamination of the sample by e.g. clay minerals. HAFELLNER (1995) pointed out that during the crushing procedure volatile phases (e.g. CO_2) can get lost. The kind of chemical elements of an inclusion are known but not the kind of chemical compound (species). The elements Na, K, Ca, Mg and Fe are supposed to occur as chlorides. Discrepancies in charge balances can also be due to H^+, CO_3^{2-} and OH^- concentrations. Taking these restrictions into account charge balances provide useful information.

Bulk fluid inclusion chemistry gives hints about the processes that influenced salinity of palaeofluids. At an initial stage of evaporation within a saline environment Na, Cl and Br are concentrated in the residual brine and their ratios do not change. The halite evaporation trend can be observed when seawater starts to precipitate halite. The composition of the bittern brine is shifting along the trend. Br is still concentrated within the residual brine. With ongoing precipitation Br is incorporated and fractionation begins. Furthermore the cations system changes from a Na dominated to Mg and K dominated system (MCCAFFREY et al. 1987). On the contrary the halite dissolution trend defines palaeofluids that gained their salinity by migration within the crust. The Br content is diluted proportional to the Na and Cl contents.

Cation exchange geothermometers (Table 2) are applied by using the cation concentration in bulk fluid inclusion solutes. The different geothermometers are empirical and should only be used within their limits. A limitation is the fact that crush-leach analysis (see 2.3) is blending shares of primary, secondary and pseudo-secondary fluid inclusions. VERMA et al. (2008) developed a computer program (SolGeo) for calculating formation temperatures using different cation exchange geothermometers. In this work the Na-Li geothermometers of FOUILLAC & MICHARD (1981); KHARAKA & MARINER (1989); VERMA & SANTOYO (1997) and Na-K geothermometers of DÍAZ-GONZÁLEZ et al. (2008) are applied for calculating formation temperatures of carbonates and quartz.

Na-Li	$\frac{1000 \pm 47}{\log(\frac{Na}{Li}) + 0.38 \pm 0.11} - 273.15$	FOUILLAC & MICHARD (1981)
Na-Li	$\frac{1590}{\log(\frac{Na}{Li}) + 0.779} - 273.15$	KHARAKA & MARINER (1989)
Na-Li	$\frac{1049 \pm 44}{\log(\frac{Na}{Li}) + 0.44 \pm 10} - 273.15$	VERMA & SANTOYO (1997)
Na-K	$\frac{883 \pm 15}{\log(\frac{Na}{K}) + 0.894 \pm 0.032} - 273.15$	DÍAZ-GONZÁLEZ et al. (2008)

Table 2: *Solute geothermometers used to calculate precipitation temperatures [°C] of carbonate minerals and quartz.*

1.2. Reconstruction of fluid provenance and evolution

Stable isotope measurements bear the possibility to reconstruct fluid provenance and evolution. Reconstructions of ore forming fluids are possible when δ^{18}O , δ^{13}C and δ^{34}S values are interpreted.

1.2.1. Oxygen isotopes

Oxygen isotopes provide information about the origin of ore forming fluids. Waters of magmatic, metamorphic and sedimentary origin occupy partly overlapping fields. Therefore the discrimination to one single fluid source is not possible. Using the $\delta D - \delta^{18}O$ diagram (Figure 3) illustrates the isotopic compositions of waters of different origin. The isotopic composition of precipitation and shallow groundwater plots along the global meteoric water line (GMWL). Meteoric water represents water that was part of the meteorological cycle (evaporation - condensation - precipitation). The isotopic composition of meteoric water excludes seawater. Formation water depicts waters of unknown origin and age within sediments. Possible overprints of the primary isotopic signature by meteoric or formation waters have to be investigated.

Today δ^{18}O of atmospheric CO_2 is about +41 ‰ (Keeling, 1961).

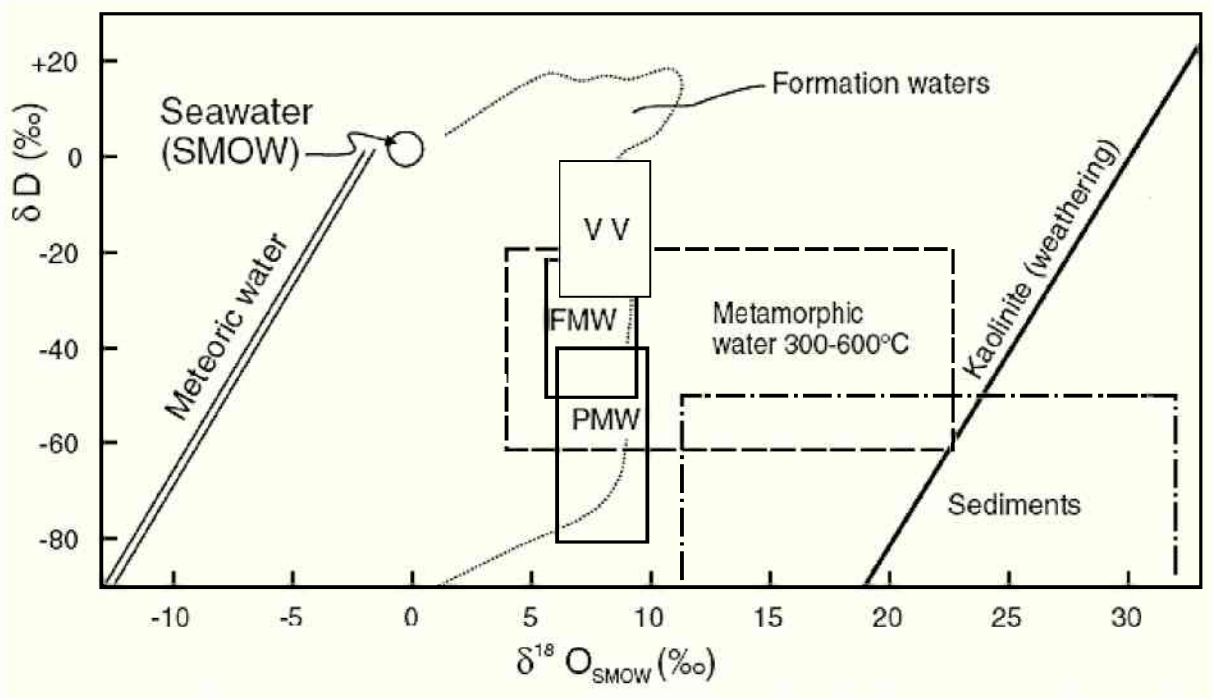

Figure 3: *Isotopic composition of fluids participating in the hydrothermal ore formation processes. Simplified after* Pohl (2011) *with data of* Hoefs (2009). *VV ... volcanic vapour, FMW ... felsic magmatic water, PMW ... primary magmatic water.*

1.2.2. Carbon isotopes

Due to the fact that the PeeDeeBelemnite (PDB) is used as a reference for δ^{13}C measurements marine carbonates show values around zero. Mantle carbon ranges from -4 to -8

(DEINES, 1980), kerogen ranges from -20 to -30 ‰ (WHITICAR, 1996) and hydrothermal carbonates show values between -6 and -9 ‰ (SCHROLL & PROCHASKA, 1997). Today $\delta^{13}C$ of atmospheric CO_2 is about -8 ‰ (KEELING et al., 1995). The determination of variations of $\delta^{13}C$ in a geological timescale is difficult but it can be estimated using marine carbonates.

1.2.3. Sulphur isotopes

The fractionation between sulphides and a solution is function of temperature and the dominant aqueous sulphide species (cf. OHMOTO, 1972). Principally four different sulphur species are present above 250 °C: $\sum SO_4^{2-}$, H_2S, HS^- and S^{2-}. The dominating species is depending on pH, $f(O_2)$ and the temperature of the fluid.

Example A: Taking an acidic, hydrothermal fluid for example: bulk $\delta^{34}S_{\sum} = 0$ ‰, $T = 300$ °C, $pH = 4.5$, $log\, f(O_2) = -38$ and total sulphur equals 1 mole per kg H_2O. Under these conditions most of the dissolved sulphur occurs in form of H_2S (Figure 5). When sulphides are precipitating in equilibrium with H_2S the following fractionation apply: $\triangle^{34}S\,(galena - H_2S) = -1.95$ (calibration after LI & LIU 2006), $\triangle^{34}S\,(chalcopyrite - H_2S) = 0.15$ (calibration after LI & LIU 2006), $\triangle^{34}S\,(sphalerite - H_2S) = 0.30$ (calibration after LI & LIU 2006) and $\triangle^{34}S\,(pyrite - H_2S) = 1.22$ (calibration after OHMOTO & RYE 1979).

Example B: If the the hydrothermal fluid of example A is oxidized $\sum SO_4^{2-}$ would be the dominant aqueous sulphur species with $\delta^{34}S_{\sum} = 0$ ‰. The initial sulphur fractionations of sulphides precipitated from such a fluid would be (applying the calibration of OHMOTO & RYE (1979) for $SO_4^{2-}\,(aq) \rightleftharpoons H_2S$): $galena = -20.06$ ‰, $chalcopyrite = -22.16$ ‰, $sphalerite = -22.31$ ‰ and $pyrite = -23.03$ ‰.

Example C: If the pH is increasing $f(O_2)$ remains similar to example A. For example the fluid is entering organic rich carbonates. In this case the dominant species is S^{2-} with $\delta^{34}S_{\sum} = 0$ ‰. The initial sulphur fractionations of sulphides precipitated from this fluid would be (using the calibration of OHMOTO & RYE (1979) for $S^{2-} \rightleftharpoons H_2S$): $galena = 2.04$ ‰, $chalcopyrite = 4.14$ ‰, $sphalerite = 4.29$ ‰ and $pyrite = 5.21$ ‰.

The examples A, B and C work for $\delta^{34}S_{\sum} = 0$ ‰. Due to the fact that the Canon Diablo Troilite (FeS) is used as an international standard mantle material and sulphides derived from it have a $\delta^{34}S$ value near zero. Marine sulphate in contrast show values from +10 to +30 ‰. Modern seawater shows +21 ‰ (CLAYPOOL et al. 1980). Another extreme values shows sulphide sulphur that is produces by organic fractionation that shows negative $\delta^{34}S$ values from -20 to -60 ‰ (CANFIELD & THAMDRUP 1994; CANFIELD et al. 2010). Magmatic and hydrothermal sulphur may contain sulphur of mixed origin but an estimation about the provenance is possible.

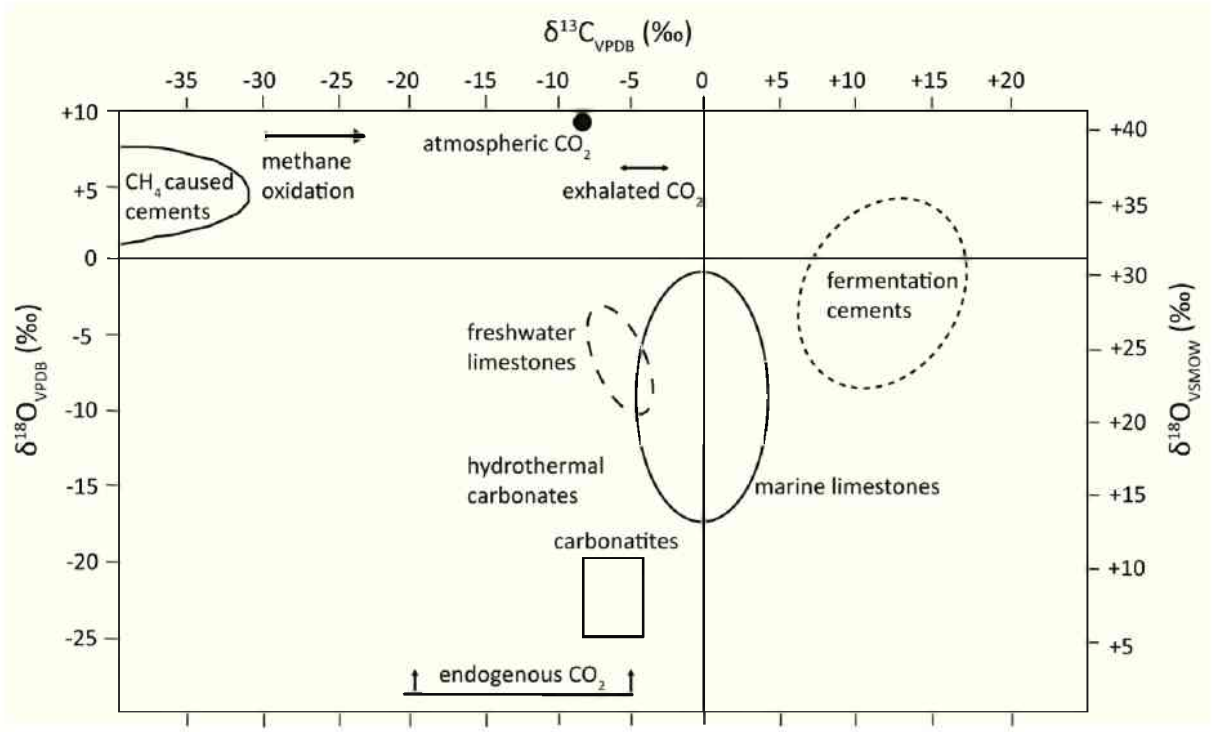

Figure 4: *Diagram showing $\delta^{18}O$ versus $\delta^{13}C$ values of carbonates and isotopic compositions of endogenous CO_2, atmospheric CO_2 and biogene fractionation of carbon through fermentation processes (modified after* Schroll & Prochaska 1997 *with data of* Keeling (1961) *and* Keeling *et al. (1995) for atmospheric carbon and oxygen).*

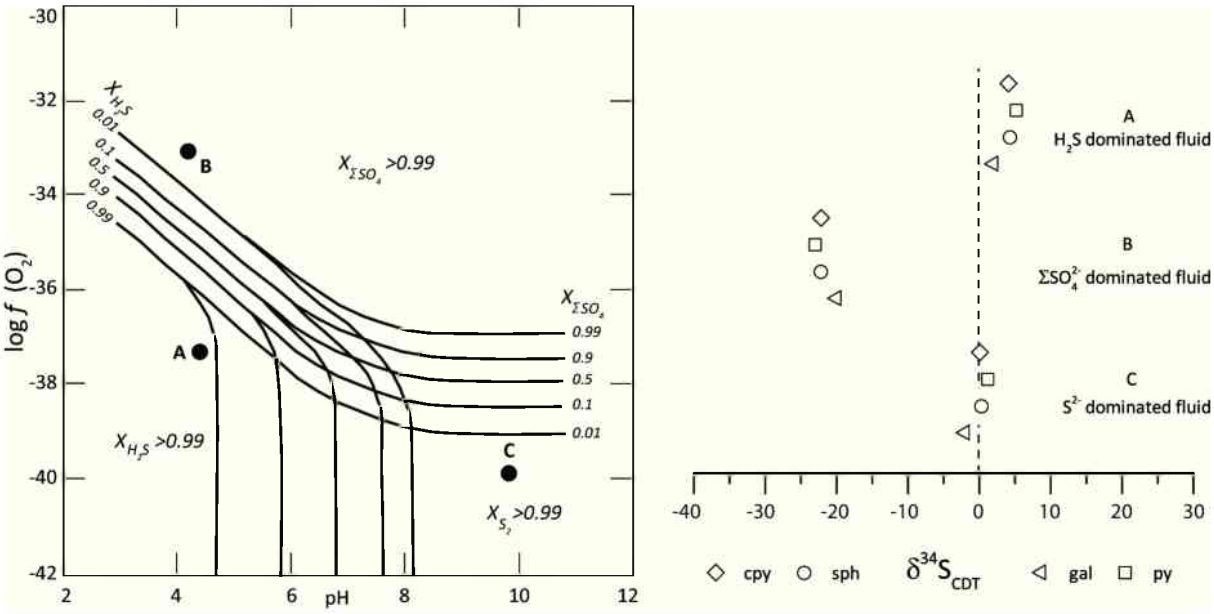

Figure 5: *left: Stability field of aqueous sulphur species as a function pH and $f(O_2)$ (modified after* Ohmoto 1972*). right: Initial $\delta^{34}S$ values of sulphides precipitating from a fluid with $\delta^{34}S_{\sum} = 0\,‰$ and various dominant aqueous sulphur species: (A) H_2S as dominant fluid species, (B) $\sum SO_4^{2-}$ as dominant fluid species, (C) S^{2-} as dominant fluid species (calculated after calibrations of* Ohmoto & Rye (1979); Li & Liu (2006)*.*

1.3. Quantification of fluid flux and fluid rock interaction

1.3.1. Zero-dimensional water-rock interaction model

Zero-dimensional water-rock interaction models after TAYLOR (1979) represent simple models for estimating fluid/rock ratios by instantaneous and constant isotopic equilibration between a fluid and rock. The basis of this model is a mass balance equation:

$$W^{i}_{H_2O} + R^{i}_{rock} = W^{if}_{H_2O} + R^{f}_{rock} \tag{10}$$

where i represents the initial value, f the final values, W is the atom fraction of the element in the fluid and R is the atom fraction of the element in rock. Covariation of δ^{18}O and δ^{13}C values of carbonates reflect a change in the isotopic composition of the solution and/or temperature during precipitation. ZHENG & HOEFS (1993) developed a two component model to describe the covariation of δ^{18}O and δ^{13}C for hydrothermal calcites. They describe three mixing processes quantitatively: (1) mixing between two different fluids, (2) mixing between fluid and rock with calcite precipitation due to fluid/rock interaction, (3) alteration of primary calcite by interaction with a subsequent fluid.

1.3.2. Mixing between two fluids

ZHENG & HOEFS (1993) discussed the mixing process of two different hydrothermal fluids and the evolving carbonates thereof intensively. The equations 11 and 12 show the oxygen and carbon isotopic composition of calcite precipitated due to the mixture of two fluids:

$$\delta^{13}C_{calcite} = \frac{X_a(\delta^{13}C_a + 10^3 \ln \alpha^{calcite}_{HCO_3^-}) + P(1 - X_a)(\delta^{13}C_b + 10^3 \ln \alpha^{calcite}_{CO_2})}{P + X_a + PX_a} \tag{11}$$

$$\delta^{18}O_{calcite} = \delta^{18}O_b + 10^3 \ln \alpha^{calcite}_{CO_2} + X_a(\delta^{18}O_a - \delta^{18}O_b) \tag{12}$$

X_a represents the mole fraction of fluid A in the mixed fluid and $10^3 \ln \alpha^{X}_{Y}$ is the equilibrium fractionation factor between the components X and Y. P denotes the carbon content of the two fluids: $P = \frac{C_b}{C_a} \approx \frac{^{12}C_b}{^{12}C_a}$. The model assumes furthermore that the predominant carbon species in the high-temperature and low-temperature fluid end members are $CO_2(aq)$ and HCO_3^-. The model assumes that mixing is a purely physical process that ignores temperature and pH. The mixing curves of fluid compositions for mixing of two fluids A with an isotopic composition of δ^{18}O = 0 ‰ and δ^{13}C = 0 ‰ and fluid B with δ^{18}O = 10 ‰ and δ^{13}C = -10 ‰ is illustrated in Figure 6. Fluid A is representing seawater or shallow formation water dominated by HCO_3^- and has a temperature of 50 °C. Fluid B is dominated by H_2CO_3 ($\approx CO_2$) and has a temperature of 300 °C and shows the isotopic composition of metamorphogenic water.

1.3.3. Secondary alteration after Zheng & Hoefs (1993)

This model assumes isotopic exchange between carbonate host rock and a percolating fluid. Taking a remobilised, stratiform ore deposit with carbonate gangue for example.

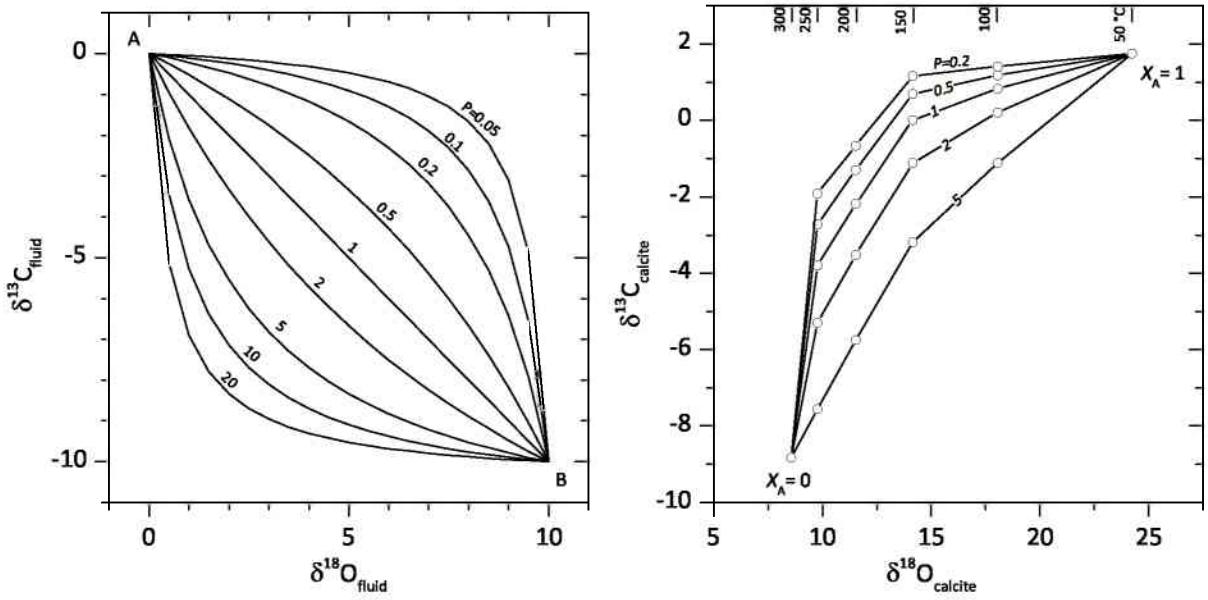

Figure 6: *(a) Simple temperature independent mixing curves of fluid compositions for mixing of two fluids calculated after* Zheng & Hoefs (1993). *Fluid A has $\delta^{18}O$ = 0 ‰ and $\delta^{13}C$ = 0 ‰ and represents seawater or shallow formation water. Fluid B has $\delta^{18}O$ = 10 ‰ and $\delta^{13}C$ = -10 ‰ and stands for metamorphogenic water. P is the concentration ratio of total dissolved carbon in fluid B to fluid A. Fluid A is dominated by HCO_3^- and has a temperature of 50 °C. Fluid B is dominated by H_2CO_3 ($\approx CO_2$) and has a temperature of 300 °C. (b) Carbon and oxygen isotopic composition of calcite precipitating due to mixing of fluid A and B.*

The remobilised carbonates are subsequently precipitated in form of a vein type deposit. By measurement of "primary" and re-deposited calcite an estimation migration distance using the water/rock ratio is possible. The model is limited by several assumptions. Knowledge of the primary isotopic composition of the involved limestone, the temperature and the isotopic composition of the fluid as well as the mole fraction of the carbon species are necessary. With known isotopic compositions of altered carbonates the covariation curves can be modelled and the temperature and isotopic composition of the involved fluid is assessable. The following equations are valid for an open system where the fluid is replenished by fluid of the same isotopic composition. This is the case for metamorphogenic fluids that have equilibrated during migration. The isotopic exchange produces initially greater changes in δ^{18}O than δ^{13}C (Figure 7).

$$\delta^{13}C_{calcite} = (\delta^{13}C^{initial}_{HCO_3^-} + \triangle\delta^{13}C^{calcite}_{HCO_3^-}) - (\delta^{13}C^{initial}_{HCO_3^-} + \triangle\delta^{13}C^{calcite}_{HCO_3^-} - \delta^{13}C^{initial}_{HCO_3^-}).e^{-\frac{W}{R}X_{HCO_3^-}}$$

$$\delta^{18}O_{calcite} = (\delta^{18}O^{initial}_{H_2O} + \triangle\delta^{18}O^{calcite}_{H_2O}) - (\delta^{18}O^{initial}_{H_2O} + \triangle\delta^{18}O^{calcite}_{H_2O} - \delta^{18}O^{initial}_{calcite}).e^{-\frac{W}{R}}$$

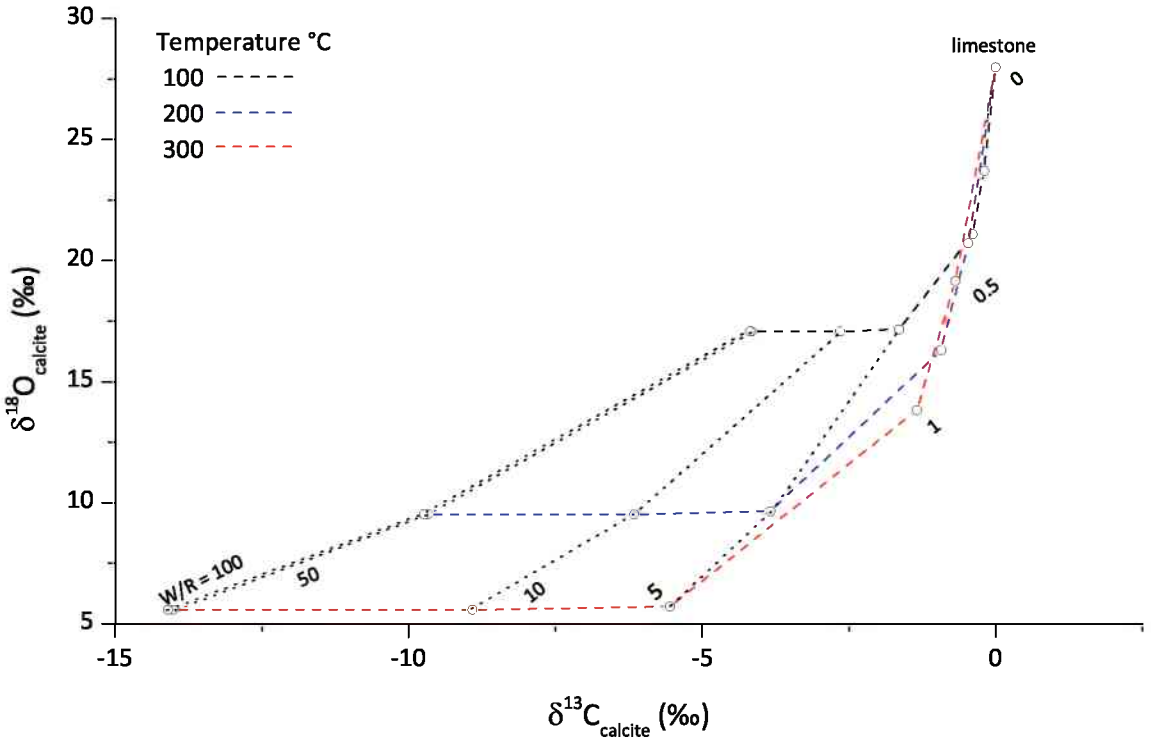

Figure 7: *Covariation of carbon versus oxygen isotopic composition during fluid/rock interaction involving a marine limestone modelled after* Zheng & Hoefs (1993). *The fresh marine limestone has* $\delta^{18}O = 28$ ‰ *and* $\delta^{13}C = 0$ ‰. *The involved fluid represents a metamorphogenic fluid with* $\delta^{18}O$ ‰ $= 0$ *and* $\delta^{13}C$ ‰ = -7. *The process takes place at 100, 200 and 300 °C and the* HCO^-_3 *forms the main dissolved carbon species.* $X_{HCO_3^-} = 0.2$ *represents the mole fraction of* HCO^-_3 *in the fluid. During hydrothermal alteration a progressively increasing fluid/rock ration (W/R) from zero to 100 is assumed.*

1.4. Selection of investigated ore deposits

This study is aimed to compare individual geothermometers applied to selected historical important ore deposits of the Eastern Alps:

- Upper Austroalpine nappe system
  - Greywacke zone nappe system
    - Cu deposit Mühlbach-Buchberg/Salzburg
    - Cu deposit Radmer/Styria
  - Silvretta-Seckau nappe system
    - Ni-Co-Bi deposit Zinkwand/Schladming/Styria
    - Magnesite deposit Kraubath/Styria
  - Ötztal-Bundschuh nappe system
    - Pb-Zn deposit Tösens/Tyrol
- Sub-Penninic units of the Tauernwindow
  - Pb-Ag deposit Erzwies-Silberpfennig/Salzburg.

All these vein systems are made up of mainly carbonate gangue (calcite, ankerite and siderite) and minor quartz. They were selected due to their large vertical extent (up to $\sim$ 300 m) to assure a wide range in crystallization temperatures of ore minerals and gangue. The variable tectonic position and differences in formation ages, metamorphic history and host rocks provide ideal conditions to study pros and cons of the individual geothermometers and their usefulness. Summarized geological and metallogenetical information about the individual deposits is found in WEBER (1997A).

1.5. Ore deposition within the Eastern Alps linked to metamorphism

Ore deposition within the Eastern Alps is closely linked to several orogenic phases during Phanerozoic. After FRANK & WEBER (1997) four phases were essential for the metallogenetical evolution of ore deposits.

Pre-Permian metal enrichments

Pre-Permian metal enrichments and ore deposits are difficult to determine due to later metamorphic overprints. In some cases remobilisation of older metal enrichments are proven. The Pb-Zn deposit Tösens within the Ötztal crystalline represents a pre-Variscan, syngenetic mineralisation with pre-Varicsan magmatic cycles as possible source for metal supply (VAVTAR, 1988).

The Pb-Zn-Ba ore district Graz Palaeozoic shows stratiform mineralisations within Devonian black schists and is interpreted as SEDEX deposit of Meggen-typus (WEBER, 1990). The Paleozoic rocks of the Gurktaler nappe system exhibit small occurrences of syngenetic magnetite-haematite mineralisations (EBNER, 1997).

Permotriassic metamorphism

During the Permian crustal extension wide spread evaporites were formed. These evaporites (Haselgebirge) are now incorporated into the Upper Austroalpine nappe system and play an important role in ore generating processes during later metamorphic processes. SCHUSTER & STÜWE (2008) propose model of lithospheric thinning accompanied by magmatic underplating with subsequent partial melting of the lower crust and lP/hT metamorphism. If the Permian metamorphic event generated concentrations of ore minerals within the younger sedimentary cover, remains unresolved.

Eo-alpidic metamorphism

During Eo-Alpidic times (92 Ma) two different scenarios leading to intense fluid mobilisation, circulation and ore deposition are discussed. Parts of the Austroalpine Palaeozoic especially the Greywackezone nappe system suffered increased fluid flow rates. These enhanced rates are due to intense metamorphic processes in the depth (see SCHRAMM 1977 and Metamorphic map of the Alps by OBERHÄNSLI et al. 2004 and BOUSQUET et al. 2008[2]) . The high number of different ore deposits within the Greywackezone nappe system accompanies this rearrangement and remobilisation processes. The Mitterberg Cu-vein is an instructive example for vein formation as a result of Cretaceous metamorphism (see Chapter 4.1). Deformation occurred during and after the temperature peak respectively. Therefore the relevant time span comprises several tens of millions of years. At the base of the Northern Calcareous Alps massive units of evaporites (Haselgebirge) occur (cf. SCHAUBERGER, 1986). Fluids migrating within these units represent acidic and chlorine or sulphate solutions (POHL & BELOCKY, 1994; PROCHASKA, 1999). Such solutions are able to dissolve ions from host rocks with subsequent deposition thereof at changing physico-chemical conditions.

The second process occurs at the frontal areas of the Austroalpine crystalline. During early nappe stacking units of the Semmering-Wechsel system were affected by intense fluid movements at the beginning subduction of the Penninic ocean (PROCHASKA, 1993).

Neogene metamorphism and lateral extrusion

Ore deposits associated with prominent fault systems like Liesing-Paltental and Lavantal fault are associated with fluid convection cells. Within such convection cells deep seated ascending Cretaceous rest-fluids were mixing with descending meteoric waters. The mixing process and degassing of CO_2 were the main driving factors for ore deposition.

The Tauerngold veins are a special case. These veins are associated with the fading Tauern metamorphosis. In the Gastein and Rauris area shear zones due to the updoming of the Hohe Tauern mountains during this late orogenic stage provide pathways for metamorphogenic fluids.

[2]Metamorphic structure of the Alps - Revised version (2008): http://http://perso.univ-rennes1.fr/romain.bousquet/Papers/MetMap/ (downloaded on 23.10.2012)

1.6. Aims of research

Metamorphic processes are assumed to be the main motor of ore genesis within the Eastern Alps. The different orogenic phases triggered remobilisation and subsequent ore deposition. Metamorphogenic fluids of similar isotopic compositions precipitate ore minerals and carbonate-quartz gangue. The application of oxygen isotope geothermometry applied to quartz-carbonate mineral pairs is evaluated in this study. The investigated deposits offer large vertical extensions and therefore a broad range in formation temperature is given. The investigated deposits are situated in different geological units of the Eastern Alps with variable geological history and formation ages.

Suitable analytical methods (Chapter 1.1) as well as literature data are applied to decipher ore forming processes in the individual study areas. Limits, problems and concluding remarks regarding metallogenesis, formation temperatures are critically examined and individually discussed. Finally the main characteristics of mineralising fluids during the different orogenic phases of the Eastern Alps and a code of practice for the use of isotope geothermometers applied to re deposits are presented.

2. Analytical procedures

2.1. Electron microprobe

Electron microprobe measurements of sulphides, arsenides etc. were carried out using a JEOL JXA 8200 Superprobe at the "Eugen F. Stumpfl Laboratory" at the Montanuniversität Leoben. Operation conditions were 20 kV accelerating voltage, a beam size of 2 μm, peak counting times of 20 s and background counting times of 10 s . Counting times for Co, Se, Ag,Ni and Pb were increased up to 100 s for peak counting time and 50 s for background. Radiation lines and crystals were used as follows: Lα TAP (As, Se), Lα PETJ (S, Sb, Pb), Lα PETH (Ag), Kα PETJ (S), Kα LIF (Cu, Fe, Zn), Kα LIFH (Co, Ni). The calculation of sample detection limits for single point measurement is based on the standard counts, the unknown background counts and the magnitude of the ZAF correction factor (Scott & Love, 1983). This determination resulted in following detection limits (in ω^3): Ag, Co, Cu, Fe, Hg, Ni, Sb, S, Se = 0.0002; As, Pb, Zn = 0.0003.

2.2. Stable isotope measurements

δ^{13}C and δ^{18}O of carbonates

Oxygen isotope ratios of carbonates were determined at the Stable Isotope lab at the Montanuniversität Leoben. The carbonate samples were prepared by drilling small aliquots from specimens using a dentist drill. The powder was transferred into autosampler vials (Labco Exetainer vials) and sealed with butyl-rubber septa. The analyses were performed on a Thermo Fisher Delta V mass spectrometer employing a Finnigan Gas Bench II following the descriptions of Spötl & Vennemann (2003). The samples (0.2 - 0.3 mg) were dissolved with anhydrous H_3PO_4 (density 1.91) in a pressurised helium atmosphere at 70 °C for 8 hours. By using multiple measurements of an in-house calcite reference material, precision of δ^{18}O and δ^{13}C measurements are $\pm$ 0.07 ‰ and $\pm$ 0.05 ‰ (1s, n=180) respectively. Carbon isotope data are reported relative to Vienna Pee Dee Belemnite (VPDB) and oxygen isotopes relative to Vienna Standard Mean Ocean Water (VSMOW) .

δ^{18}O of quartz

Quartz mineral separates were prepared by hand-picking under a binocular microscope. Quartz was finely crushed to avoid contamination by fluid inclusions. The quartz powder was washed with HCl (12 mol/l) for several hours to remove residual carbonates and subsequently cleaned with deionized water. Oxygen isotope ratios of quartz were measured at the Scottish Universities Environmental Research Center (SUERC) in East Kilbride/GB. Oxygen of quartz aliquots ($\sim$ 1.5 mg) was converted to CO_2 by the laser fluorination method of Sharp (1990) with ClF_3 as fluorine source as described by Macaulay et al. (2000). A carbon dioxide laser is used as a heat source in order to bring quartz grains

[3]The mass fraction ω is defined as the mass of a constituent divided by the total mass of all constituents in the mixture. The sum of all the mass fractions within the mixture is equal to 1 (c.f. Bakker, 2011).

to incandescence whereupon it reacts with the atmosphere of fluorinating reagent and releases oxygen. The oxygen is purified cryogenically and by passage through an in-line Hg diffusion pump whereby it is transferred to the vicinity of a heated graphite rod. The resultant carbon dioxide is transferred to a capacitance manometer where the chemical yield is measured as a monitor of complete reaction. Replicate analyses of in-house silicate (garnet, quartz, agate) reference material give a long-term precision better than 0.2 ‰ (1s). The reference standard for $\delta^{18}O$ analyses is VSMOW.

$\delta^{34}S$ of sulphides

Sulphide samples were prepared by drilling sulphide crystals on polished blocks using a standard dentist drill . Sulphur extraction for $\delta^{34}S$ analyses on sulphides was carried at SUERC using the method of ROBINSON & KUSAKABE (1975). Sulphide samples were converted to SO_2 by reaction with excess Cu_2O at 1070 °C for 25 min. SO_2 was analysed using a standard vacuum line technique on a dual-inlet gas-source mass spectrometer. The reproducibility based on multiple measurements of an in-house chalcopyrite reference material is ± 0.2 ‰ (1s). The reference standard for $\delta^{34}S$ analyses is troilite from the Canyon Diablo meteorite (CDT).

2.3. Bulk fluid inclusion analysis

The chemical composition of solutes was determined using the technique modified after BOTTRELL et al. (1988) as described in PROCHASKA (1999). The rock samples were crushed to $1 - 2$ mm grain size and subsequently carbonate minerals were hand-picked under the binocular microscope. The carbonates were washed with distilled water. Hand-picked quartz samples were washed with hydrochloric acid to remove residual carbonate mineral grains. Between 0.5 and 1 g of cleaned grains were ground together with 5 ml double distilled water in an agate mortar. The solution was subsequently filtered. A DIONEX DX- 500 system at Montanuniversität Leoben was used for analyses of halogens and anions (F^-, Cl^-, Br^-, I^-, SO_4^{2-}). Cations (Li^+, Na^+, K^+, Mg^{2+}, Ca^{2+}) were analysed in the aliquots of the same solution using atomic absorption spectrometry.

2.4. Geochemical analysis of carbonate minerals

Carbonates and quartz are strongly interdigitated in many cases when they occur as gangue minerals in vein deposits. Following the instructions of HEINRICHS & HERRMANN (1990) the samples were treated with $ClCH_2COOH$ (4 g/100 ml) to digest the acid-solvable carbonates. The dissolution reaction of carbonates took about 24 h. The filtrate was subsequently filtered by a membrane filter. The solution was analysed for Ca, Mg, Fe, Mn, Sr, Li and Na using atomic absorption spectrometry.

3. Geological framework of investigated deposits

Genetical aspects and fluid evolution of ore deposits affiliated with an orogen can only be studied with proper knowledge of the geological evolution thereof. The following section briefly outlines the connections between geology, tectonics and ore genesis in the Alpine parts of Austria. Detailed geological characterizations and discussions are given in the descriptions of the individual deposits (Chapter 4). The investigated deposits are located in different geological units within the Eastern Alps which are described below.

Sub-Penninic units of the Tauernwindow

The rocks of the Sub-Penninic nappes are characterized by Variscan metamorphic, continental crust with overlying late Palaeozoic and Mesozoic metasediments. After the opening of the Penninic ocean during Middle Jurassic Sub-Penninic rocks formed the southern margin of the European continental plate. The Alpidic orogeny segregated the Sub-Penninic nappes from the lower crust and subcontinental mantle and pushed them to the north on the European plate (SCHMID et al. 2004). In the Eastern Alps rocks of the Sub-Penninic are exposed in the Tauernwindow. The lowest unit inside the Tauernwindow is the Venediger nappe system. It consists of pre-Variscan rock complexes, Variscan intrusive rocks (Zentralgneis) and post-Variscan rocks. Parts of the pre-Variscan rocks were metamorphosed and migmatised during Variscan orogeny. Variscan orogeny lead to the intrusion of intermediate and acid plutonites (Zentralgneis). The bulk of the Zentralgneise are of Upper Carboniferous age (FINGER et al., 1993). Post-Variscan metasediments comprise Upper-Carboniferous and Permotriassic metasediments (Hochstegen marble and Silbereck marble) directly deposited on Variscan basement (PESTAL et al. 2009). Alpine metamorphism reached greenschist to amphibolite facies during Oligocene (SCHUSTER et al. 2004) .

The Zentralgneis unit of the Sub-Penninic nappe is characterised by numerous, small scheelite deposits, vein type and disperse molybdenite occurrences (Alpeiner Scharte & Richterhütte). The world-class scheelite deposit of the Felbertal ore district is bound to the Palaeozoic rocks of the Habach group within the Venediger nappe (HÖLL, 1975; THALHAMMER et al., 1989; HÖLL & EICHHORN, 2001; WEBER 1997A, B). Au bearing veins within the Zentralgneis unit occur at the ore districts of Schellgaden-Oberdorf and Rauris-Gastein. The Erzwies-Siglitz deposit is part of the ore district Rauris-Gastein. Only of mineralogical interest are different U-Th enrichments in augengneisses, vein type fluorite and small beryllium and lazulithe occurrences (WEBER & PAAR, 1997).

Austroalpine thrust system

The Austroalpine thrust system is distinguished in a Lower and an Upper Austroalpine nappe system. The Lower Austroalpine is characterised by rocks that were deposited at the south-eastern shelf of the Penninic ocean during Jurassic and Cretaceous. The closure of the Penninic ocean resulted in structural and metamorphic evolution of these rocks. Now these units form the tectonic lowest parts of the Austroalpine directly superposing the Penninic nappes (SCHMID et al. 2004, FROITZHEIM et al. 2008).

The Upper Austroalpine is a nappe system that formed during subduction and extrusion processes during Eo-Alpine orogeny (Cretaceous). Since the beginning of early Cretaceous the subduction process and the closure of the Meliata ocean formed enormous sedimentary basins (NEUBAUER, 1994). During Late Cretaceous parts of the crystalline rocks were sheared off the mantle. Until Middle Late Cretaceous a complex nappe system evolved and was pushed to northwestern direction onto the Penninic nappes (SCHMID et al. 2004, FROITZHEIM et al. 2008). The Upper Austroalpine nappe system is characterised by crystalline rocks, Palaeozoic and Mesozoic (meta-)sediments (Figure 8). Metamorphism during Eo-Alpine orogeny mostly reached greenschist facies (Greywackezone nappe system) and is increasing to amphibolite and even eclogite facies (Schneebergzug and Kor- & Saualpe) (FRANK, 1987).

Greywackezone nappe system

The Greywackezone nappe system is is subdivided into 4 different nappes (NEUBAUER et al. 1994): Veitsch-nappe, Silbersberg-nappe, Kaintaleck-nappe and Noric-nappe (from footwall to hangingwall). The Greywackezone nappe system is superposed by the Tirolic-Noric nappe system[4]. The individual nappes show variable lithologies, metamorphic and structural overprint during Variscan orogeny against each other as well as against the Palaeozoic part of the Tirolic-Noric nappe system. During Permian the different nappes were exposed to the surface and were trangressively overlain by a sedimentary cover. During Alpine orogeny the Greywackezone nappe system was sheared off the basement and overthrusted in northwestern direction (FROITZHEIM et al. 2008).

The Greywackezone nappe system represents one of the main ore and commodity bearing units of the Austroalpine. Noteworthy are the following ore districts: Magnesite and Graphite districts Veitsch nappe, Fe-(Cu) district Noric-nappe, Magnesite district Hochfilzen and Dienten, polymetallic Cu-ore districts (fahlore district Schwaz-Brixlegg, Cu-district Röhrerbühel-Kitzbühel, Cu-Ni-Co-Hg-Ag district Leogang, Cu-district Jochberg, Cu-district Mitterberg-Mühlbach-Larzenbach (cf. WEBER, 1997A,B). These mineralisations are bound to the Noric nappe and the Western Greywackezone nappe system. The western parts of the Greywackezone nappe system are comparable with units of the Noric nappe in the Eastern parts of the Austroalpine. Within this work the Mitterberg-Buchberg deposit of the Cu-district Mitterberg-Mühlbach-Larzenbach and the Radmer deposit within the Fe-(Cu) district Noric-nappe are investigated.

Silvretta-Seckau nappe system

The Silvretta-Seckau nappe system form the lowest unit of the Upper Austroalpine. It is tectonically superposing the Lower Austroalpine and is overthrusted by the Greywackezone nappe system and the Koralpe-Wölz nappe system (SCHMID et al. 2004). Several kilometres thick crystalline rock and superposing, post-Variscan metasediments form the lithological inventory. In some areas as the Schladming crystalline the nappe fronts are overtiltet and inverted (SLAPANSKY & FRANK, 1987). Post-Variscan sedimentation is

[4]Note: The Noric nappe after NEUBAUER et al. (1994) is added to the Tirolic-Noric nappe system by FROITZHEIM et al. (2008).

beginning with Carboniferous/Permian. Pre-Variscan rocks suffered Variscan metamorphism up to amphibolite facies.

Eo-Alpidic orogeny lead to different retrograde metamorphic influence up to 300 °C in the western parts and amphibolite facies in the eastern parts (Seckauer Tauern and Gleinalpe).

The Silvretta-Seckau nappe system lacks extended ore deposits. The Chromite-asbestos-magnesite ore district Kraubath-Hochgrössen is famous for its former chromite mining and the type locality of cryptocrystalline, vein type magnesite. The Cu-Fe-Pb-Zn mineralisation of the Arlberg area and the polymetallic ore district Schladming are only of historical importance (cf. WEBER 1997A,B, THALHAMMER et al. 2010). The Kraubath magnesite deposit (Chromite-asbestos-magnesite ore district Kraubath-Hochgrössen) and the Co-Ni-Bi mineralisation of the Zinkwand within the polymetallic ore district Schladming are investigated.

Ötztal-Bundschuh nappe system

The Ötztal-Bundschuh nappe system consists of the Ötztal nappe (west of the Tauern Window) and the Bundschuh nappe (east of the Tauern Window) (SCHMID et al. 2004). Both nappes consist of thick crystalline basement units (Ötztal-Stubai complex, Bundschuh complex) and are superposed by transgressive, Permomesozoic metasediments (Brenner- and Stangalm Mesozoic) (TOLLMANN, 1977). FRISCH et al. (1998) are postulating a connection between the Ötztal and the Bundschuh nappe before the uplift of the Tauern Window due to only partly Alpidic penetrative deformation. Eo-alpidic metamorphism is decreasing from epidote-amphibolite facies in footwall rocks to greenschist facies in hangingwall rocks. Units of the Ötztal-Bundschuh nappe system have not been subducted during Alpine orogeny (after FROITZHEIM et al. 2008).

The Ötztal-Stubai complex is only bearing small Cu-Fe-Zn-Pb occurrences (polymetallic ore district Stubai-Ötztal). Mesozoic carbonates of the Brenner- and the Stangalm Mesozoic exhibit Fe mineralisations and occurrences of Pb-Zn and Cu mineralisations (cf. WEBER, 1997A,B). The Tösens deposit represents one of the most important Pb-Zn deposits within the polymetallic ore district Stubai-Ötztal and is worked in this thesis.

Figure 8: *Geological map of Austria with localities of the investigated deposits. Map modified after Geological map of Austria 1: 2 000 000 - Geological Survey of Austria, Vienna 1999*

4. Studied ore deposits

The following chapter provides information about the investigated deposits in different geological units (Figure 8). It focuses on the geological evolution of each individual deposit and provides information on the formation temperatures and genetical models. Different geothermometers are compared with each other. Especially the method of stable isotope geothermometry is tested for quality and applicability. Microthermometric data from literature and bulk fluid inclusion data give information about formation temperature and fluid chemistry. The overall examination of all available data results in a comprehensive discussion of the metallogenetical evolution of each individual deposit.

4.1. Mitterberg and Buchberg Cu

4.1.1. Geological setting

The former copper deposits of Mitterberg and Buchberg are located in the Upper Austroalpine Greywackezone nappe system. The „Mitterberger Hauptgang" copper vein is steeply dipping to the south and crosscutting the Late Palaeozoic stratigraphic sequence (*grey & pink series*). The vein pinches out in the post-Variscan trangressional metasediments (*pink series*) and is no longer detectable within the stratigraphic youngest schists of the *green series* (Figure 10). The main ore vein „Mitterberger Hauptgang" has a striking extension of ~11 km and reached a thickness between 0.2 and 4 m.

BERNHARD (1965) is subdividing a three-phase mineralisation: an old pyrite, Ni-Co-sulphide, arsenopyrite, quartz and ankerite bearing phase followed by a younger generation with chalcopyrite, pyrite, galena, sphalerite, tetraedrite-tennantite, quartz and ankerite. The last paragenesis is dominated by chalcopyrite, pyrite, arsenopyrite, galena, tetraedrite-tennantite, ankerite and quartz. The last paragenesis is dated with ca. 90 – 95 Ma using a pitchblende-gold mineralisation. Pitchblende is occurring in form of nodules and equals the formation age of the „Mitterberger Hauptgang" (PAAR, 1978; PETRASCHECK, 1975).

The Buchberg vein is bound to a SW dipping structure (254/30) and crosscutting south dipping phyllites. The Buchberg deposit is only bearing the last paragenetic succession after BERNHARD (1965). The thickness of the vein was about 1 to 4 m (BUTTMANN, 1913).

The Mitterberg and Buchberg deposits are grouped to the Mitterberg - Mühlbach - Larzenbach ore district (WEBER, 1997A). The Mitterberg mine is abandoned since 1976 and the adits are closed. Therefore samples from the former mine dumps south of the Arthurhaus are used for investigation. The Buchberg mine was closed 1959 and thereafter used by the Austrian Armed Forces. Samples are taken from the top of the emergency shaft.

4.1.2. Results

Paragenesis

The Paragenesis at the Mitterberg vein is dominated by pyrite followed by chalcopyrite. The ore minerals are bound to a ankerite - quartz gangue. Quartz grains do not

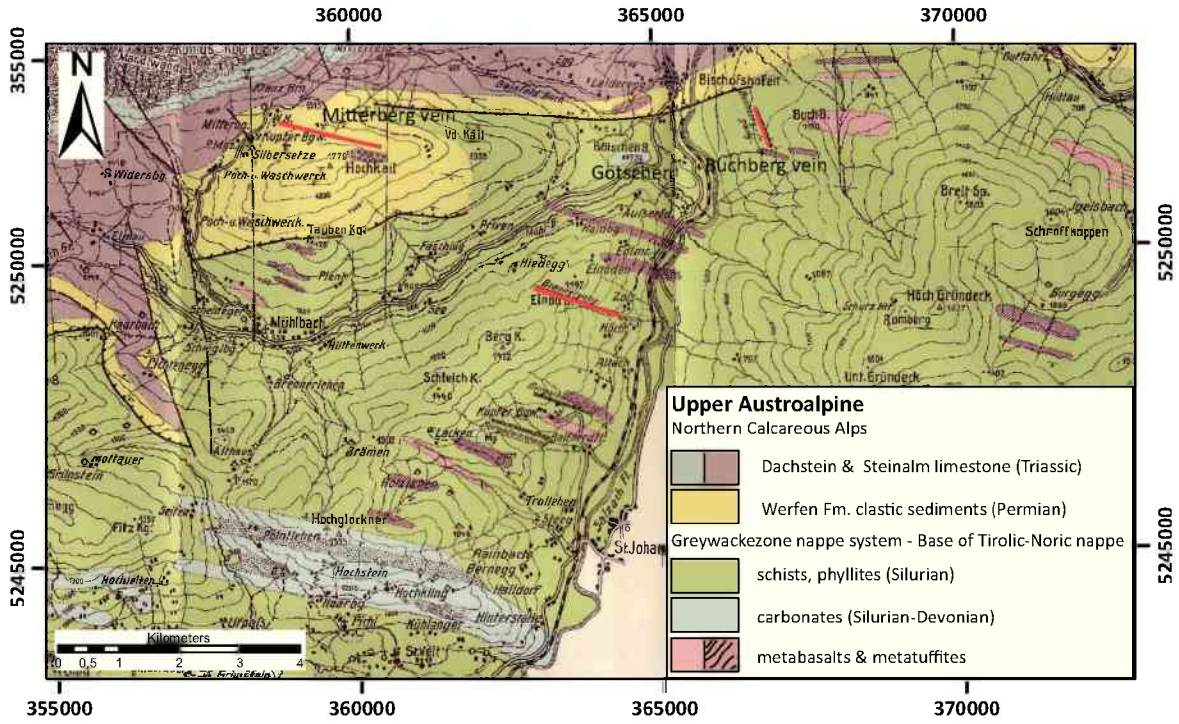

Figure 9: *Geological overview of the Mitterberg and Buchberg deposits simplified after* BUTTMANN (1913). *The veins are marked in red The orientation of the Buchberg vein (254/30) is angular against the Mitterberger Hauptgang. Note: The Brandergang vein is not worked in this thesis.*

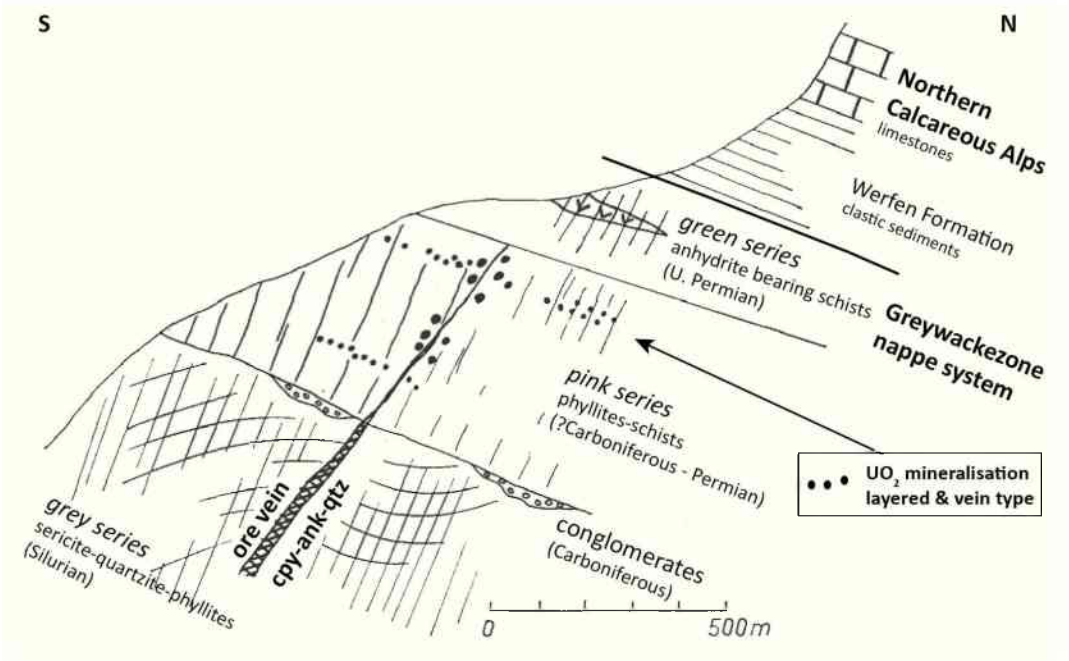

Figure 10: *Scheme of the Mitterberg ore vein presenting the discordant character of the vein. Sketch modified after* PETRASCHECK (1975). *The formation of the pitchblende (UO_2) nodules is dated with* $\pm 90 - 95$ *Ma* (PAAR, 1978).

show undulatory extinction and are therefore assigned to the last, Alpidic paragenesis. BERNHARD (1965) is describing microcrystalline and undulatorious extincting quartz in the older paragenetic sequences. The Paragenesis at the Buchberg vein comprises pyrite, chalcopyrite, ankerite and quartz. The samples of the Buchberg vein show pinolitic ankerite and void filling quartz. The void filling quartz is not showing undulatory extinctions and therefore the mineralisation is also correlating with the last paragenesis of Mitterberg (Figures 11 & 12).

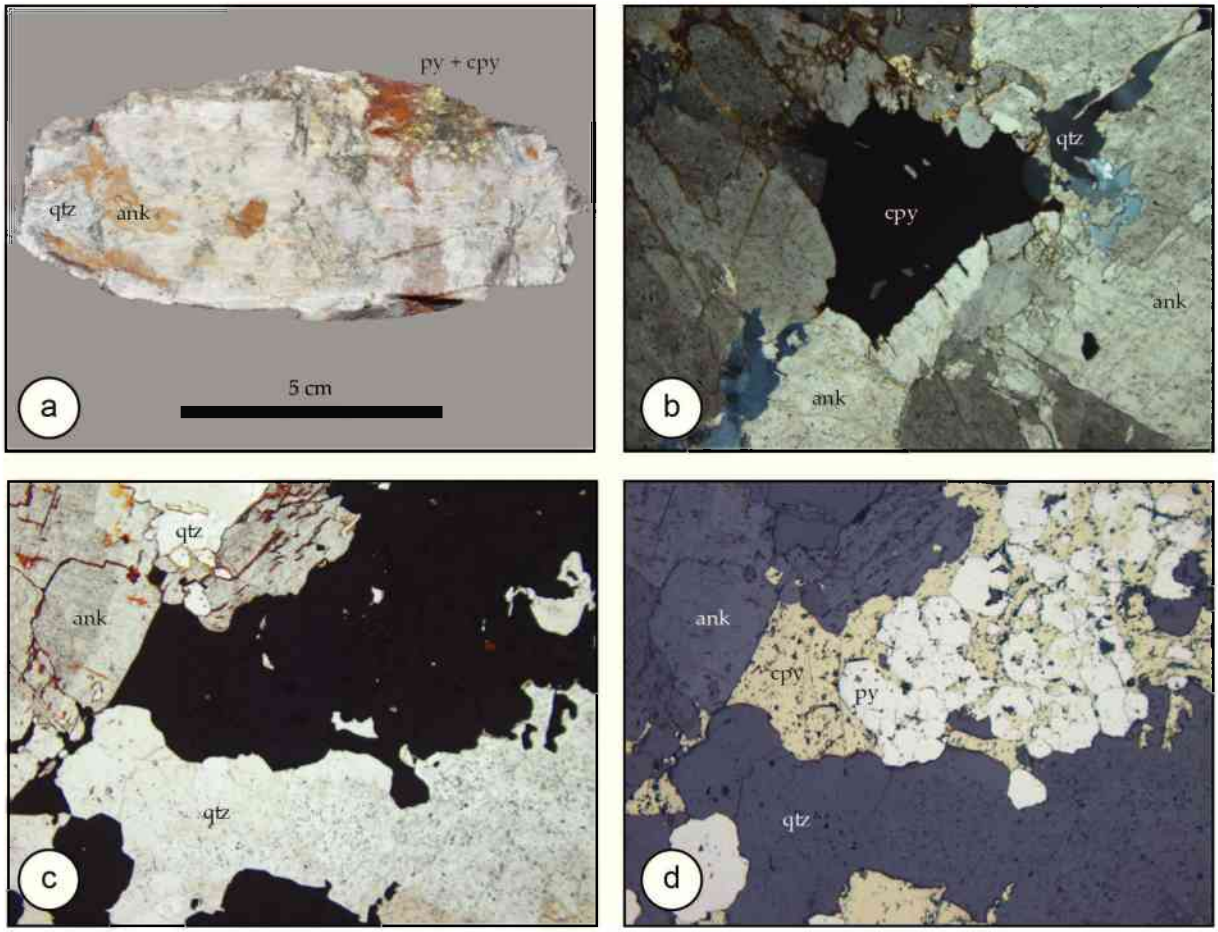

Figure 11: *(a) Hand specimen of the Mitterberg deposit, (b) Chalcopyrite with ankerite and minor quartz gangue (polished thin section, TL, XN), (c) Cleavage parallel corroded ankerite and quartz (polished thin section, TL), (d) Pyrite and chalcopyrite with ankerite and quartz gangue (polished thin section, RL, air).*

Mineral Chemistry

Pyrites from Mitterberg show ideal stoichiometric composition. The chemical composition of chalcopyrite is nearly stoichiometric $Cu_{1.00-1.04}$ $Fe_{0.99-1.02}$ S_2. Sulfarsenides from the Mitterberg deposit form a solid solution series between gersdorffite and arsenopyrite. The chemical composition of these sulfarsenides is varying:

$(Fe_{0.28-0.37}, Ni_{0.62-0.65}, Co_{0.01-0.09})_{\sum 1.00}$ $As_{0.74-0.76}$ $S_{1.24-1.26}$. The sulfarsenides show high S for As substitution. The As/S ratios are between 0.59 and 0.61 (Figure 13b).

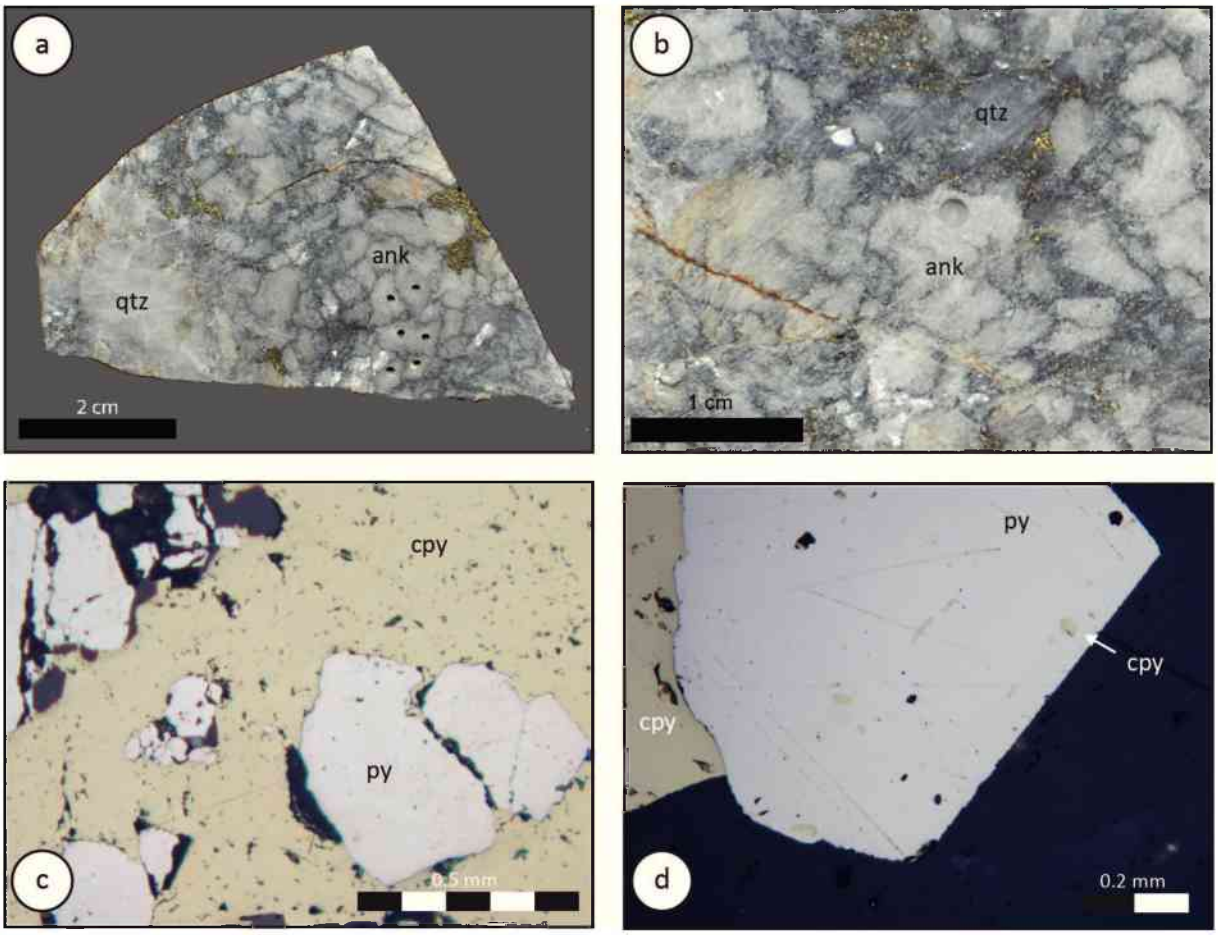

Figure 12: *Paragenesis at the Buchberg vein: (a) Hand specimen of chalcopyrite and pyrite filling voids in ankerite-quartz gangue , (b) Intergrowth between ankerite and quartz associated with sulphides, (c) Pyrites associated with chalcopyrite (polished thin section, RL, air), (d) Hypidiomorph pyrite with chalcopyrite exsolutions (polished thin section, RL, air).*

Tetrahedrite-tennantite solid solution series show compositions of:
$(Cu_{9.87-10.03},Ag_{0.01},Zn_{0.74-0.97},Fe_{0.98-1.24},Hg_{0.05-0.08})_{\sum 11.86-12.00}$
$(As_{0.41-2.17},Sb_{1.83-3.74})_{\sum 4.00-4.15}S_{12.82-13.09}$.

Bulk fluid inclusion composition

The composition of bulk fluid inclusion analyses is presented in Appendix B. The values are believed to represent the composition of the ore forming fluids with minor contamination by secondary fluid inclusions. This assumption is applicable due to the fact that Pohl & Belocky (1999) are reporting that high saline primary fluid inclusions are followed by lower saline secondary fluid inclusions in quartz from the Mitterberg deposit. This is confirmed by the fact that the total dissolved salt contents are getting gradually lower in the paragenetic sequence from ankerite to quartz (Figure 14).

The data for Mitterberg samples show considerable variability in both cation and anion ratios. The I/Cl ratios are between $19 \times 10^{-6}$and 139×10^{-6} for ankerite and between 17×10^{-6} and 34×10^{-6} for quartz. These values are higher than modern seawater (0.86×10^{-6}). The Br/Cl mass ratios for ankerites and quartz of the Mitterberg veins are ranging from 1.8×10^{-3} to 4.9×10^{-3} (slightly elevated against the seawater value of 1.54×10^{-3}). The K/Na ratios for quartz and ankerite are scattering between 0.034 and 0.086. The Li/Na ratios range from 0.0001 to 0.0913; the Ca/Na ratios are between 0.11 and 1.27. These three parameter are significantly higher than modern seawater (McCaffrey et al., 1987). The analyses of ankerite samples exhibit imperfect charge balance (i.e. Q^+/Q^- =1), because some dissolved species (e.g. bicarbonate, sulphide) have not been analysed. In contrast the charge balance of quartz samples range from 0.9 to 1.23.

The data for the Buchberg vein is showing similar variability. The I/Cl ratios are relatively homogeneous between $42 \times 10^{-6}$and 53×10^{-6} for ankerite but more irregular for for quartz samples ($4 \times 10^{-6}$to 45×10^{-6}). Br/Cl mass ratios for ankerites and quartz from the Buchberg vein are ranging between 2.2 and 5.7. The K/Na ratios are ranging from 0.028 to 0.047; Ca/Na ratios are between 0.05 and 1.16. The Li/Na values are from 0.0004 to 0.0349. These values are similar to the Mitterberg samples.

Stable Isotopes

Carbon isotope values of the Mitterberg mine dump samples range from -5.59 to -3.21 ‰ and oxygen values are from 16.08 to 18.65 ‰. The value of ankerite at Götschen (MB 09_012) is representing the eastward continuation of the Mitterberger Hauptgang (Figure 9). The low $\delta^{18}O$ value of 16.36 ‰, the $\delta^{13}C$ value of -3.36 ‰ in combination with the absence of quartz are representing slightly higher precipitation temperatures than the other samples. Stable isotope values of ankerites of the Buchberg vein show relatively homogeneous values for oxygen ranging from 15.45 to 15.72 ‰ and -5.70 to -5.16 ‰ for carbon respectively (Table C).

$\delta^{18}O$ of quartz samples for Mitterberg shows values ranging from 14.3 to 17.9 ‰. Buchberg quartz samples are ranging between 16.62 and 18.51 ‰ (Table C).

Formation temperatures calculated using the equations of Sharp & Kirschner (1994) and Zheng (1999) result in temperatures of 343 ±19 °C to 614 ±33 °C for Mitterberg

vein and 207 ±14 °C to 550 ±29 °C for Buchberg.

$\delta^{34}S$ ratios are showing values ranging from 3.9 to 5.7 ‰ for chalcopyrite and 3.7 to 9.1 for pyrite of the Buchberg vein. The Mitterberg chalcopyrite samples are relatively homogeneous with values around 2.5 ‰. The values for δ^{34}S are slightly rising from chalcopyrite to pyrite (Figure 15).

4.1.3. Discussion

The Mitterberg and the Buchberg veins show a similar paragenetic sequence. For both depots a multi-phase mineralisation is assumed. In this study samples of the last mineralisation phase are investigated.

Texturally in Mitterberg and Buchberg samples ankerite and quartz are in equilibrium (cf. Figures 11c & d and 12a & b). Therefore the application of the computed quartz-ankerite fractionation equation (with data of SHARP & KIRSCHNER 1994 and ZHENG 1999) is possible. The calculation leads to formation temperatures between 343 and 449 °C (maximum 658 °C) for the Mitterberg vein and 207 to 447 (maximum 550 °C) for Buchberg. The maximum values are due to low $\Delta_{qurtz-ankerite}$ values (0.31 and 0.19 ‰) and therefore not to be considered. These temperatures are generally elevated against crush-leach temperatures using the equ. of VERMA & SANTOYO (1997). Crush-leach temperatures of ankerites (Mitterberg) are in the range of 387 to 436 °C and ankerites of Buchberg lie between 228 and 280 °C. Quartz samples show irrealistic low temperature values. Due to very low salinities (Appendix B) cation exchange geothermometers are not applicable. POHL & BELOCKY (1994) report trapping temperatures of over 240 °C in fluid inclusions of gangue quartz and pressures about 0.2 GPa which correspond with formation depths of ~7 km. Metamorphic conditions during Eo-Alpine metamorphism reached sub-greenschist to greenschist facies (KRALIK et al., 1987)(KRALIK ET AL., 1987).

The mineralising fluid shows enriched values for δ^{18}O between 16 and 17 ‰ for Mitterberg and 15.5 to 16 ‰ for Buchberg samples. δ^{13}C values of the fluid show depleted values between -6 and -4 ‰ (Figure 16). The fractionation curves of the calcite-H_2O systems (ZHENG 1999; FRIEDMAN & O'NEIL 1977) are shown for comparative purpose against the fractionation curve of ankerite-H_2O (ZHENG 1999). Fluid evolution after POHL & BELOCKY (1999) is relativity simple starting with high salinities which diminish progressively with time. This is also represented by the Br/Cl and Ca/Na ratios which are lowering with the precipitation of ankerite and subsequently quartz. The decreasing salinities of fluid inclusion with progressing precipitation of gangue minerals suggest that fluid inclusion chemistry represents the ore forming solutions.

Sulphur isotopic composition show slightly enriched values for chalcopyrite and pyrite against CDT. Comparing these values with the seawater sulphate isotopic composition during Cenomanium shows that the ore bearing solutions are influenced by formation waters. This assumption is reinforced by the fact that primary fluid inclusions show high saline (elevated values of Na and Cl) compositions. Migration distance of the metal bearing fluids is therefore limited. Sulfarsenide compositions of the series arsenopyrite-gersdorffite indicate formation temperatures of 450 - 500 °C.

4.1.4. Interpretation

The Mitterberg and Buchberg veins formed during Eo-alpidic metamorphism along E-W striking extensional structures. The youngest ore generation is about 90 Ma old. Migrating brines leached metals of metasedimentary Palaeozoic rocks and partly remobilised older ore generations as described by BERNHARD (1965). The ore forming solutions show enrichment in $\delta^{18}O$ (15 to 17 ‰) and are depleted in $\delta^{13}C$ (-6 to -4 ‰). These values indicate metamorphogenic waters influenced by a deep carbon source (HOEFS, 2009).

Ankerite precipitated mostly due to degassing of CO_2 in depths of about 7 km. The metal bearing solutions precipitated sulphides and sulfarsenides at temperatures well above 400 °C. The sulphur isotopic composition shows influence of sulphate bearing formation waters. Subsequently quartz and ankerite evolved at temperatures of 340 to 450 °C for Mitterberg and significantly lower temperatures of 230 to 280 °C for Buchberg. The lower temperatures of the Buchberg vein substantiate the fact that this vein is representing a subordinate oblique shear zone with more distance to the main fluid pathways. Also the fact that the ore quantity at Buchberg is lower than at Mitterberg matches this picture.

The application of the quartz-siderite geothermometer gives temperatures from 210 to 550°C. Quartz and ankerite are in textural and isotopic equilibrium. Therefore the temperatures gained from isotope geothermometry are realistic and in good agreement with temperatures gained from bulk fluid inclusions thermometry and microthermometric analyses (POHL & BELOCKY, 1999).

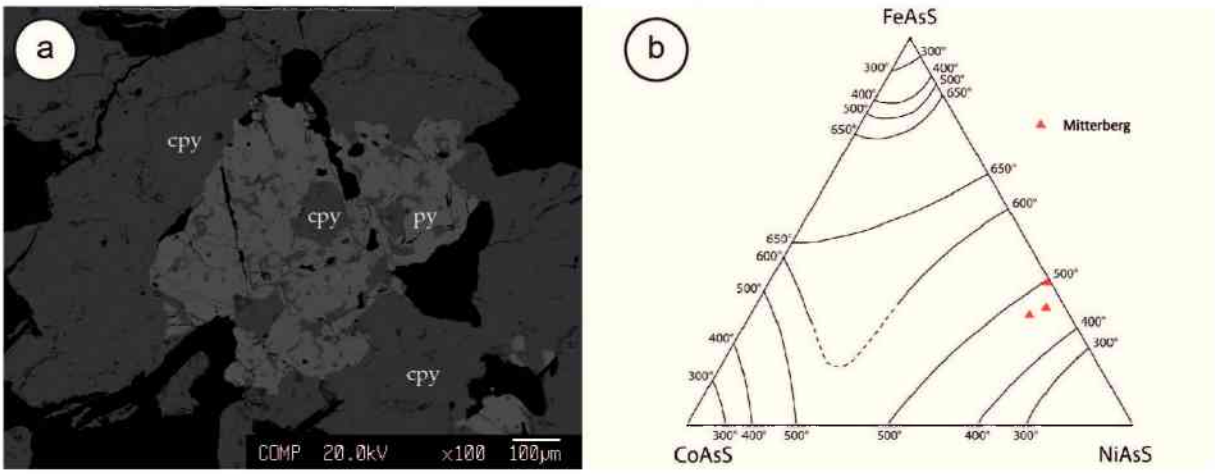

Figure 13: *(a) BSE images of a chalcopyrite-pyrite interdigitation with minor galena and ankerite gangue, (b) Compositional plot of Mitterberg sulfarsenides in the system FeAsS-CoAsS-NiAsS. Solvus lines at different temperatures are taken from* KLEMM (1965).

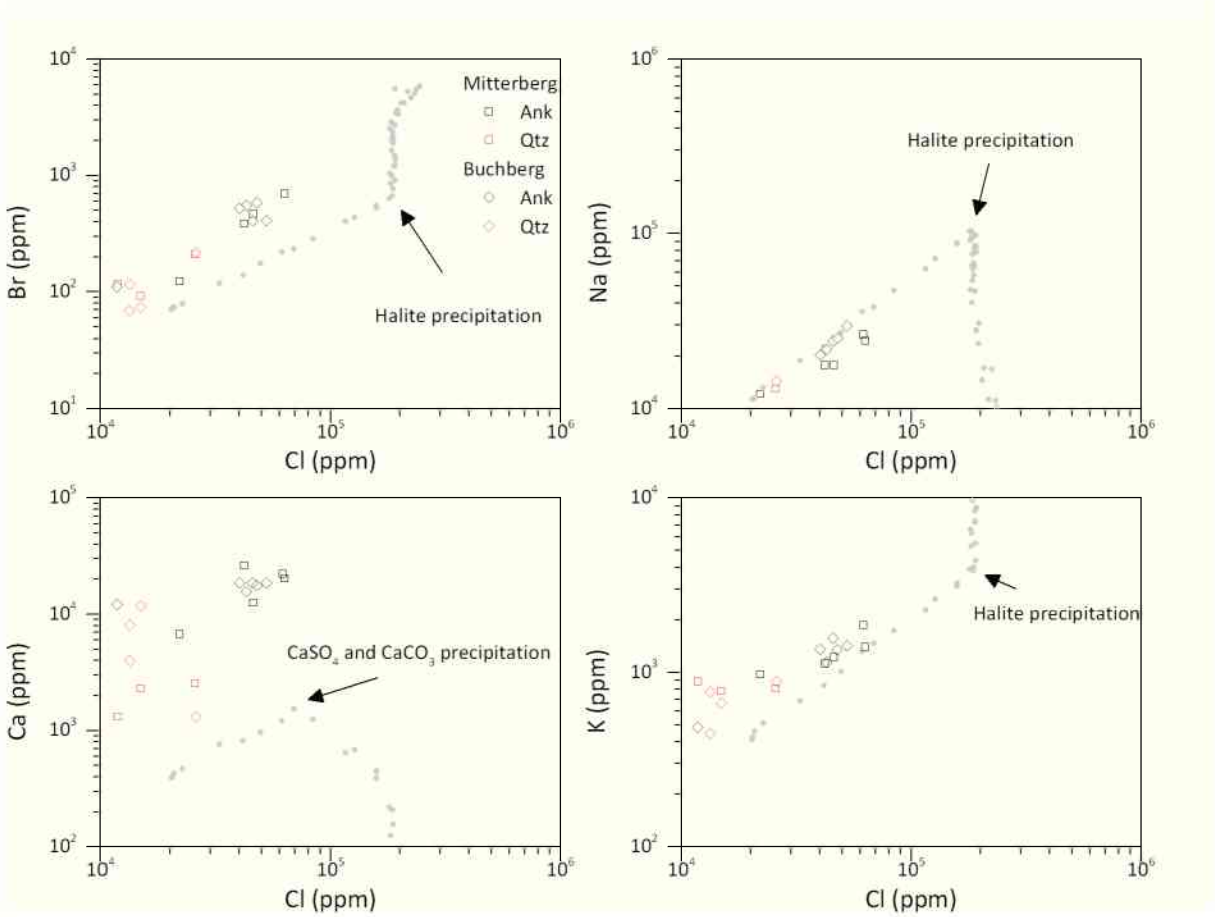

Figure 14: *Log-Log plots of major cations Na, Ca, K and Br versus Cl. The grey points are the seawater evaporation trajectory (data taken from* MCCAFFREY *et al. 1987)*

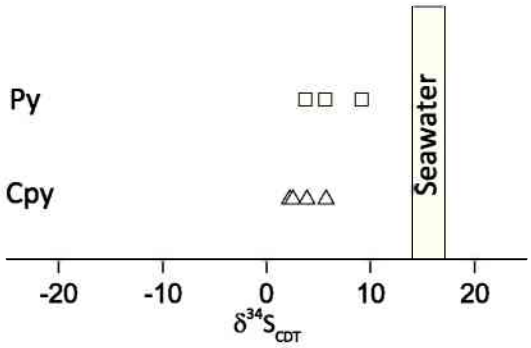

Figure 15: *Sulphur isotope distribution of sulphides of the Mitterberg and Buchberg deposits. Comparative seawater range for Cenomanium is taken from* Kampschulte & Strauss (2004).

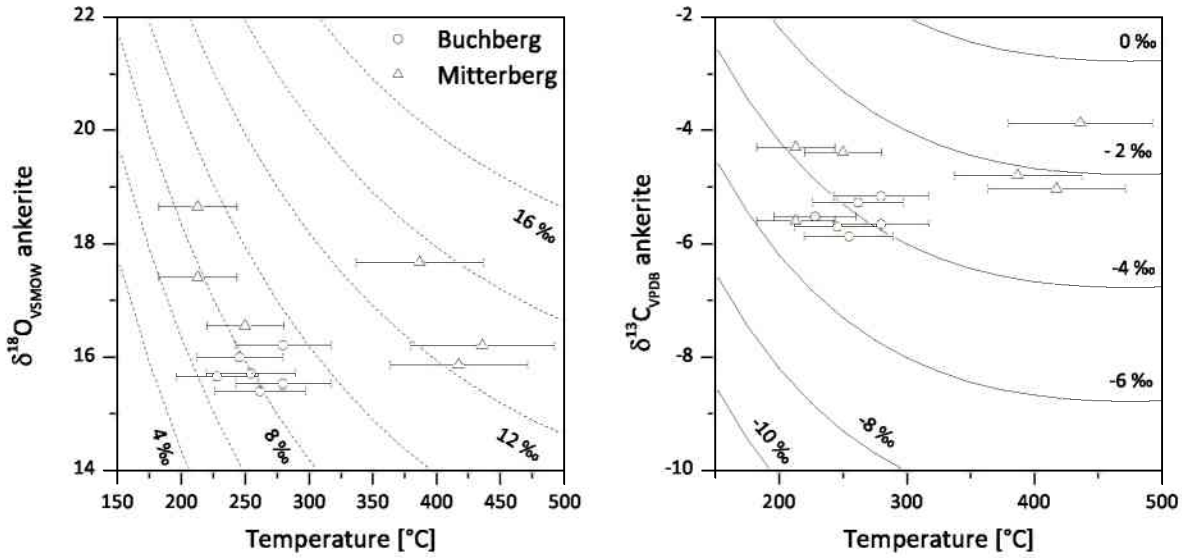

Figure 16: *Oxygen and carbon isotope compositions of ankerite forming fluids for the Buchberg and the Mitterberg deposits calculated from the Na-Li geothermometer* Verma & Santoyo (1997) *and equilibrium oxygen isotope fractionation in the ankerite-H_2O system (dashed curves:* Zheng (1999)*) and carbon isotope fractionation in the calcite-CO_2 system (solid curves:* Ohmoto & Rye (1979)*).*

4.2. Radmer Cu

4.2.1. Geological setting

The copper district Hinterradmer-Johnsbach is situated in the Upper Austroalpine Noric nappe of the Eastern Greywackezone (Figure 8). The mineralisation is bound to the uppermost parts of the Noric nappe (Weber, 1997a). The Noric nappe is tectonically superposed by the Upper Austroalpine Northern Calcareous Alps (Figure 17). The Noric Nappe in the Radmer area is dominated graphitic, phyllitic schists with interdigitations of crystalline, banked carbonates of Devonian(?) age. Redlich & Sellner (1923) describe 4 different vein systems in the Radmer area. In the following section the vein system of the Haselbachgraben and the Paradeis adit respectively are described in detail. The thickness of the mineralisation of the Paradeis adit has reached up to 3.5 m (Redlich & Sellner, 1923). The ore vein of the Paradeis adit is situated approximately 340 m below the base of the Northern Calcareous Alps within the Noric nappe. The direct surroundings of the Paradeis adit are formed by different phyllitic schists (sericite schists, graphite schists, calcareous schists) and marbles. Ankerite and quartz form the gangue minerals of the deposit (Ofner 2002; Sperl et al. 2010).

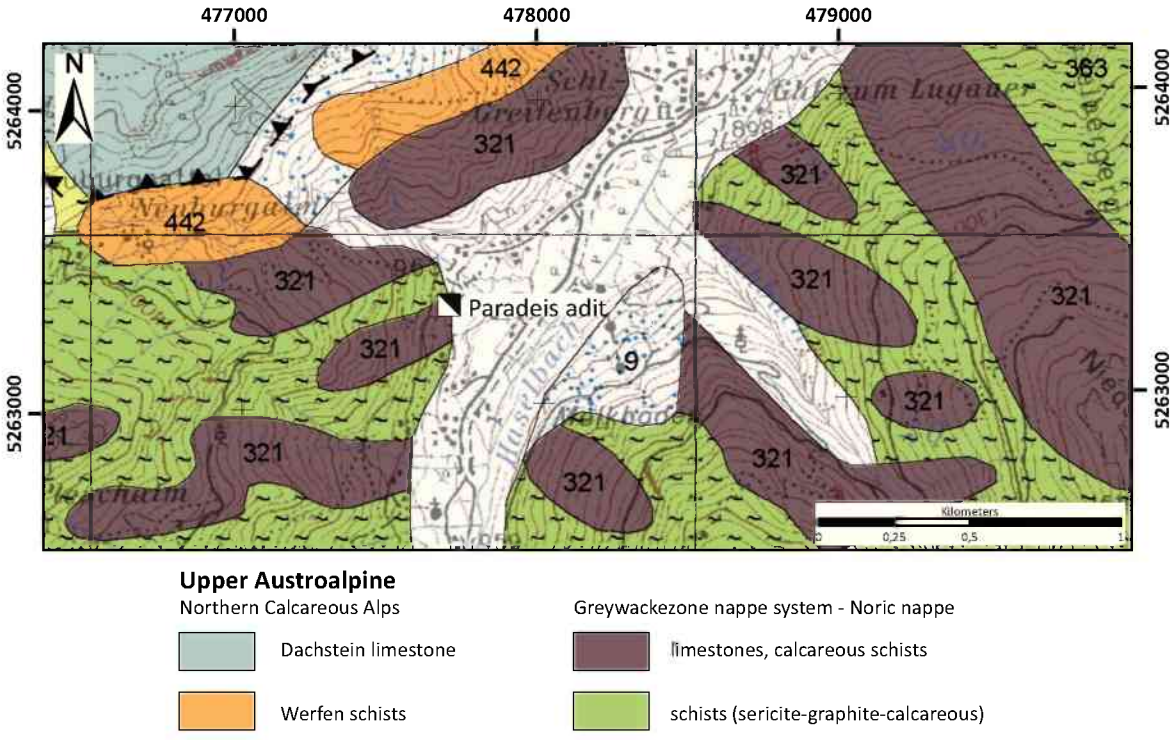

Figure 17: *Geological map of the Radmer area after (Map section modified after Geofast-vorläufige Geologische Karte 1:50.000 - 100 Hieflau: Stand Okt. 2001)*

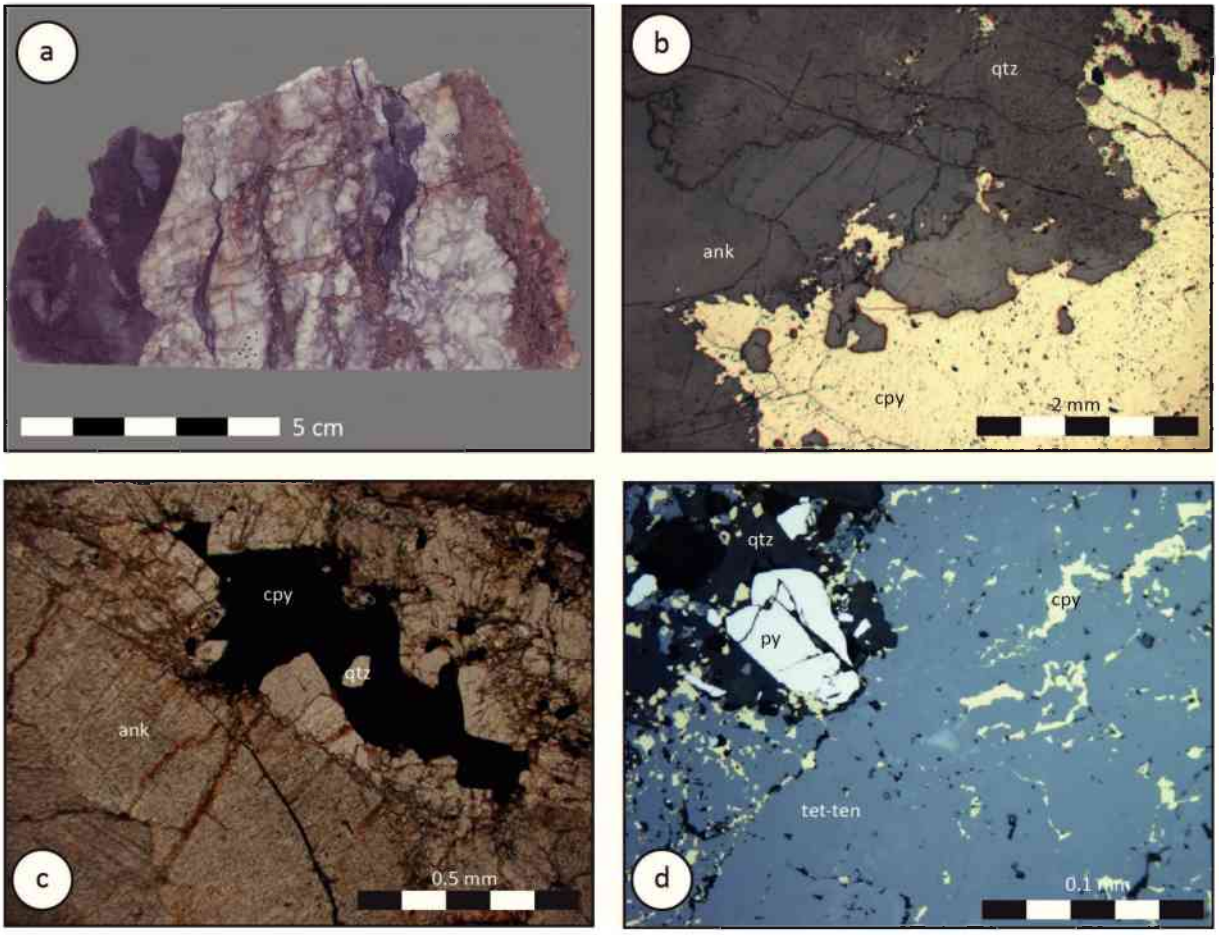

Figure 18: *(a) Chalcopyrite-pyrite ore specimen of the Paradeis adit with ankerite-quartz gangue within graphitic schist, (b) Chalcopyrite interdigitated with quartz-ankerite (polished thin section, RL, air) ,(c) Chalcopyrite filled voids within ankerite gangue with minor quartz (thin section, TL), (d) Pyrite - fahlore (tet-ten) - chalcopyrite succession with quartz gangue (polished thin section, RL, air)*

4.2.2. Results

Paragenesis

The mineral succession in the Paradeis adit consists of chalcopyrite, fahlore, gersdorffite, arsenopyrite and pyrite. Subsidiary galena and sphalerite occurs. Ofner (2002) subdivided ore formation into 3 generations : sulphides with ankerite-quartz gangue (generation 1), remobilized primary sulphide bearing veinlets (generation 2) and remobilized small scale sulphide veins ($<$ 1 mm) inside primary ankerites (generation 3).

Samples were taken from the mine backfill in the Paradeis adit and are focused on specimens with macroscopic ankerite-quartz interdigitations. The following descriptions and interpretations are applied to specimens from the first ore generation.

Bulk fluid inclusion composition

The data for Radmer ankerite and quartz samples (Appendix B) show considerable variability in both cation and anion ratios. The I/Cl ratios are relatively consistent between

20×10^{-6} and 87×10^{-6} for ankerite. Fluid inclusions in quartz show similar values ranging from 9×10^{-6} and 89×10^{-6}. The Br/Cl mass ratios for ankerites are very low (up to 8.3×10^{-3}). Br/Cl ratios of quartz are between 1.1×10^{-3} and 4.8×10^{-3}. The K/Na ratios for ankerite are scattering between 0.049 and 0.135. K/Na ratios for fluid inclusions in quartz are higher by one power of ten and ranging between 0.305 and 0.816. The Li/Na ratios for ankerite range from 0.0157 to 0.0611 and Li/Na ratios for quartz are significantly lower between 0.0007 and 0.091 ; the Ca/Na ratios are scatter between 0.10 and 2.31. The analyses of ankerite samples exhibit elevated charge balances from 2.5 to 4.01 (one outliers with 8.53). The quartz samples have lower charge balance values from 1.00 to 2.91 (outlier with 6.15).

The calculation of ankerite precipitation temperatures using the Na-Li geothermometer of VERMA & SANTOYO (1997) gives temperatures ranging from 234±32 °C to 343±45 °C. Bulk fluid inclusion temperatures for gangue quartz are significantly lower and give temperatures around 190 °C using the geothermometer of KHARAKA & MARINER (1989).

Mineral chemistry

Chalcopyrite samples show stoichiometric compositions of $Cu_{0.97-1.02}$ $Fe_{0.95-1.01}$ $S_{2.00-2.03}$. Fahlore (ore generation 1) from the Radmer deposit exhibit two different generations: an older disrupted tennantite generation that is cemented by a younger tetrahedrite generation (Figure 19). The tennantite composition ($Cu_{9.85-10.26}$, $Zn_{0.54-1.64}$, $Fe_{0.53-1.25}$, $Hg_{0.08-0.22})_{\sum 11.84-12.33}$ ($As_{1.21-2.38}$, $Sb_{1.42-2.66})_{\sum 3.71-3.94}$ $S_{12.84-13.25}$ as well as the tetrahedrite composition
($Cu_{9.84-10.28}$, $Zn_{0.56-2.02}$, $Fe_{0.18-1.22}$, $Hg_{0.05-0.36})_{\sum 11.92-12.35}$ ($As_{0.12-2.23}$, $Sb_{1.51-3.84})_{\sum 3.74-4.01}$ $S_{12.74-13.20}$ show significant Zn^{2+} values up to 2.02 apfu. OFNER (2002) is reporting compositional data from gersdorffites (Figure 20) that can be classified to a clean gersdorffite and gersdorffite with remarkable amounts of Fe (up to 0.17 ω). Pyrites show zonation with substitution of S with As at the rims[5].

Stable Isotopes

Ankerite samples are showing carbonate ratios ranging from -4.46 to -3.59 ‰ and oxygen values from 16.97 to 18.72 ‰. Oxygen isotope values of quartz are slightly higher with values ranging from 19.6 to 21.6 ‰. Formation temperatures calculated using the equations of SHARP & KIRSCHNER (1994) and ZHENG (1999) result in temperatures ranging from 139 ±12 to 333 ±18 °C for quartz-ankerite mineral pairs.

Chalcopyrite samples show positive $\delta^{34}S$ values from 2.1 to 4.8 ‰. SPÖTL & PAK (1996) determined $\delta^{34}S$ values of + 11.1 for gypsum in hangingwall Permian evaporites.

4.2.3. Discussion

Genetical aspects of the Radmer deposit are intensely discussed by OFNER (2002). The Radmer deposit is formed by three different hydrothermal mineralisation types and bound to pinolitic ankerite veins in mostly graphite phyllites. Host rock fragments and graphite

[5]Ongoing research at sulphide chemistry is done together with F. MITTERMAYR (TU Graz).

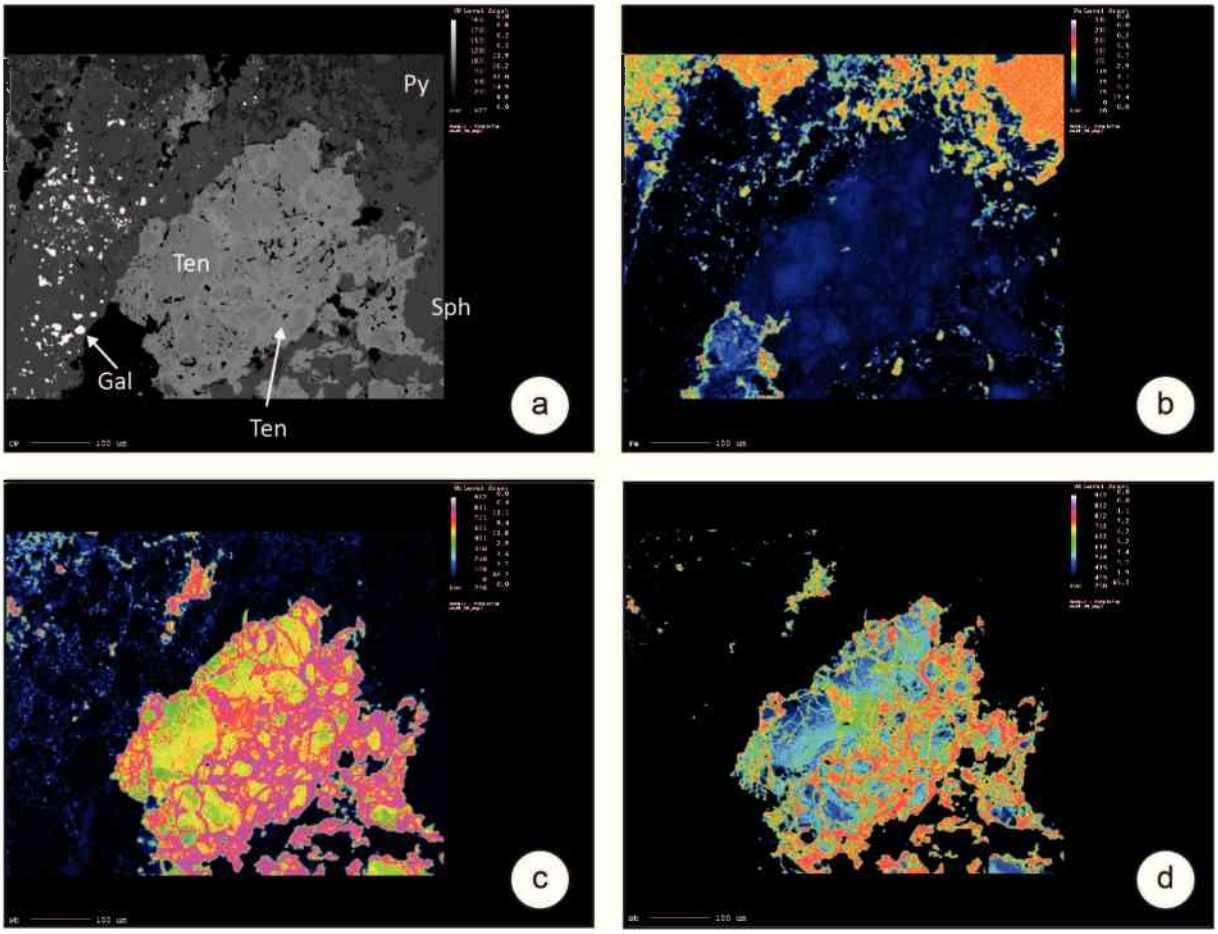

Figure 19: *Element mapping (EMP) of tetraedrite-tennantite fahlore containing two different generations: (a) BSE image, (b) Fe-content, (c) Sb-content, (d) As-content. The fahlore mineralisation is representing the first ore generation sensu* Ofner (2002).

plates embedded within the ankerite veins argue for a post-diagenetic formation of the ankerite-quartz veins.

The application of the quartz-calcite fractionation equation of SHARP & KIRSCHNER (1994) and ZHENG (1999) leads to formation temperatures between 139 and 333 °C. These temperature coincide or fall into the calculated uncertainties of crush-leach temperatures using the equation of VERMA & SANTOYO (1997). Crush-leach temperatures of ankerites are in the range of 230 to 360 °C. Quartz samples show lower values of 140 to 200 °C. OFNER (2002) is reporting microthermometric formation temperatures for ankerite between 170 and 210 °C and 170 to 270 °C for quartz respectively. The temperature estimations of both methods (oxygen isotope geothermometry, crush-leach geothermometry and microthermometry) show comparable results.

The mineralising fluid shows enriched values for δ^{18}O between 9 and 13 ‰. δ^{13}C values of the fluid show values between -4 and -2‰ (Figure 21). Carbon values seem to derive from marine carbonates. Leaching hangingwall gypsum under reducing conditions leads to a δ^{34}S depleted, H_2S - dominated fluid. At 350 °C[6] such a fluid would have a δ^{34}S of -8.55 ‰ (calculated after OHMOTO & RYE 1979). Precipitating chalcopyrite from such a fluid would result in enriched δ^{34}S values of about 9 ‰. Temperatures of more than 350 °C would lower the δ^{34}S of the evolving chalcopyrite. Therefore formation temperatures of chalcopyrite result in temperatures of more than 350 °C.

4.2.4. Interpretation

The copper mineralisation at the Paradeis adit in the Radmer area consists of three hydrothermal ore generations within graphitic schists. Gangue minerals are formed by pinolitic ankerite and quartz. Host rock fragments and graphite flakes within the vein are arguments for a post-metamorphic emplacement of the ore veins. The third ore generation sensu OFNER (2002) reinforces this assumption because it does not show undulatory extinction within quartz grains. Following the paragenetic sequence sulphides, sulfarsenides and sulfosalts precipitated from a metal bearing solution at temperatures of more than 300 °C. Ankerite gangue was formed simultaneously at lowering temperatures down to 250 °C and quartz filled up remaining gaps at relatively low temperatures of about 200 °C. The mineralising fluid was migrating at elevated temperature of more than 350 °C through hangingwall Permian evaporites and leaching gypsum. This acid, H_2S rich fluid defined the transport medium for the metals. δ^{18}O values between 9 and 13 ‰ plot within the metamorphogenic field. Carbon is showing values between -4 and -2 ‰ and is derived from marine carbonates.

[6] 350 °C represents the maximum of the usable temperature range for the fractionation equation for $CaSO_4.2H_2O \leftrightharpoons H_2S$ of OHMOTO & RYE (1979).

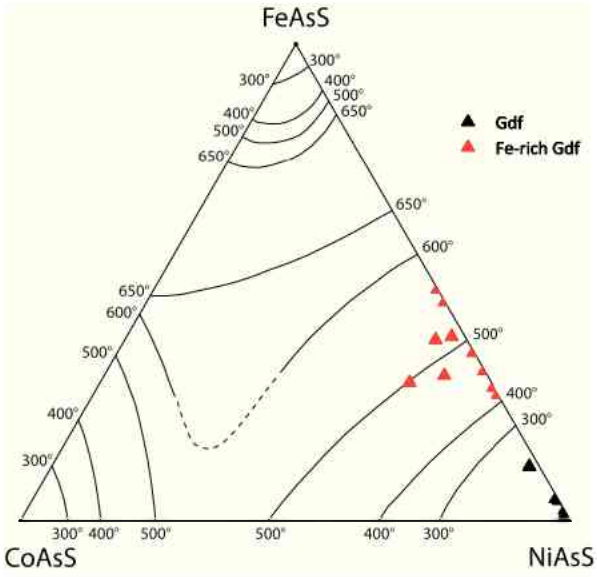

Figure 20: *(a) Compositional plot of gersdorffites from the Radmer deposit: Clean Gdf with formation temperatures well below 300°C and Fe-rich Gdf with formation temperatures ranging from 550 to 400°C. Solvus lines at different temperatures are taken from Klemm (1965). Data includes measurements of* Ofner (2002) .

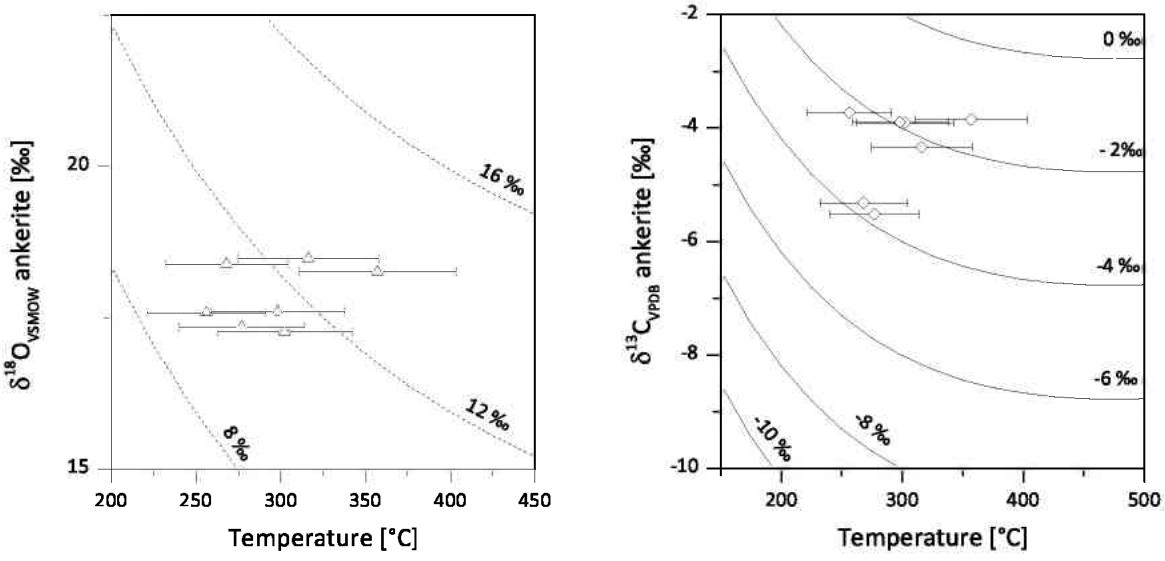

Figure 21: *Oxygen and carbon isotope compositions of ankerite-forming fluids of the Radmer deposit calculated from the Na-Li geothermometer* Verma & Santoyo (1997) *and equilibrium oxygen isotope fractionation in the ankerite-H_2O system (dashed curves:* Zheng, 1999*) and carbon isotope fractionation in the calcite-CO_2 system (solid curves:* Ohmoto & Rye, 1979*).*

4.3. Zinkwand Ni-Co-Bi

4.3.1. Geological setting

The medieval Obertal-Zinkwand-Vöttern mines are situated in the Schladming crystalline of the Weißpriach nappe within the Silvretta-Seckau nappe system (MATURA, 1980; LIU et al., 2001) (Figure 8). The Silvretta-Seckau nappe system represents the lowest unit of the Upper Austroalpine. Nappes of the Greywackezone and rocks of the Koralpe-Wölz nappe system superpose it in the north and south respectively (SCHMID et al. 2004, LIU et al. 2001).

The Schladming crystalline is dominated by polymetamorphic ortho- and paragneisses (MATURA, 1980, 1987). The gneisses were affected by Variscan amphibolite grade metamorphism (HEJL & SLAPANSKY, 1984). During the Alpidic event the Schladming crystalline was influenced by a retrograde greenschist facies metamorphic overprint (HEJL et al. 1987). The continuous cooling of the Schladming Crystalline Complex started from above 350 °C in the Cretaceous and is related to Cretaceous extensions (HEJL, 1997; THÖNI, 1999), similar to comparable units in the Eastern Alps (NEUBAUER et al. 1995). Alpidic tectonics resulted in a complete inversion of the Schladming crystalline and the formation of thick phyllonite zones (MATURA, 1987; SLAPANSKY & FRANK, 1987).

Ore deposits within the Schladming crystalline are often bound to quartzite-schists, quartzite-phyllites, gneiss-phyllites and phyllonites as well as foliation-parallel Fe-sulphide rich phyllitic beds. After FRIEDRICH (1975) and WEBER (1997A) the polymetallic Schladming ore district can be subdivided into five types due to different genetical aspects and formation ages:

- two-dimensional Ag-rich Pb-Zn mineralisations (Eschach, Roßblei, Bromriese, Eiskar)
- two-dimensional Ag-bearing chalcopyrite-fahlore mineralisation within sericite - quartzites (Krombach)
- lenses of massive pyrite and chalcopyrite ores
- Cu-(Co-Ni) mineralisation bound to diaphtoritic tectonic trajectories (Obere Giglerbaue)
- vein type Ni-Co-Bi-Ag mineralisations (Vöttern, Zinkwand)

Primary, polymetallic metal supply during Early Palaeozoic seems to be due to bimodal, calcalcaline volcanism in the range of a magmatic arc or rift zone (SCHEDL, 1981). Leaching and mobilisation processes during the Alpidic orogeny are believed to be the driving factors of the different types of mineralisation (FRIEDRICH, 1975; SCHEDL, 1981).

In the following section the Ni-Co-Bi-Ag mineralisation of the Zinkwand area is described and discussed in detail (Figure 22 & 23). Gneisses, black schists and minor amphibolites form the host rocks of the deposit. The main mineralisation is bound to carbonate veins crosscutting blackschists. The blackschists are characterised by limonitic weathering and reach up to several meters thickness. The rock texture shows fine layering and is caused by tectonic movement (FUCHS, 1988). Former workers (HIESSLEITNER, 1929) highlighted the fact that the Ni-Co mineralisation is confined to the intersection

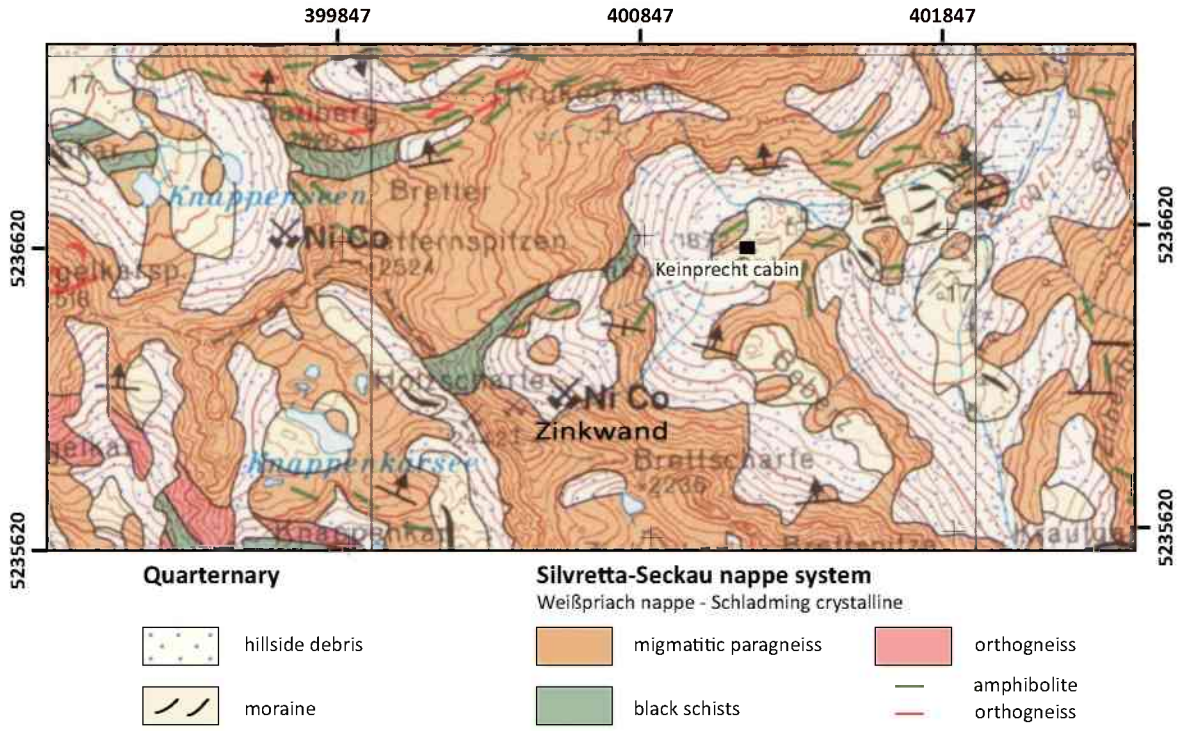

Figure 22: *Geological map of the Zinkwand area (Map section modified after* MANDL & MATURA, 1995)

area of carbonate veins with the blackschist. The following descriptions are focused on Ni-Co ore samples with ankerite and minor quartz gangue. Samples are taken from different elevation levels in the underground workings as well as from the mine dumps.

4.3.2. Results

Paragenesis

The paragenesis of the carbonate veins intersecting the blackschists is dominated by nickeline that is characterised by its copper red colour. Frequently the nickeline is intergrown with gersdorffite. Nickeline is sometimes replaced by more As-rich minerals of the löllingite group (löllingite - rammelsbergite - safflorite) or minerals of the skutterudite series. Subsidiary safflorite occurs intergrown with gersdorffite. Arsenopyrite appears in form of idiomorphic crystals as well as dense masses (Figures 24 & 25). Chalcopyrite, sphalerite, phyrrothite, galena, pyrite, tetrahedrite, boulangerite, bournonite and jamesonite occur as accessory minerals. FUCHS (1988) is furthermore describing the appearance of native arsenic. PAAR & CHEN (1979) are reporting the occurrence of parkerite[7] as a mineralogical speciality.

Quartz and calcite are intergrown with granular texture.

[7] $Ni_3(Bi,Sb)_2S_2$

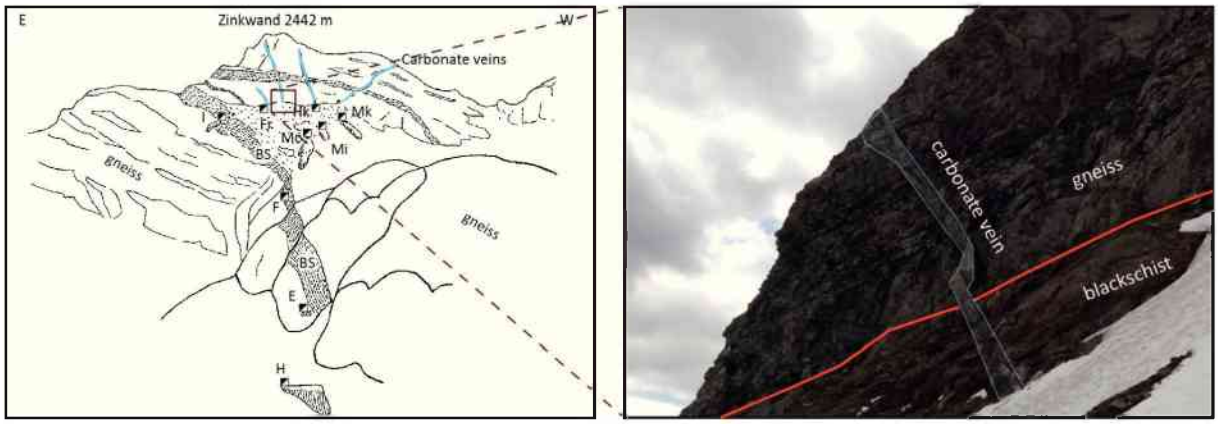

Figure 23: *left: Overview of the Zinkwand ore deposit seen from the Keinprecht cabin with locations of the different adits: HK Himmelkönigin, MK Mutterkirchental, Mi Mitterstollen, Mc Michaeli, Fr Franziski, I Ignatzi, F Fund, E Elisabeth, H Hermann. Sketch modified after* HIESSLEITNER (1929). *right: Detail of a carbonate vein crosscutting blackschists and gneisses. The thickness of the vein is about 40 cm.*

Mineral chemistry

Arsenopyrite of the Zinkwand deposit shows minor replacement of S against As and and incorporation of Co up to 0.074 ω. Stoichiometric compositions are as follows: $(Fe_{0.78-1.00}, Ni_{0.00-0.04}, Co_{0.00-0.20})_{\Sigma=1.00} As_{0.94-1.15} S_{0.85-1.06}$. Gersdorffites also show enrichment in Co ans substitution of S against As: $(Fe_{0.02-0.08}, Ni_{0.64-0.94}, Co_{0.04-0.29})_{\Sigma=1.00} As_{1.29-1.46} S_{0.54-0.71}$. Loellingite shows nearly stoichiometric compositions with sulphur contents up to 0.03 ω: $(Fe_{0.81-1.00}, Ni_{0.00-0.06}, Co_{0.00-0.14})_{\Sigma=1.00} As_{1.80-2.00}$. Safflorite shows variable composition of: $(Fe_{0.62-0.84}, Ni_{0.06-0.14}, Co_{0.10-0.25})_{\Sigma=1.00} As_{1.92-1.98}$. Another diarsenide intergrown with gersdorffite showing similar contents of Fe,Co and Ni is also occurring and probably to be named as safflorite[8] (see Figure 25a). This *unnamed (Fe,Ni,Co)As_2* is showing compositions of: $(Fe_{0.34-0.37}, Ni_{0.33-0.35}, Co_{0.29-0.32})_{\Sigma=1.00} As_{1.97-1.98}$. Nickeline is stoichiometric with compositions of: $Ni_{0.99-1.00} As_{0.99-1.00}$.

Sulphides occur in form of chalcopyrite $Cu_{0.97-1.01} Fe_{0.98-1.02} S_{1.98-2.05}$, sphalerite $(Zn_{0.90-.095}, Fe_{0.08-0}$ galena showing compositions of $Pb_{0.99-1.05} S_{0.94-0.99}$ and up to 0.006 ω Bi, stoichiometric pyrite as well as phyrrothite. Tetrahedrite shows high values of silver and compositions of $(Cu_{9.49-9.81}, Zn_{0.51-0.58}, Fe_{1.50-1.58}, Ag_{0.19-0.21}, Bi_{0.00-0.01})_{\sum 11.80-12.09}$ $(As_{0.23-0.41}, Sb_{3.64-3.78})_{\sum 4.01-4.09}$ $S_{12.98-13.15}$. Boulangerite is bearing high values of bismuth: $Pb_{5.02-5.37}(Sb_{3.72-4.02}, Bi_{0.10-0.18})S_{10.45-11.09}$. Bournonite represents stoichiometric compositions: $Pb_{0.96-1.05} Cu_{1.00-1.07} Sb_{0.95-1.03} S_{2.83-3.04}$. One single jamesonite crystal shows: $Pb_{4.20} Fe_{1.34} Sb_{5.73} S_{13.06}$.

Bulk fluid inclusion composition

The data for Zinkwand calcite and quartz samples (Appendix B) show variable cation and anion ratios. The I/Cl ratios are between $107 \times 10^{-6}$and 405×10^{-6} for calcite. Fluid inclusions in quartz show values ranging from 16×10^{-6} to 237×10^{-6}. These

[8]Presently the mineral is conducted as *unnamed (Fe,Ni,Co)As_2*.

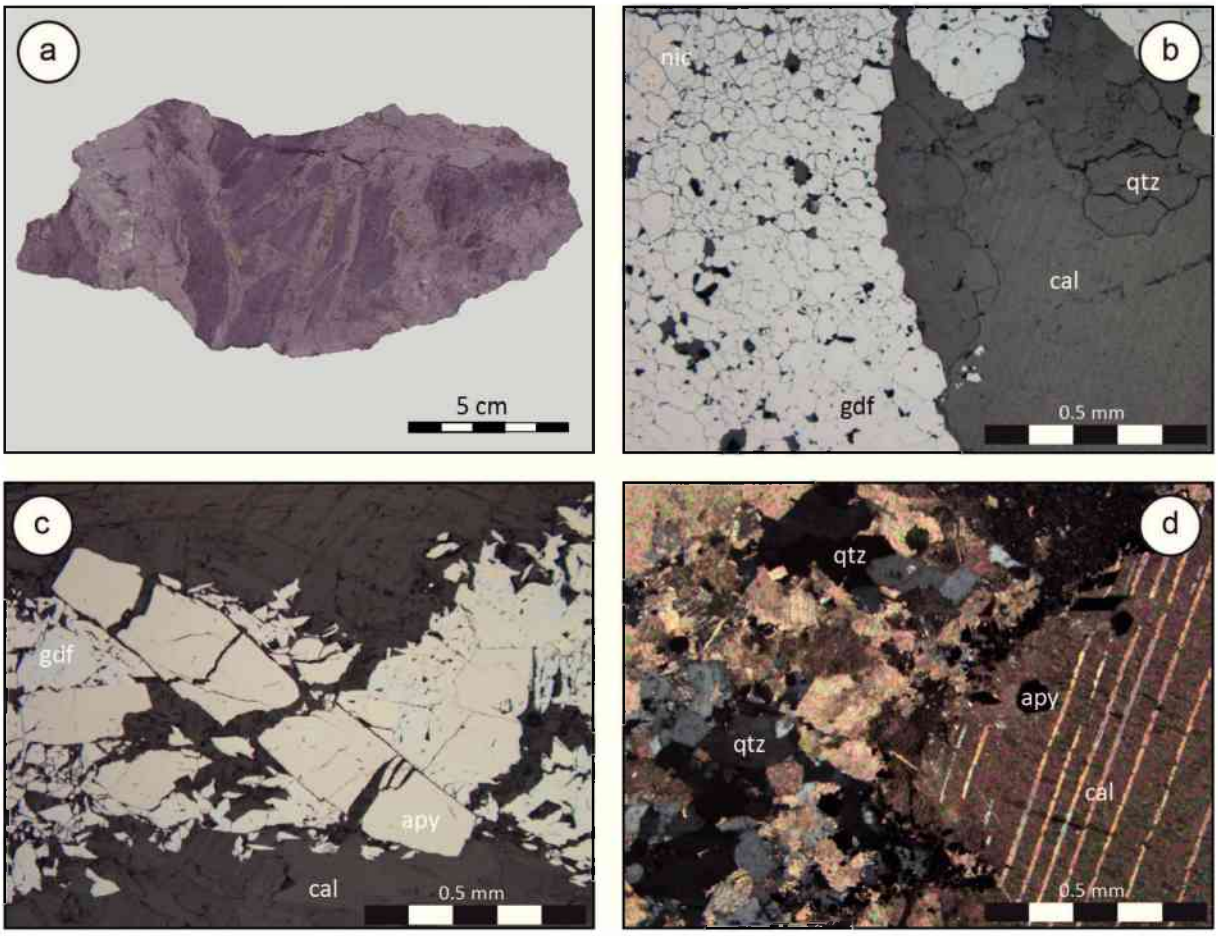

Figure 24: *(a) Typical ore specimen from Zinkwand mostly consisting of gersdorffite-arsenopyrite with minor quartz-carbonate gangue, (b) Nickeline intergrown with gersdorffite (polished thin section, RL, air), (c) Euhedral arsenopyrite crystal intergrown with gersdorffite within calcite gangue (polished thin section, RL, air), (d) Succession of calcite-quartz gangue with minor apy (thin section, TL, XN).*

values are elevated against seawater (0.86×10^{-6}). The Br/Cl mass ratios for calcites are generally low with values up to5.0×10^{-3} with one sample as high as 20.6×10^{-3} . Br/Cl ratios of quartz are between 2.8×10^{-3} and 19.5×10^{-3} and are therefore slightly higher than seawater 1.54×10^{-3}. The K/Na ratios for calcite are scattering between 0.058 and 0.120. K/Na ratios for fluid inclusions in quartz are ranging between 0.067 and 0.140. The Li/Na ratios for calcite range from 0.0028 to 0.0491 and Li/Na ratios for quartz are significantly lower (up to 0.0025) ; the Ca/Na ratios are scattering between 0.19 and 4.52. Calcite samples show elevated charge balance from 1.97 to 13.19. The quartz samples have charge balance values from 1.21 to 11.29.

The comparison of different cation exchange geothermometers applied to bulk fluid inclusions give similar values for both quartz and carbonate samples. The Na-K geothermometer of Díaz-González et al. (2008) gives formation temperatures of 190 ±11 to 337 ±18 °C for carbonate and 186 ±11 to 309 ±16 °C for quartz samples. The application of different Na-Li geothermometers for comparison was not successful due to very low Li contents in the eluate.

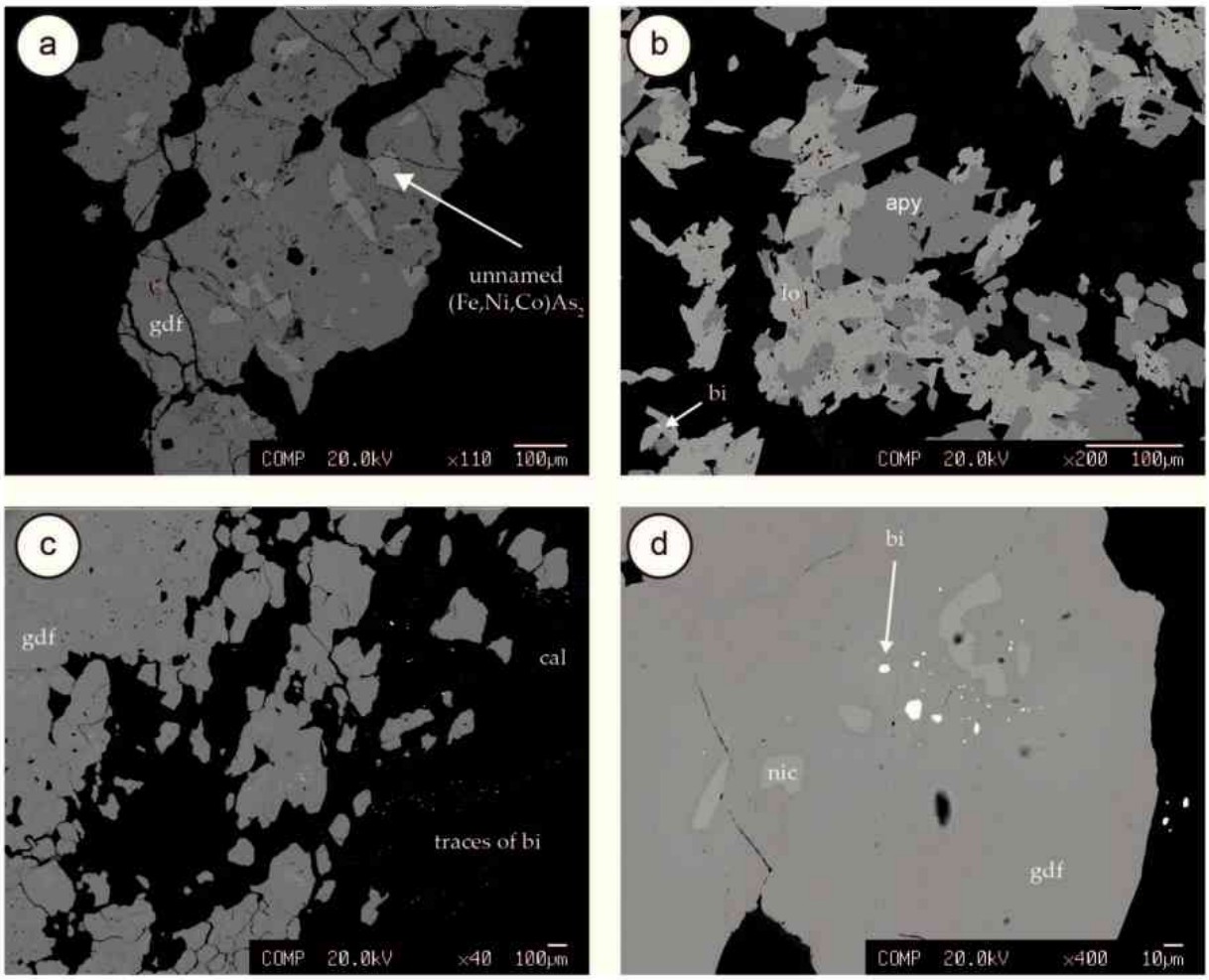

Figure 25: *BSE images of: (a) Gersdorffite intergrown with safflorite, (b) Arsenopyrite-löllingite succession with native bismuth fracture fillings, (c) Mass of gersdorffite with traces of bismuth in calcite fractures, (d) Detail of gersdorffite with nickeline exsolutions and native bismuth.*

Stable Isotopes

Oxygen isotope measurements quartz resulted in values from 13.21 to 19.18 ‰. Carbon and oxygen isotope measurements of vein carbonates form two distinct groups (Figure 26). The vein carbonates of the Zinkwand deposit show a high variability of $\delta^{18}O$ (11.79 to 19.18 ‰) and of $\delta^{13}C$ respectively (-7.07 to -3.29 ‰). Some values of sample material of the Mutterkirchental dump overlap with values measured at the Bromriese deposit.

Formation temperatures calculated using the equation of Sharp & Kirschner (1994) result in temperatures of 180 to 334 °C for the lowest vein parts (Mutterkirchental adit), 465 °C for the central parts (Himmelkönigin adit) and 276 to 337 °C (with one outlier at 595 °C) for the highest reachable vein areas (Lobkowitz opening). $\delta^{34}S$ values for gersdorffite show negative values ranging from -1.3 to -10.0 ‰.

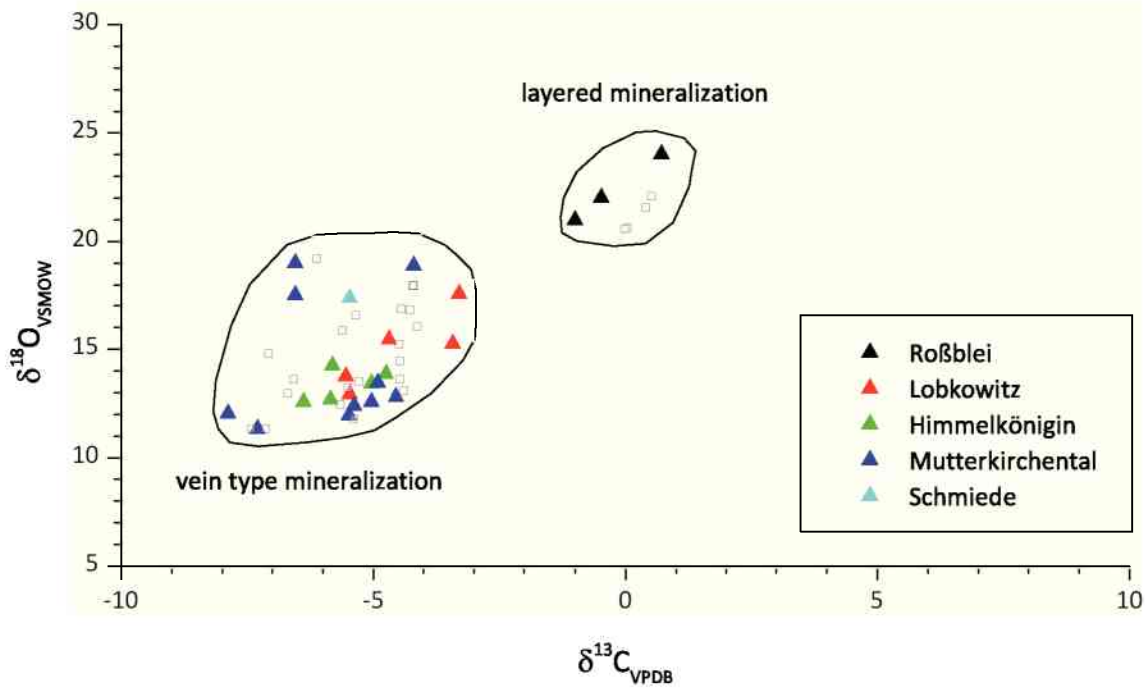

Figure 26: *$\delta^{18}O$ vs. $\delta^{13}C$ of vein carbonates of the Zinkwand deposit. The two groups represent carbonates veins associated with the Ni-Co veins at the Zinkwand deposit and the two-dimensional Bromriese Pb-Zn deposit for competitive reasons. Note: Open squares mark samples taken from the mine dumps where the exact position within the deposit is not reconstructable.*

4.3.3. Discussion

KLEMM (1965) reported experimentally determined data on the solid solution system NiAsS-CoAsS-FeAsS. The gersdorffite and arsenopyrite analyses form two populations well within the experimentally determined solid solution fields at 300 °C (Figure 27). Population A is suggesting slightly higher formation temperatures than population B (< 300 °C). Dendritic bismuth is texturally comparable to natural assemblages precipitating from hydrothermal solutions at temperatures below its melting point. Above the melting point of 271 °C native bismuth forms liquid droplets and retains this morphology during cooling (GODOVIKOV & KOLONIN, 1966). Native bismuth fills cleavages and fissure within carbonate gangue. The not detectable low S concentrations detected in nickeline also indicate formation temperatures below 300 °C. At 300 °C nickeline can incorporate as much as 5.0 wt.% S (e.g. YUND, 1962; WAGNER & LORENZ, 2002). The arsenopyrite geothermometer of SHARP et al. (1985) shows formation temperatures of arsenopyrite ranging from 365 to 400 °C. Boulangerite, jamesonite and bournonite usually form at low to moderate temperature hydrothermal veins.

Using the mineral pair of quartz-calcite as a isotope geothermometer gives contradictory results. Formation temperatures dependent from elevation level is not reconstructable. But the overall range of formation temperatures is between 180 and 465 °C. It seems feasible that oxygen isotope geothermometry can only be applied when the results are crosschecked with other geothermometers.

Reconstructing a mineralising fluid using the hydrothermal alteration model of ZHENG & HOEFS (1993) results in a metamorphogenic fluid with $\delta^{18}O = 7 - 10\,‰$ and $\delta^{13}C \sim -5\,‰$ and temperature of 350 to 400 °C. Assuming that the primary sedimentary mineralisation is remobilised small water/rock ratios of 0.5 to 1 and therefore limited migration distances are plausible. The difference in the carbon and oxygen isotopic composition of calcite within the layered and the vein type mineralisation provide information about the migration distance of the mineralising fluid.

The relative low $\delta^{18}O$ values indicate a possible mixing with meteoric water. Sulphur isotopic composition of gersdorffite is heavily depleted against CDT. The lack of fractionation factors for the gdf-sulphur system results in an estimation of sulphur provenance. The negative values indicate a migration of the ore forming fluids within metasedimentary rocks containing biogenic depleted sulphide (e.g. pyrite). The black schists within the Schladming crystalline provide these conditions. Bulk fluid inclusion data show increased I/Cl against seawater. Diagenetic modified seawater (BOTTOMLEY et al. 2002) shows enriched I/Cl contents. Organic-rich marine sediments release iodine during diagenesis to a migrating brine (BOTTOMLEY et al. 2002).

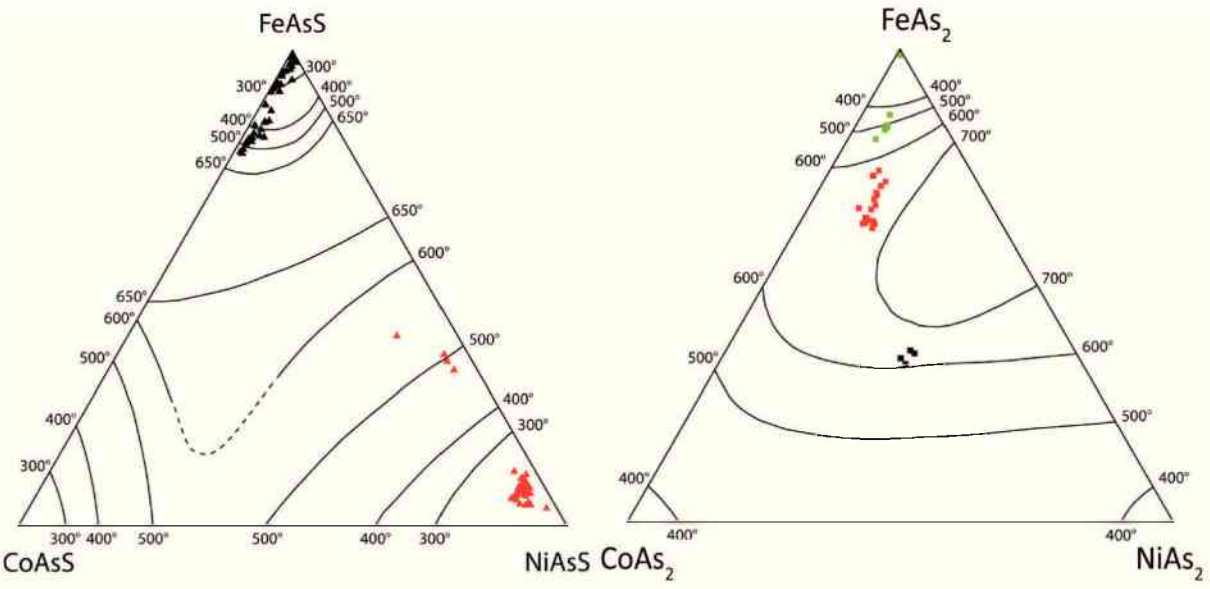

Figure 27: *(left): Compositional plot of arsenopyrites and gersdorffites from the Zinkwand deposit in the FeAsS-CoAsS-NiAsS field. Arsenopyrites represent a gradual cooling down from 550 to < 300 °C. Gersdorffite compositions form two groups: a high temperature (around 500 °C) and low temperature group (around 300 °C). (right): Compositional plot of loellingite (green squares) and safflorite (red & black squares) in the $FeAs_2$-$CoAs_2$-$NiAs_2$ field. Formation temperatures of 600 to 700 °C are too high and therefore not meaningful. Solvus lines at different temperatures for both systems are taken from* KLEMM (1965).

4.3.4. Interpretation

The mineral paragenetic sequence of the Zinkwand arsenide mineralisation started with high temperature phases of Ni monoarsenides (nickeline) and followed by Ni diarsenides at temperatures well above 400 °C. Subsequently sulfarsenides precipitated at temperatures

of 300 to 400 °C. Contemporaneously calcite and quartz started to precipitate at lowering temperatures. The last mineral phase is defined by native bismuth that formed below 271 °C.

The mineralizing fluids at the Zinkwand deposit was a mixture of two different fluids: a relatively high tempered, metamorphogenous brine derived from phyllonitic blackschist due to retrograde leaching and low tempered meteoric waters. The mixing process between these fluids led to an increase in pH and sulphur activity and a decrease of oxygen fugacity and resulted therefore in the formation of quartz-carbonate gangue and late stage hydrothermal sulphide. The extreme negative sulphur isotopic composition of gersdorffite is due to an influence of fluid migration within blackschists and depicting an influence of biogenic sulphur derived from pyrite.

The Ni-Co-Bi mineralisation was formed after the Eo-Alpine metamorphic peak when extensional tectonics provided pathways for fluid migration.

4.4. Kraubath Mg

4.4.1. Geological setting

The Kraubath Ultramafic Complex (Figure 28) forms an integral part of the Speik complex (NEUBAUER & FRISCH, 1993) in the Silvretta-Seckau nappe system (Figure 8). The Kraubath Ultramafic complex is dominated by ultramafic rocks like serpentinised peridotites, dunites and pyroxenites. Subsidiary metabasalts, metagabbros, augengneisses and metasediments occur.

The magmato-metamorphic history of the Speik complex starts during Proterozoic when a partial melting of not depleted mantle rocks in MOR or back-arc setting occurred and a harzburigitic residuum was formed. In Lower Cambrian times repeated partial melting in a supra-subduction environment or sub-arc setting occurred and strongly depleted harzburgites evolved. Early Variscan (Lower Devonian) orogenesis expressed itself in amphibolite- to eclogite facies metamorphism. During Variscan agglomeration to Variscan units (Carboniferous) moderate to high grade metamorphism in combination with the intrusion of granites occurred. Eo-alpidic subduction and crustal thickening heated the Speik complex to greenschist and amphibolite facies conditions (NEUBAUER 1988, MELCHER et al. 2002, MELCHER & MEISEL 2004). During Miocene the ultramafic complex was affected by Mur-Mürz shear zone and E-W trending faults created the Fohnsdorf-Seckau pull apart basin (SACHSENHOFER et al. 2000).

Magnesite is occurring in form of cryptocrystalline magnesite[9] hosted by serpentinites. Two main types of cryptocrystalline magnesite occur: veins and networks of magnesite (WENINGER, 1981) and sedimentary magnesite in form of breccias or conglomerates (cf. KROISSENBRUNNER 2012; THALHAMMER et al. 2010). The magnesite mineralisation is part of the chromite-asbestos-magnesite district Kraubath-Hochgrössen (WEBER, 1997A).

4.4.2. Results

Magnesite

The cryptocrystalline variety of magnesite was first described in Kraubath by REDLICH (1909). WENINGER (1981) classified five different types of magnesite:

1. magnesite veins with thicknesses ranging from a few cm to 2 m. The borders of these veins often show slickensided discontinuities. The magnesite is partly brecciated and solidified by magnesite cement.

2. coarse grained serpentinite breccias in a magnesite mass

3. fine magnesite filled fissures forming a magnesite network

4. cauliflower shaped magnesite

5. red coloured magnesite due to small amounts of haematite

[9]Hereafter the term "magnesite" is used for cryptocrystalline variety of $MgCO_3$.

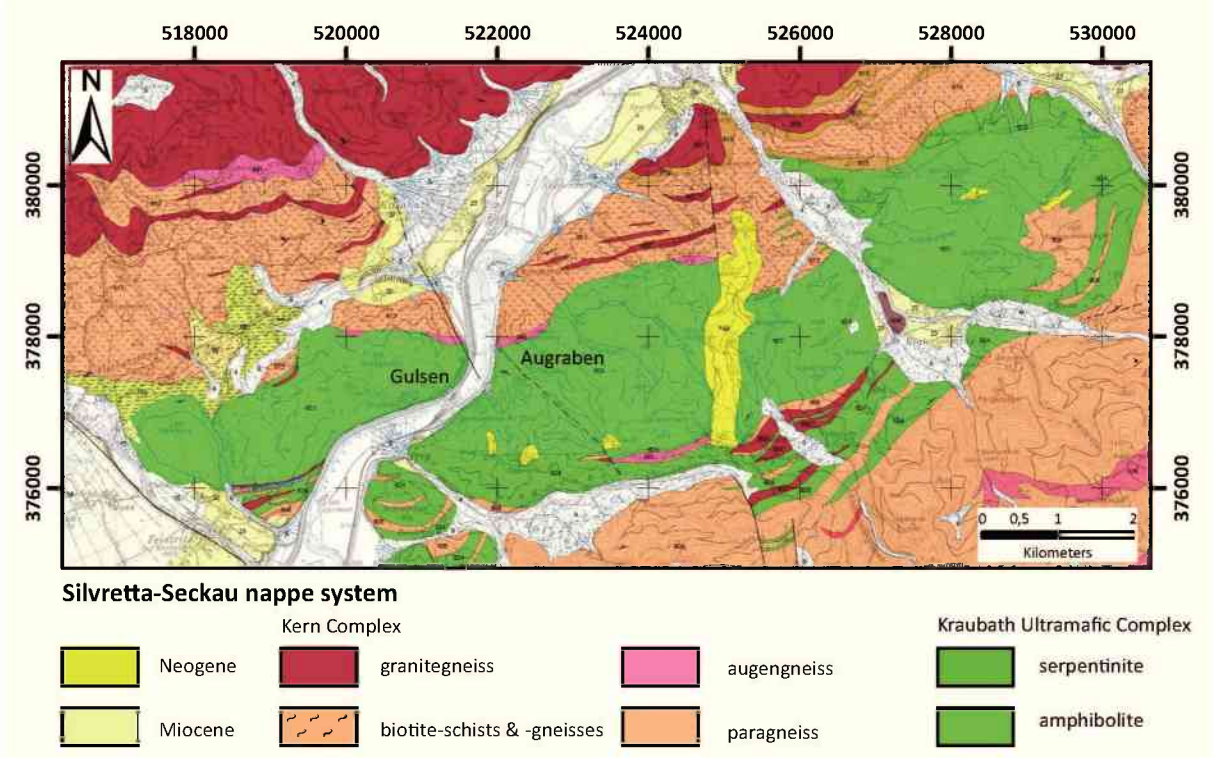

Figure 28: *Geological map of the Kraubath area. The Augraben and Gulsen Area are marked. (Map section modified after Geofast-Provisorische Geologische Karte der Republik Österreich 1:50.000 - 132 Trofaiach: Stand 1999, Ausgabe 2005/10)*

This tectonically controlled magnesite mineralisation in form of veins, fissures and networks is labelled as "Kraubath type magnesite" in international literature. The Kraubath type magnesite is strictly controlled by depth (THALHAMMER et al. 2010). Vein type magnesite of the Augraben area is investigated within this thesis. KROISSENBRUNNER (2012) is describing conglomerates with magnesite components and magnesite cement at Gulsen. The conglomerates are interpreted as alluvial fans that filled the Neogene Fohnsdorf basin (SACHSENHOFER et al. 2010). This sedimentary type magnesite is similar to Bela Stena type magnesite (EBNER et al. 2012, HORKEL 2012, EBNER & WILSON 2006, POHL 1990, FALLICK 1991).

Stable isotopes

Stable isotope values for oxygen and carbon show two different populations for Kraubath type and sedimentary magnesite (Figure 30). The Kraubath type is characterised by a broad range of $\delta^{13}C$ values between -23 and -10 ‰. $\delta^{18}O$ values show relative constant amounts of 24 to 27 ‰. A further subdivision of of Kraubath type magnesite due to its appearance shows a very focused data set of vein type magnesite ($\delta^{18}O$: 26 - 27 ‰; $\delta^{13}C$: -12.5 to -15 ‰). Sedimentary magnesite in form of breccia and conglomerate cement shows lower $\delta^{18}O$ values ranging from 25 to 18 ‰. $\delta^{13}C$ values are slightly higher than vein type magnesite an lie between -7 and -14 ‰. Both sub-types overlap, because the discrimination of vein and network is not unfailingly possible and both types are closely

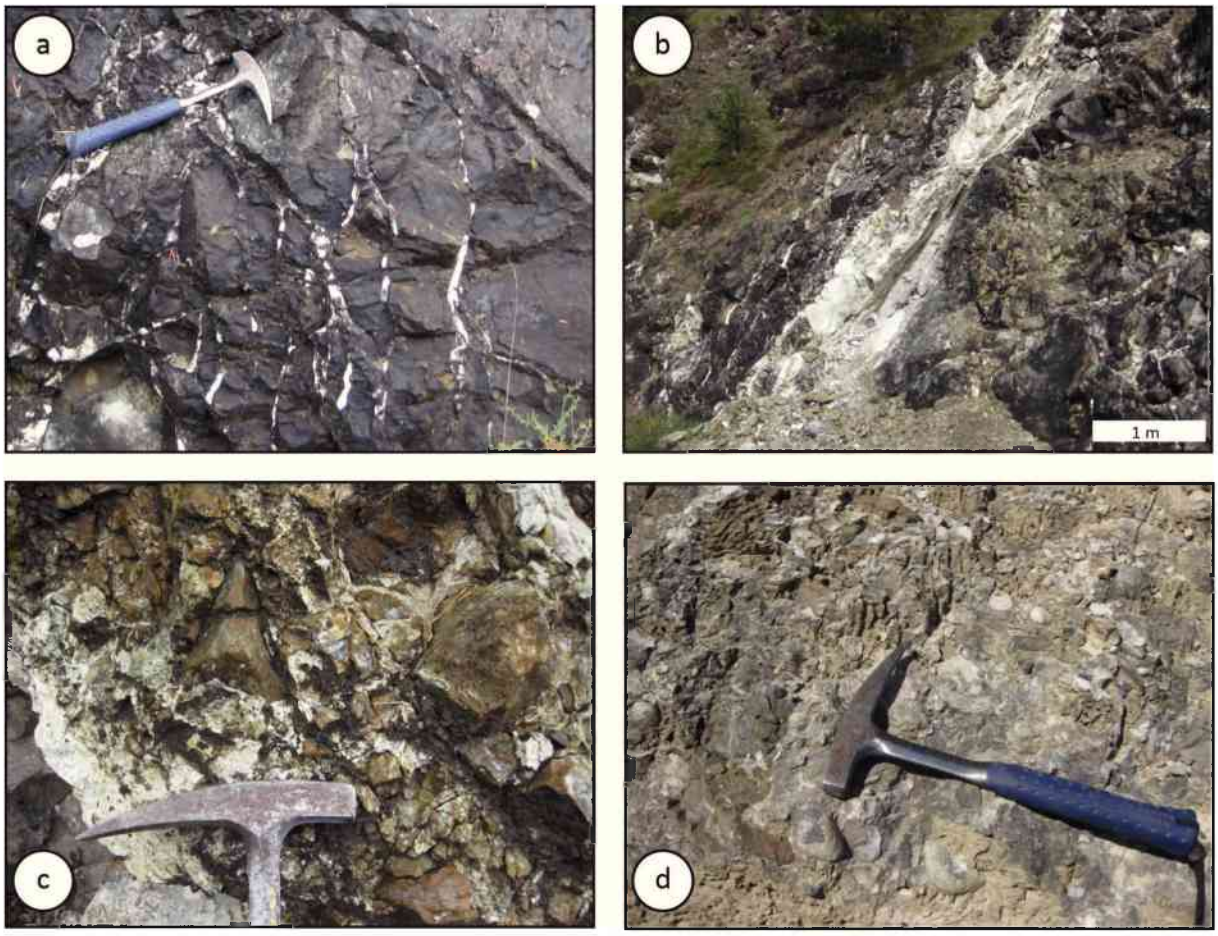

Figure 29: *Different types of cryptocrystalline magnesite: (a) Network mineralisation (Augraben), (b) Vein type (Augraben), (c) Serpentinitebreccia cemented by magnesite (Augraben), (d) Sedimentary magnesite in form of conglomerate with magnesite cement (Gulsen). Photographs used with permission of* P. KROISSENBRUNNER.

linked with each other. For comparison measurements of chalk and calcitic breccia matrix from lacustrine sediments within the comparable Rein basin are shown in Figure 30 as grey triangles.

4.4.3. Discussion

The genesis of cryptocrystalline magnesite has been the subject of controversial discussions for years. Two different models of magnesite formation are proposed. The ***ascendant model*** favours ascending carbonated fluids from the depth that precipitate magnesite in surface near positions (cf. KADIR et al. 2012; ECE & ÇOBAN 2005; UNTERWEISSACHER et al. 2009; POHL 1990).

In contrast the ***descendent model*** associates magnesite formation with alteration and weathering of ultramafic rocks due to the infiltration of CO_2-rich, surface derived waters (cf. BASHIR et al. 2009a & b; ZEDEF et al. 2000). Choosing between "one side" or "the other" is rather difficult or even not possible regarding to stable isotope investigations. The source of Mg^{2+} is clearly attributed to the serpentinised, ultramafic rocks (numerous

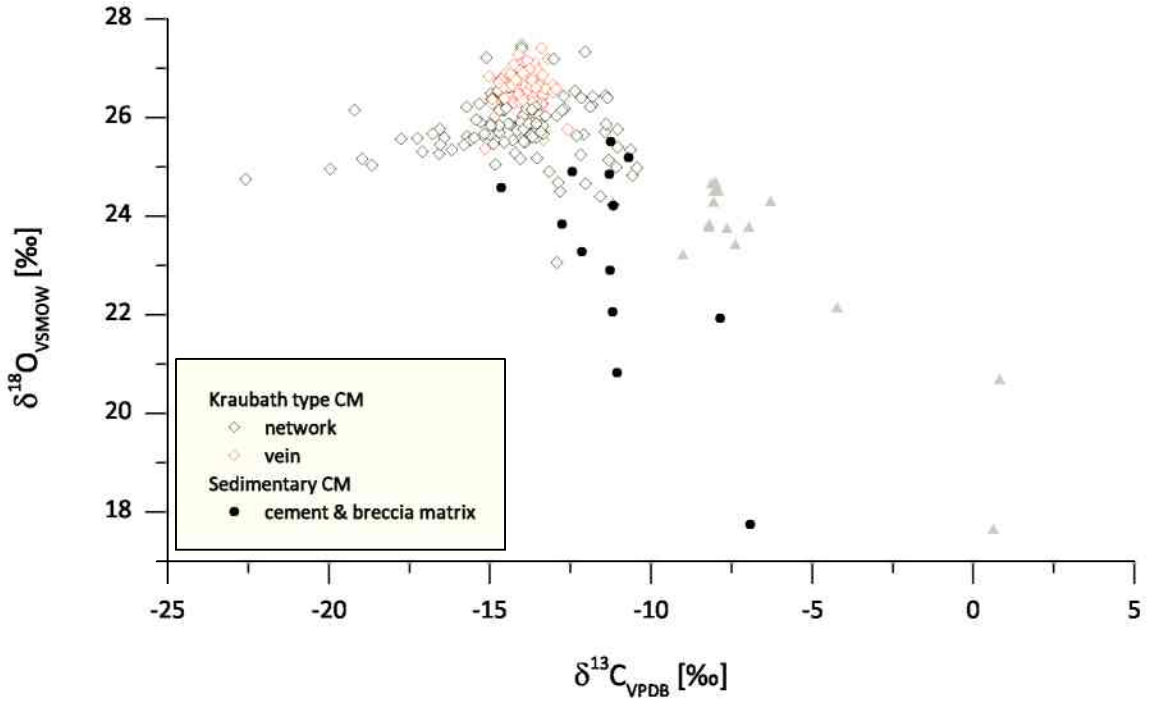

Figure 30: *Covariation plot of $\delta^{18}O$ and $\delta^{13}C$ magnesite samples from Kraubath. Vein and network type magnesite forms a distinct group of samples. Magnesite showing sedimentary appearance like cement and/or breccia matrix is depleted in $\delta^{18}O$. For comparison values for lacustrine sediments (chalk) and breccia matrix (calcite) from the Rein basin (Miocene) are shown in grey. The data set includes measurements of* Horkel (2012) *(network and vein type) and* Dietmayer-Kräutler (2013); Kroissenbrunner (2012) *(sedimentary).*

works since Barnes & O'Neil, 1969; Dabitzias, 1980).

In contradiction to the source of Mg^{2+} the origin of HCO_3^- is still the matter of debate. Using the values of $\delta^{18}O$ and $\delta^{13}C$ of magnesite sheds some light to the issue (Figures 30 & 31). Positive $\delta^{13}C$ values indicate alkaline, surface near environments. Sedimentary magnesite deposits in Serbia (Bela Stena) show values ranging from -5 to +5 ‰ (Dietmayer-Kräutler 2012; Jurkovic & Pamic 2003, Fallick et al. 1991). Recent magnesite stromatolithes from Salda Gölü in Turkey show values from 0.2 to 4.5 ‰ (Braithwaite & Zedef, 1996). Sedimentary magnesite from the Tethys Ophiolite Magnesite Province shows similar values for $\delta^{13}C$ but $\delta^{18}O$ does not display values below 23 ‰ (Ebner et al. 2012).

The fractionation of oxygen between magnesite and H_2O is a function of temperature (see Table 1). Using the fractionation equation of Zheng (1999) and an oxygen fractionation of H_2O of -2 ‰ leads to formation temperatures of Kraubath type magnesite of around 40 to 50 °C. The $\delta^{18}O_{H_2O}$ value of -2 ‰ reflects Miocene alkaline lake waters similar to the early state of Lake Pannon (Harzhauser et al. 2007).

Calculating formation temperatures of sedimentary magnesite the same way results in temperature up to 90 °C. Such high temperatures are irrealistic for lacustrine sediments . Presuming the formation temperatures of sedimentary magnesite with ambient Miocene conditions ($\sim$ 30 °C) leads to a strongly depleted lake water ($\delta^{18}O_{H_2O}$: -6 to -12 ‰) from

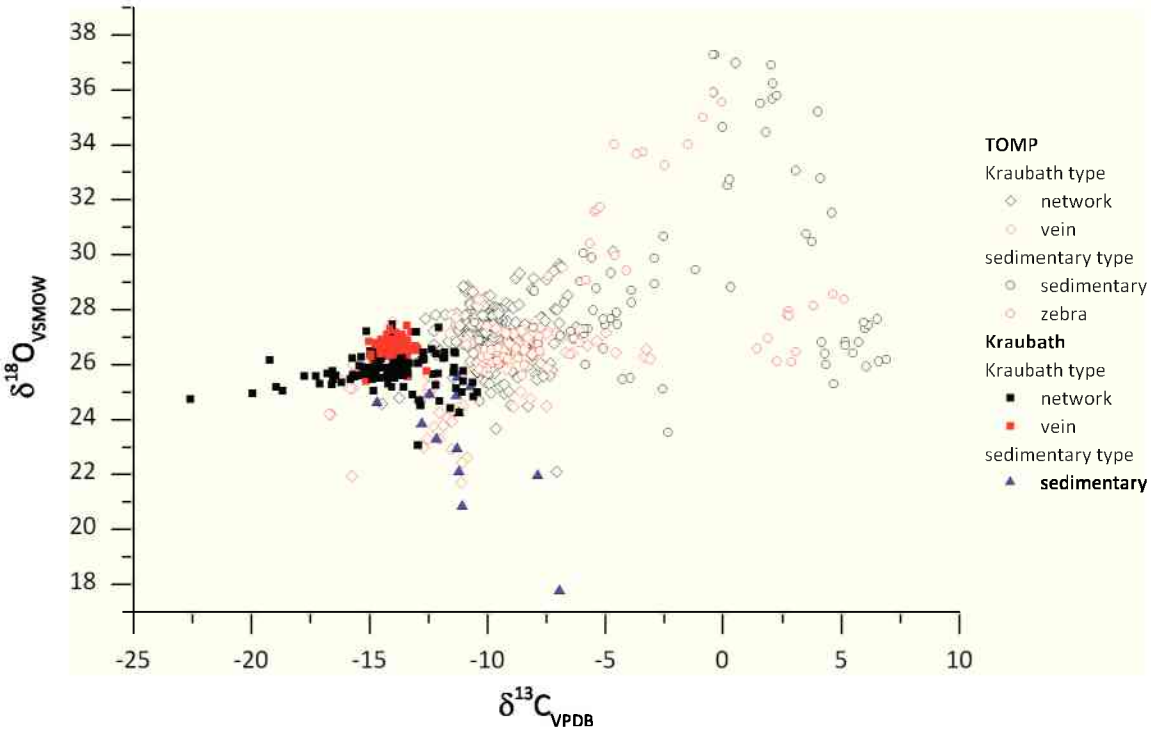

Figure 31: *$\delta^{18}O$ and $\delta^{13}C$ covariation plot of Kraubath type and sedimentary magnesite samples from the Tethys Ophiolite Magnesite Province (TOMP) and Kraubath Ultramafic complex. The data set includes measurements of* HORKEL (2012) *(network and vein type) and* DIETMAYER-KRÄUTLER (2013); KROISSENBRUNNER (2012) *(sedimentary).*

which the magnesite precipitated. Such a depleted fresh water is more or less corresponding with fresh water end members for Miocene basins comparing the Fohnsdorf basin with similar basins like the Pannonian basin (HARZHAUSER et al. 2007).

The values of $\delta^{13}C$ for vein type and network magnesite is due to the migration distance of the mineralizing fluids within the Kraubath Ultramafic complex. Vein type mineralisations occur at the fluid pathways where an infinite reservoir of mineralizing fluid ($\delta^{18}O_{H_2O}$: -2 ‰) can be assumed. Network mineralisations show a broader range in $\delta^{13}C$ and therefore subsequent fractionation depending on migration distance from the main pathways occurs. The reason for this fractionation effect is that carbon represents the limiting factor in the fluid system. Assuming atmospheric carbon as the main carbon source of precipitating magnesite seems feasible. The lack of footwall carbonates or shales providing the carbon reinforces this assumption.

Generally the previously published model (THALHAMMER et al. 2010, POHL 1990) of descendent fluids precipitating the cryptocrystalline magnesite within the Kraubath Ultramafic complex and the superposing sediments is substantiated and the carbon source is specified.

4.4.4. Interpretation

The cryptocrystalline magnesite mineralisation at Kraubath formed during Miocene along the prominent extensional shear zone that formed the Fohnsdorf basin. Two types of

mineralisation occur: (1) vein (Kraubath-) type magnesite and (2) sediment (Bela Stena type) hosted magnesite.

The Kraubath type mineralisation (veins and network) is bound to extensional structures within a NE-SW striking extensive shear zone. Parallel to the opening of fractures during extensional movements meteoric waters were infiltrating the ultramafic rock and leaching Mg^{2+}. With ongoing extension the infiltration depths were increasing and lake waters were filling the Fohnsdorf pull-apart basin. The convective hydrothermal fluid flow reached at least 2 km.

Within the superposing alkaline lake sedimentary magnesite precipitated as cement in coarse grained sediments.

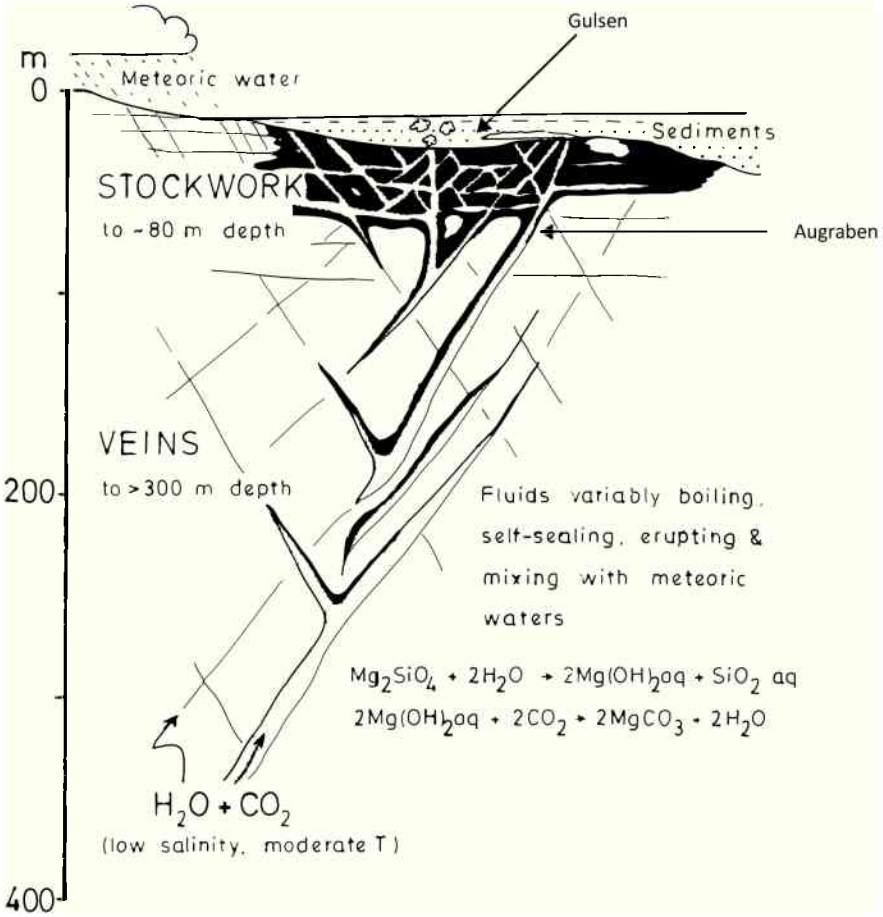

Figure 32: *Genetical model for the Kraubath magnesite deposit after* POHL (1990). *The formation of sedimentary magnesite (Gulsen) occurs contemporaneously with precipitation of vein type magnesite (Augraben) during Miocene.*

4.5. Tösens Pb-Zn

4.5.1. Geological setting

The Pb-Zn deposit Tösens is situated in the Ötztal nappe of the Upper Austroalpine Ötztal-Bundschuh nappe system (SCHMID et al. 2004). The Ötztal nappe (Figure 8) is located west of the Tauernwindow and consists of crystalline basement (Ötztal-Stubai complex) and transgressive, Permomesozoic metasediments (Brenner Mesozoic) (TOLLMANN, 1977). The Ötztal nappe is confined by the Unterengadin window and the Silvretta-Seckau nappe system in the west. The southern margin is represented by the Vinschgau shear zone and the Schneeberg nappe of the Koralm-Wölz nappe system. The eastern boundary against the Penninic nappes of the Tauernwindow and the Innsbruck Quartzphyllite nappe is formed by the Brenner normal fault (SELVERSTONE, 1985).

The Pb-Zn deposit Tösens is part of the polymetallic Cu-Fe-Zn-Pb Stubai-Ötztal ore district. Two different regional, substantial and genetic types of pre-metamorphic mineralisations are distinguished (after WEBER, 1997A; VAVTAR, 1988):

- Cu-Fe sulphide paragenesis in amphibolite-rich areas within the crystalline basement
- Zn-Pb sulphide paragenesis in amphibolite-poor areas within the crystalline basement (including the Tösens deposit)

The mined Pb-Zn mineralisation is bound to concordant sulphide enrichments in mylonitic shear zones inside ortho- and paragneisses. VAVTAR (1988) is describing a stratiform mineralisation located to two distinct ore horizons. These mineralisations are about 4 km east of the gently SE dipping thrust fault, that defines the border between the Ötztal-Stubai Crystalline and the Unterengadin window. The metal enriched zones are concordant to the S dipping gneisses.

The adits of the Tösens deposit is not accessible at the moment (cf. UCIK 2006) but the collection of samples from mine dumps in different elevation levels is possible (Appendix A).

4.5.2. Results

Paragenesis

The mineral paragenesis is characterised by sphalerite, galena, pyrite, chalcopyrite, and arsenopyrite. Minor phyrrothite, tetraedrite-tennantite, boulangerite, jamesonite, bournonite, pyrargyrite, marcasite, ullmannite, cobaltite, covellite, digenite, antimonite and gudmundite (after VAVTAR, 1988). Host rocks are ortho- and paragneisses with a clearly developed schistosity. Concordant to these gneisses metabasalts occur. Gangue minerals are quartz and carbonates of the dolomite - ankerite group. Minor calcite is occurring.

Mineral chemistry

Galena shows stoichiometric compositions of $Pb_{0.97-1.00}S_{0.99-1.01}$ with minor contents of antimony (up to 0.004 ω) and zinc (up to 0.006 ω). Sphalerite incorporates remarkable amounts of iron and shows compositions as follows:

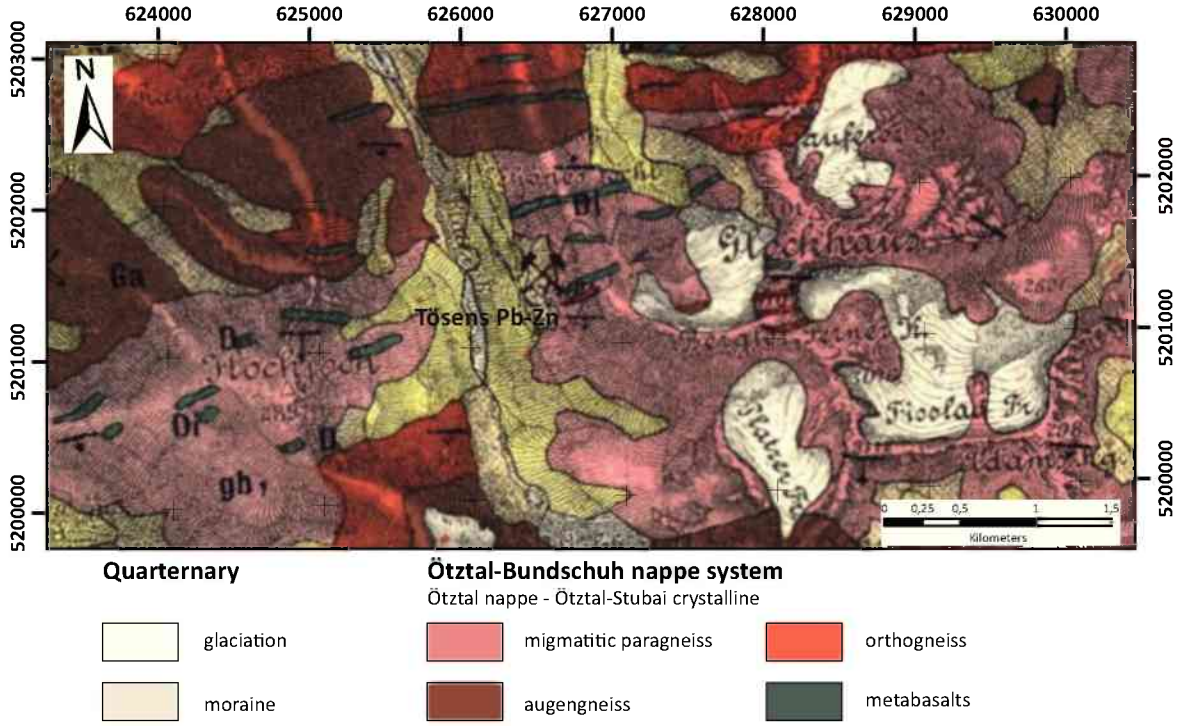

Figure 33: *Geological map modified after (Map section modified after* Hammer, 1923*)*

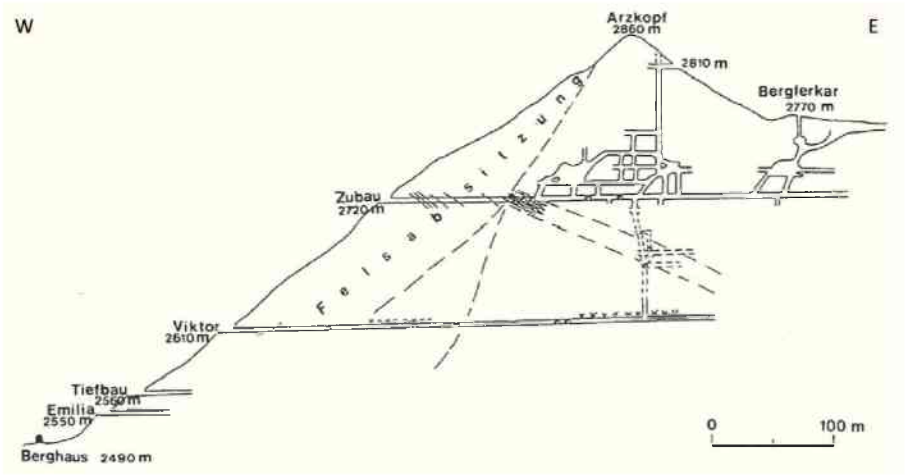

Figure 34: *Cross section of the former adits at the Tösens deposit (Obernbergler vein). Sketch simplified after* Hiessleitner & Clar (1950) *in* Vavtar (1988).

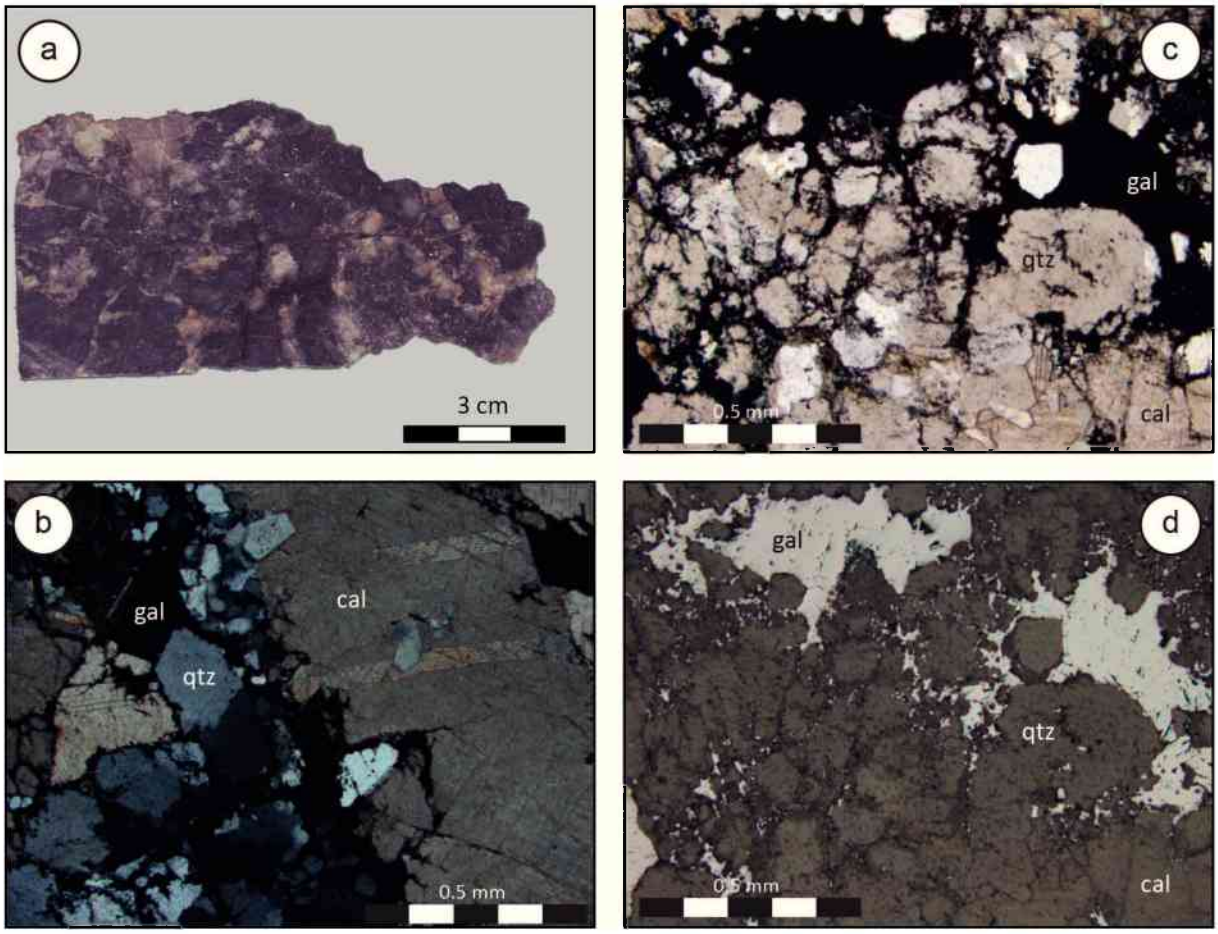

Figure 35: *(a) Ore specimen of the Tösens deposit, (b) Galena within calcite-quartz gangue (polished thin section, TL, XN), (c) Galena within calcite-quartz gangue (polished thin section, TL), (d) Galena filling voids within calcite-quartz gangue (polished thin section, RL, air).*

$(Zn_{0.89-0.92},Fe_{0.08-0.10})S_{0.99-1.01}$. Cobalt contents in pyrite samples reach up to 3.53 wt.% and have minor added arsenic (maximum 1.4 wt.%) and zinc (maximum 0.73 wt.%). The calculated stoichiometric composition of pyrite is $(Fe_{0.94-1.01},Co_{0.00-0.07})S_{1.97-1.99}$. Boulangerite occurs as exsolutions in galena and shows a non stoichiometric composition of $(Pb_{4.99-6.00}(Sb_{3.20-3.86},Cu_{0.37-0.44})S_{10.46-10.64}$. Gudmundite has normal compositions of $Fe_{1.00-1.02}Sb_{0.99-1.02}S_{0.97-0.98}$ and occurs as exsolutions in galena (Figure 36).

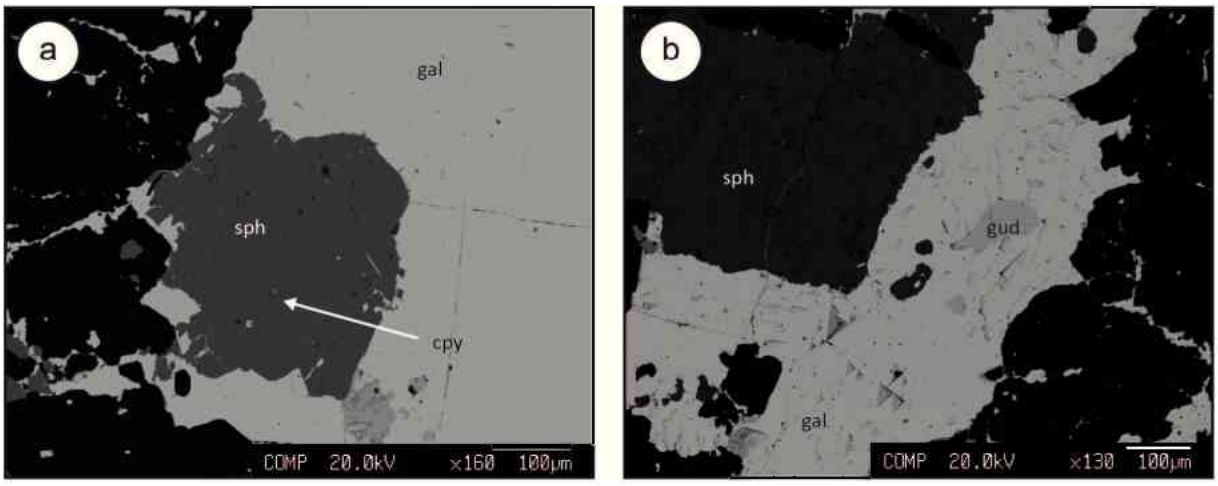

Figure 36: *(a) BSE image of galena - sphalerite interdigitations with small exsolutions of chalcopyrite within sphalerite, (b) Remarkable gudmundite exsolutions within galena (BSE image).*

Bulk fluid inclusion composition

Bulk fluid inclusion data for Tösens quartz samples (Appendix B) have to be treated with caution due to small sample weights. The I/Cl ratios are ranging between $16 \times 10^{-6}$and 123×10^{-6}. The Br/Cl mass ratios are very low (up to7.3×10^{-3}). The K/Na ratios for quartz are scattering between 0.086 and 0.234. The Li/Na ratios are not meaningful due to the very low Li values; the Ca/Na ratios are scattering between 0.11 and 0.57. The quartz samples show charge balances from 0.86 to 2.33.

The N-K cation geothermometer of Verma & Santoyo (1997) gives temperature between 253 and 366 °C with errors ranging from 50 to 68 °C for quartz samples and 212 ±44 °C for a single carbonate sample. These estimated temperatures are relatively concordant with the geothermometers of Fouillac & Michard (1981). The geothermometer of Díaz-González et al. (2008) gives similar temperatures (238 ±13 to 266 ±15 °C for quartz and 184 ±11 °C for calcite) but lower relative errors.

Stable Isotopes

Oxygen isotope measurements quartz resulted in values from 12.8 to 15.2 ‰. The vein carbonates of the Tösens deposit show relative constant values of $\delta^{18}O$ (14.57 to 17.47 ‰) and of $\delta^{13}C$ respectively (-5.89 to -7.43 ‰).

Formation temperatures calculated using the equation of Sharp & Kirschner (1994) and Zheng (1999) result in temperatures of 366 ± 7 °C and 372 ± 17 °C(with one value of 555 ±27 °C) for quartz-calcite mineral pairs.

δ^{34}S values (Appendix D) for galena show negative values ranging from -0.1 to -1.5 ‰. Pyrite is showing values from 0.8 to 1.2 ‰. Sphalerite is constantly enriched in heavy sulphur and showing values of 2.4 to 2.6 ‰. One single chalcopyrite sample is producing a value of 6.1 ‰. The share of heavy sulphur is normally rising in the queue of galena - chalcopyrite - sphalerite - pyrite (OHMOTO, 1972). The Tösens deposit however shows the series galena - pyrite - sphalerite - chalcopyrite (Figure 37).

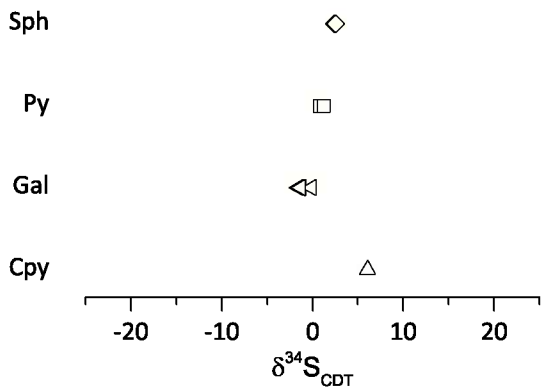

Figure 37: *$\delta^{34}S$ values of sulphides of the Tösens deposit*

4.5.3. Discussion

VAVTAR (1988) is considering the Pb-Zn mineralisation within the Ötztal-Stubai crystalline as pre-Variscan, syngenetic mineralisations with pre-Variscan magmatic cycles as a possible source for extrusive or hydrothermal metal supply. VOHRYZKA (1968) is postulating an Alpine age for the mineralisation. Lead isotopes show model ages around 350 Ma with a maximum at 406 Ma for the Tösens deposit (KÖPPEL, 1997).

The combination of the results of oxygen isotope measurements of quartz with cation geothermometry leads to quartz precipitating fluids enriched in oxygen with $\delta^{18}O$ between 13 and 15.5 ‰)(Figure 38). Formation temperatures range from about 250 to 350 °C. Vein carbonates show similar $\delta^{18}O$ values than quartz. The assumption of oxygen isotopic equilibrium between quartz and calcite seems applicable and the calculated temperatures accompany with cation geothermometry. Carbon isotopic composition of gangue carbonates show depletion in heavy carbon. The sulphur isotopic composition of galena formed at 300 °C from a H_2S dominated fluid is -1.65 ‰ (LI & LIU, 2006) and copes with measured values of galena (Appendix D). Using $\triangle_{galena-sphalerite} = 3.9$ ‰ with values of VAVTAR (1988) give no result for a temperature calculation. Therefore it is assumed that galena and sphalerite are not in equilibrium. Boulangerite and gudmundite usually form at low to moderate temperature hydrothermal veins. The appearance of boulangerite and gudmundite as exsolution textures within galena points out that they formed at lowering temperatures (below 300 °C).

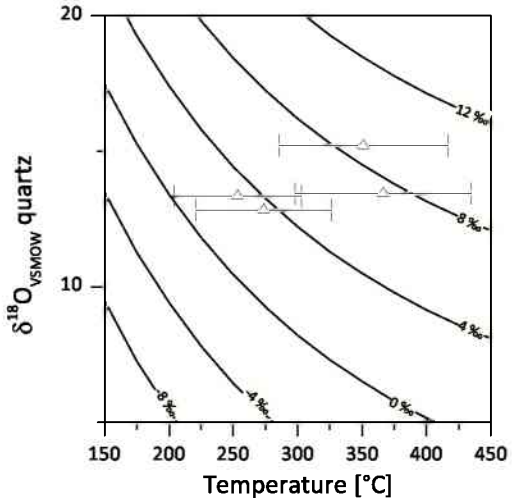

Figure 38: *Oxygen isotope compositions of quartz-precipitating fluids for the Tösens deposit versus mineralisation temperature calculated from the Na-K geothermometer* (Díaz-González *et al.* 2008)*and equilibrium oxygen isotope fractionation in the quartz-H_2O system (solid curves:* Sharp & Kirschner, 1994*).*

4.5.4. Interpretation

The Pb-Zn deposit was formed during Alpine orogeny from metamorphic fluids. The migrating metal bearing fluids remobilised an older stratiform mineralisation. The older mineralisation is about 350 Ma old. The mineralizing fluids were enriched in heavy oxygen and depleted in heavy carbon. Quartz and gangue carbonates show similar values for $\delta^{18}O$ and evolved from the same fluid. The low $\delta^{13}C$ values indicate a metamorphogenic carbon source like metasediments. Relatively high tempered metamorphogenous brines were leaching metal enriched meta-sediments. Sulphur isotopic composition of sulphides indicates an acidic brine with H_2S as the main sulphur species. The values around zero point out that migration distances were not too far. Therefore a local remobilisation of an older mineralisation is proven. The ore mineralisation formed at temperature above 350 °C. Subsequently at lower temperature quartz and carbonates precipitated from the solution.

4.6. Erzwies-Siglitz Pb-Zn-Ag-Au

4.6.1. Geological setting

The ore veins of the Erzwies-Siglitz area are located in Sub-Penninic Venediger nappe system (Figure 8). The Venediger nappe system forms the lowest unit inside the Tauern-window. Pre-Variscan and post-Variscan rock complexes are distinguished.

During Variscan orogeny pre-Variscan rocks underwent high-grade metamorphism and migmatisation as well as the intrusion of intermediate to acidic plutonites (Zentralgneis unit). Post-Variscan metasediments (Silbereck marble group) comprise Upper-Carboniferous to Permomesozoic rocks, that were deposited directly on Variscan surface (PESTAL et al. 2009).

The Silbereck marble group in the Erzwies area consists mainly of dolomitic and calcitic marbles as well as rauhwackes and calcareous mica schists (Figure 40). Alpine greenschist- to amphibolite facies metamorphism affected the Venediger nappe during Oligocene (HOECK & KOLLER, 1999).

The Erzwies-Siglitz ore district is part of the Au-district Rauris-Gastein (WEBER, 1997A). The main part of ore veins is bound to NNE-SSW striking, steeply inclined tectonic structures (Figure 39). The ore veins are extended over a total elevation of more than 1000 m (PAAR, 1997).

The ore veins are well recognizable in the field due to old mine dumps (see Figure 45). Two parallel veins crosscut the Zentralgneis unit (lower parts) and the overlying metasediments (upper parts). The ore veins are dominated by quartz gangue in the lower parts and by siderite gangue in the upper parts, that are crosscutting the Silbereck marble group. The lower parts within the Zentralgneis unit are characterised by its high gold concentrations together with arsenopyrite. The upper parts within the Silbereck marbles were mined for silver, lead and zinc within siderite gangue.

The ore bearing structures in the southern slope of the Silberpfenning mountain can be followed from the bottom of the valley near the Bockhart lake (2070 m) towards an elevation of 2380 m near the Baukarl pass. The rock material of the mine dumps is changing in a remarkable way from limonitic oxidised rocks in the Zentralgneis unit to black coloured rocks in the Silbereck marble group. This colour change is due to a quantitative change in the primary paragenesis as well as the oxidised products thereof (VAVTAR, 1982). Samples were taken from mine dumps of the different adits.

4.6.2. Results

Paragenesis

The paragenesis of the quartz veins is dominated by arsenopyrite, pyrite, minor galena and quartz (Figure 41).

The siderite veins are characterised by siderite[10], pyrite and minor galena, sphalerite, chalcopyrite, ankerite, calcite, quartz and muscovite. Siderite and ankerite are altered under surface conditions to goethite-limonite and Mn-oxides. Euhedral quartz is inter-

[10]In the following the term "siderite" is used for carbonates from mesitine (Fe/Mg = 50/50) over pistomesite (Fe/Mg = 70/30) to siderite (Fe/Mg = 100/0).

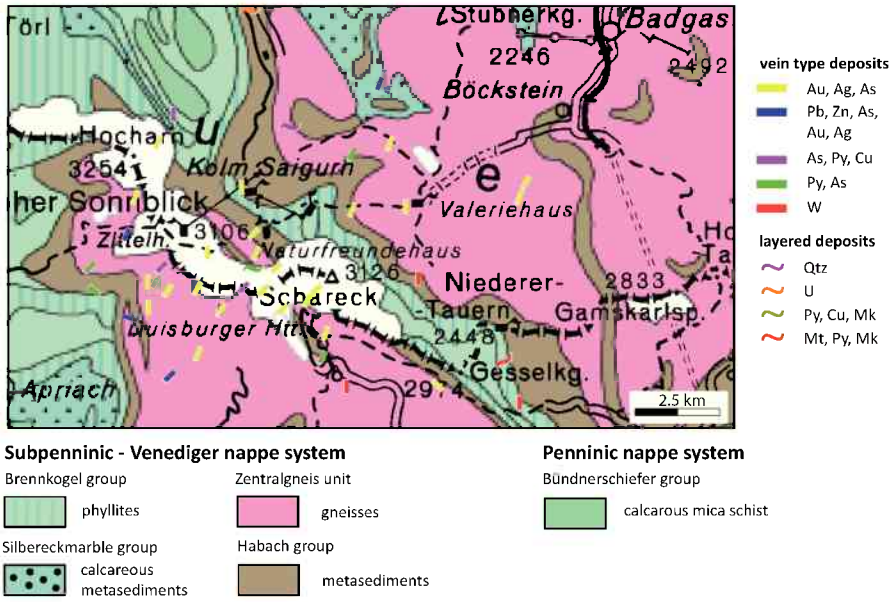

Figure 39: *Metallogenetical map of the Sonnblick area. The strike direction of the Tauerngold veins is parallel NE-SW. Note the transition of the apy-py veins at the Erzwies area within the Zentralgneis into the siderite paragenesis within the Silbereck marbles. Map section adapted from* Weber (1999).

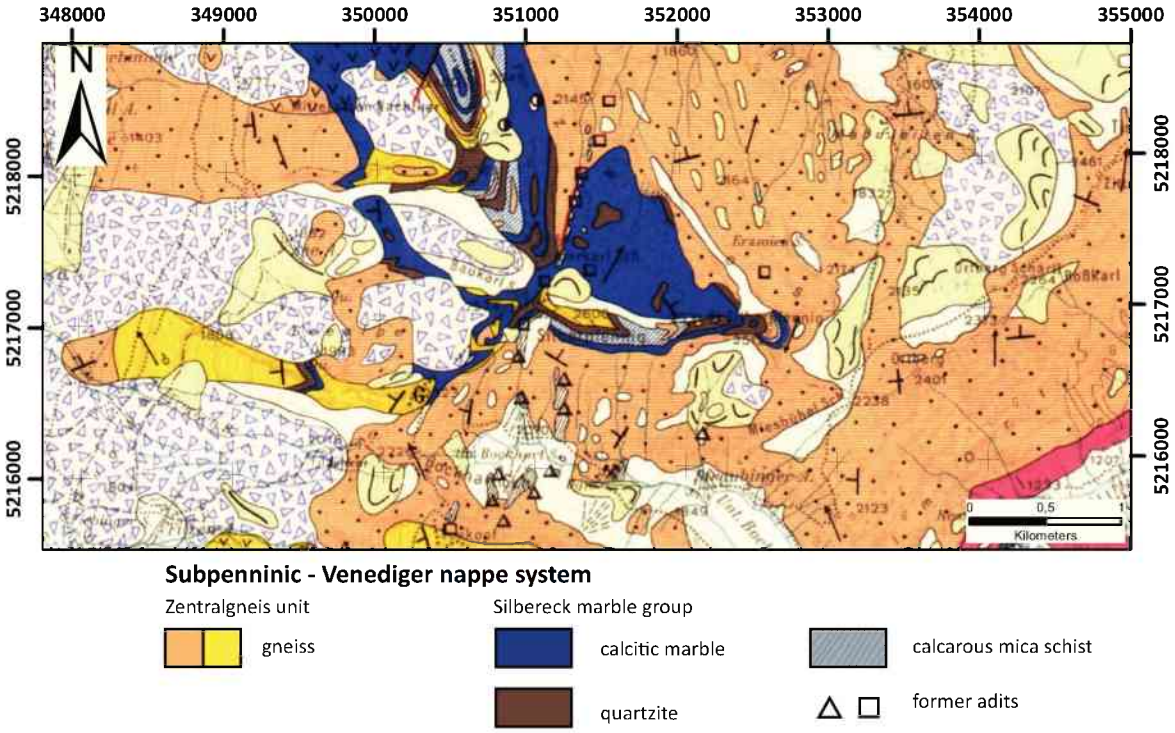

Figure 40: *Geological map of the Erzwies-Siglitz area (Map section modified after* Exner, 1962*)*

grown with siderite (Figure 42b, c & d). VAVTAR (1982) is furthermore describing the occurrence of native Au, native Ag, schapbachite[11] and anglesite.

Mineral chemistry

Geochemical analysis of siderite samples show relative constant amounts of Fe_2O_3 ranging from 0.61 to 0.69 ω. Remarkable amounts of MnO between 0.192 to 0.223 ω occur. CaO (0.012 - 0.027 ω), MgO (0.019 - 0.041 ω) and SiO_2 (0.028 - 0.067 ω) show relative low values. Galena within the quartz veins crosscutting the Zentralgneis unit show traces of silver (up to 0.02 ω) and compositions of $Pb_{0-92-1.00}S_{0.98-1.02}$. Arsenopyrite samples exhibit replacement of S against As and therefore compositions of $Fe_{1.03-1.05}As_{0.85-0.90}S_{1.06-1.15}$. Pyrites show traces of As and calculated stoichiometric formulas of $Fe_{0.98-1.03}S_{1.96-2.01}$.

Galena of siderite veins show stoichiometric compositions of $Pb_{0.98-1.01}S_{0.98-1.01}$. Cogenetic sphalerite exhibits minor emplacement of iron: $(Zn_{0.93-0.94}, Fe_{0.04})S_{1.02-1.03}$. Accessory occurring chalcocite shows enrichment in lead: $(Cu_{1.88-1.90},Fe_{0.03-0.04},Pb_{0.06-0.08})S_{1.00-1.01}$.

Bulk fluid inclusion composition

Fluid inclusion data for Erzwies quartz samples (Appendix B) show variable cation and anion ratios. The I/Cl ratios are between $112\times10^{-6}$and 400×10^{-6} and therefore increased against modern seawater (0.86×10^{-6}). Br/Cl mass ratios are generally low with values up to 2.8×10^{-3} ($Seawater = 1.54 \times 10^{-3}$). The K/Na ratios are scattering between 0.061 and 0.601; the Ca/Na ratios scatter between 0.17 and 11.61. The quartz samples have elevated charge balance values from 2.92 to 17.68. The elevated charge balance is probably due to siderite contamination of the sample.

Bulk fluid inclusion geothermometry of quartz of the apy-py paragenesis (222 ±46 °C) as well as the siderite paragenesis (435 ±81 to 530 ±101 °C) give no meaningful results . Calculated temperatures for the apy-py-qtz samples give lower and the siderite-quartz veins give exaggerated temperatures compared to fluid inclusion temperatures (300 - 350 °C) of BELOCKY (1992).

Stable Isotopes

Oxygen isotope measurements of vein quartz resulted in values from 11.1 to 20.3 ‰. The oxygen isotope ratio is constantly rising with vein level. Carbon and oxygen isotope values of siderites show relatively constant values ($\delta^{18}O$: 12.7 - 13.7 ‰, $\delta^{13}C$: -6.2 to -7.0 ‰). Carbonates of the Silbereck marbles show similar values than seawater ($\delta^{18}O$: 22.40 - 24.30 ‰, $\delta^{13}C$: 0.20 - 2.30 ‰), see Appendix C. Sulphur isotope ratios are showing values ranging from 0.9 to 4.6 ‰ for pyrite and 1.4 to 2.9 ‰ for arsenopyrite. $\delta^{34}S$ values for galena show values around -1.3 ‰ and sphalerite values are ranging between -5.9 and 1.4 ‰ (Figure 43).

[11] $AgBiS_2$

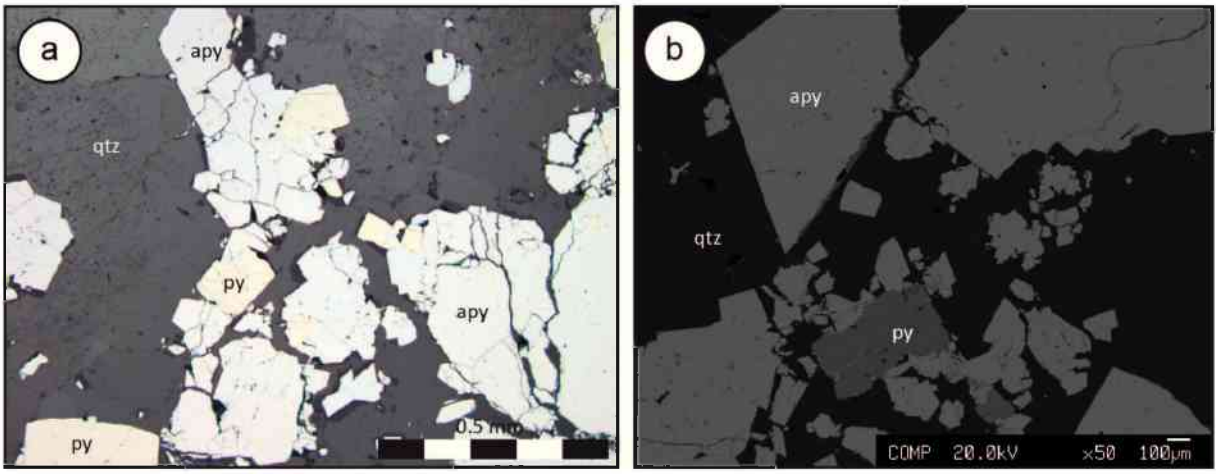

Figure 41: *(a) Polished section of a pyrite-arsenopyrite interdigitation inside quartz, (b) BSE-image of arsenopyrite-pyrite-quartz paragenesis.*

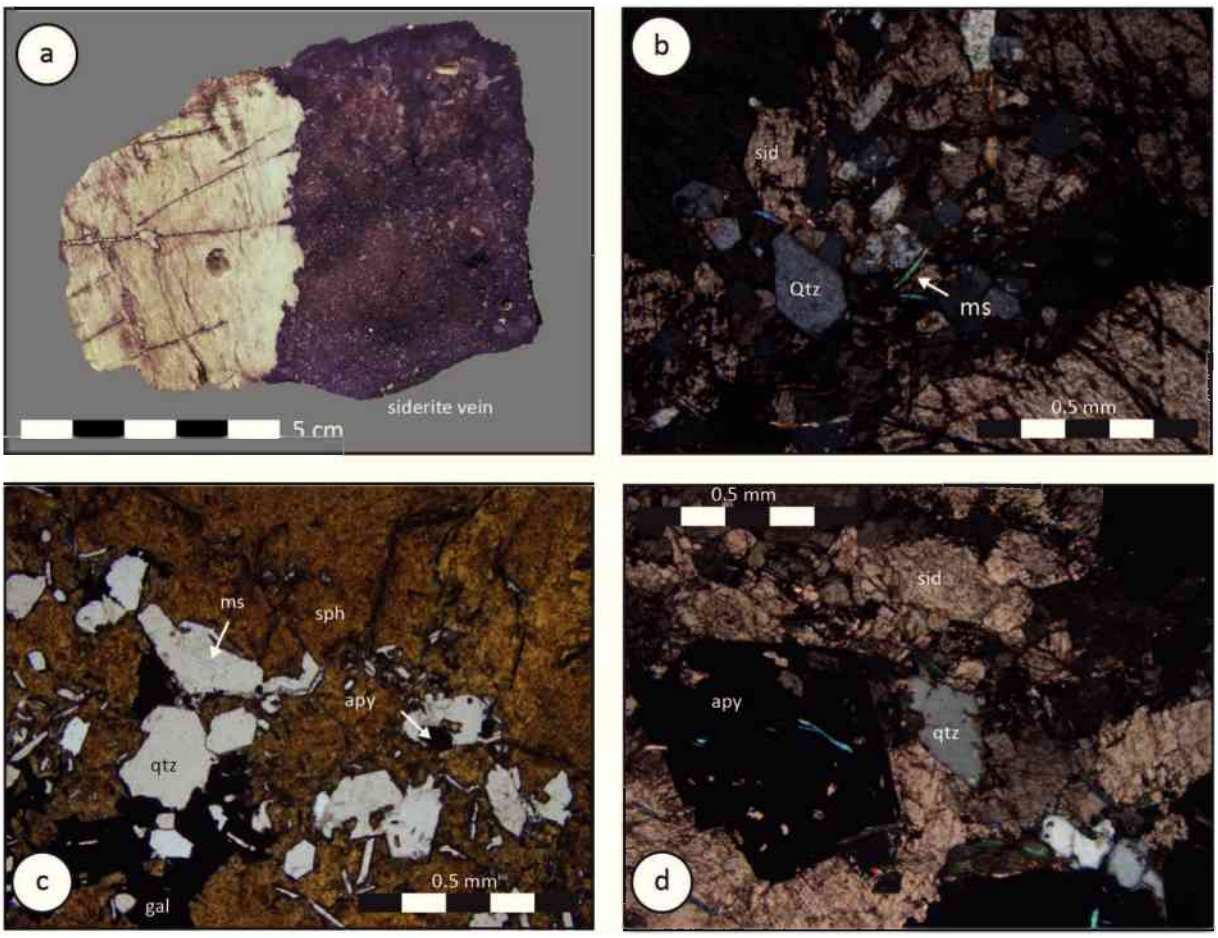

Figure 42: *(a) Siderite vein (dark brown) crosscutting carbonate host rock (grey). Sample taken near the Baukarl pass 2380 m. (b) Siderite-quartz interdigitation. Opaque phases along cleavage are Fe- and Mn-oxides (polished thin section, XN, TL), (c) Euhedral quartz inside sphalerite and galena matrix with minor arsenopyrite (polished thin section, TL), (d) Arsenopyrite within siderite-quartz gangue. Minor muscovite is occurring (polished thin section, XN, TL).*

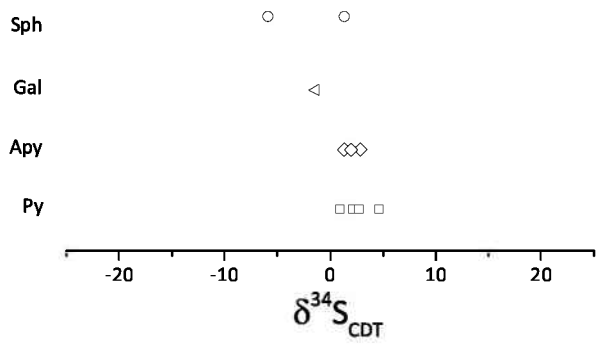

Figure 43: *$\delta^{34}S_{CDT}$ values of sulphides of the Erzwies-Siglitz district (Appendix D)*

4.6.3. Discussion

The use of the fractionation factors of SHIRO & SAKAI (1972) for the quartz-H_2O and of ZHENG (1999) for siderite-H_2O in order to calculate the equilibrium precipitation temperatures is only applicable with caution for the siderite-quartz mineral pair of the Erzwies deposit. The calculated temperatures for the siderite paragenesis range between 284 ±25 and 426 ±30 °C and coincide with microthermometric results of fluid inclusions of BELOCKY (1992). A elevation dependent trend of the temperatures is not evident.

Measurement precision of stable isotope measurements affects small $\Delta_{siderite-quartz}$ values relatively strong and results in elevated temperature estimations. But generally the calculated temperatures are slightly above the temperature field of vein quartz. Vein quartz in the Sonnblick area show formation temperatures of 365-410 °C (FEITZINGER & PAAR, 1991) and total homogenisation temperatures of fluid inclusion in the Goldzeche area of 275-380 °C (ROBL & PAAR, 1994).

Data from the Erzwies siderite veins fall along a positive trend on the $\delta^{13}C - \delta^{18}O$ plot (Figure 44). The conditions of precipitation of siderite and vein quartz are investigated by applying a model for precipitation from a single fluid over a defined temperature range. The siderite curve is calculated using the fractionation factors of ZHENG (1999) for $\Delta_{CO_2-siderite}$ and $\Delta_{siderite-H_2O}$. The temperature range is defined by quartz-siderite geothermometry and fluid inclusion data of BELOCKY (1992) and ranges between 300-350 °C for vein quartz. Fractionation between $H_2CO_{3(ap)}$ and CO_2 above 100 °C is negligible, therefore the fractionation factor of CO_2 is used to account for both species (OHMOTO, 1972).

A set of different fluid $\delta^{13}C$ and $\delta^{18}O$ compositions was tested to fit the siderite data. The modelled mineralising fluid is characterised by $\delta^{18}O = 7$ ‰ and $\delta^{13}C = -14.5$ ‰. The oxygen isotope value of the model fluid is ambiguous and can be interpreted both as magmatic and/or metamorphogenic. In contrast carbon isotope composition is strongly depleted in heavy carbon. Such a signature may represent (1) carbon originating from the lower crust or (2) carbon from the homogenized Earth´s crust (HOEFS, 2009) and/or a possible influence of oxidized organic matter. Oxygen isotopic composition of the fluid forming the apy-py paragenesis is about $14 - 16$ ‰. The oxygen isotopic composition of the fluid creating the siderite paragenesis is slightly lighter and lies between $4 - 8$

‰. These values coincide with the isotopic compositions reconstructed with siderite data (Figure 44). Sulphur isotopic compositions of pyrite show more depleted values for the apy-py paragenesis than for the siderite paragenesis. This is a result of the sudden pH change when the migrating fluids entered the Silbereck marbles. It can be assumed that the fluid is changing from a H_2S dominated fluid to a S^{2-} dominated one.

Bulk fluid inclusion data show increased I/Cl and Cl/Br values against seawater. Fluids generated in deeper parts of crystalline basement (e.g. Bohemian Massif; DOLNICEK et al. 2009) exhibit similar Br/Cl ratios than the Erzwies data. Diagenetic modified seawater (BOTTOMLEY et al. 2002) shows enriched I/Cl contents similar to the Erzwies data. Organic-rich marine sediments release iodine during diagenesis to a migrating brine (BOTTOMLEY et al. 2002).

VAVTAR (1982) is discussing the provenance of the metal bearing solutions and proposing the model of a topomineralic influence and lateral secretion of primary metal enriched carbonate sequences of the Silbereck marbles. The application of the open-system carbonate alteration model of ZHENG & HOEFS (1993) results in high water-rock ratios. These high ratios ($water/rock > 10$) indicate long migration distances. Lateral secretion of metals and migration of mineralizing fluids through host rock carbonates should also result in higher CaO values of vein siderites or result in the deposition of ankerite.

PAAR (1997) indicates that the CO_2 derives from the mantle or from metamorphic fluids generated in deep seated Penninic series. Also POHL & BELOCKY (1994, 1999) rank the Au-veins of the Rauris-Gastein district among metamorphogenic mineralisations. They assume that fluids migrated along deep seated convection zones and that the mineralisation is influenced both by meteoric and metamorphogenic fluids. BELOCKY (1992) delineates tectonically incorporated carbonates within the Zentralgneis as the main source of CO_2 during pro-grade Alpine metamorphism.

4.6.4. Interpretation

Mineralisation temperatures of the Au-veins in the Erzwies-Siglitz area are decreasing from the lower parts (apy-py paragenesis) of the veins to the upper areas (siderite paragenesis) (Figure 45). The lower apy-py-qtz veins formed at temperatures around 300 to 350°C. The abrupt change of the paragenesis from apy-py-qtz to siderite veins is due to the different geochemical environment. The sudden rise in pH forced siderite to precipitate.

The application of the quartz-siderite geothermometer gives scattering temperatures from 426 to 284°C. But the grade of isotopic equilibrium (cooling effect) is variable and cannot be derived from textural analysis. Therefore a statistical significant number of measurements has to be done to get meaningful results. Otherwise the results have to be crosschecked with different geothermometers.

The mineralising fluid is characterised by negative $\delta^{13}C$ values of -14.5 ‰ and positive $\delta^{18}O$ values of 7 ‰ for the siderite veins and by more enriched $\delta^{18}O$ values of 14 - 16 ‰ for the apy-py veins. It seems feasible that the mineralising fluids are influenced by oxidized carbon. Therefore migration of meteoric waters and mixing with metamorphogenic fluids as well as large migration distances are plausible. The high water/rock ratios and the lack of alteration of the host rock carbonates reinforces this assumption. The lateral secretion model of VAVTAR (1982) is therefore not applicable anymore. The sulphur species is changing from H_2S at the vein parts crosscutting the Zentralgneis unit to S^{2-}

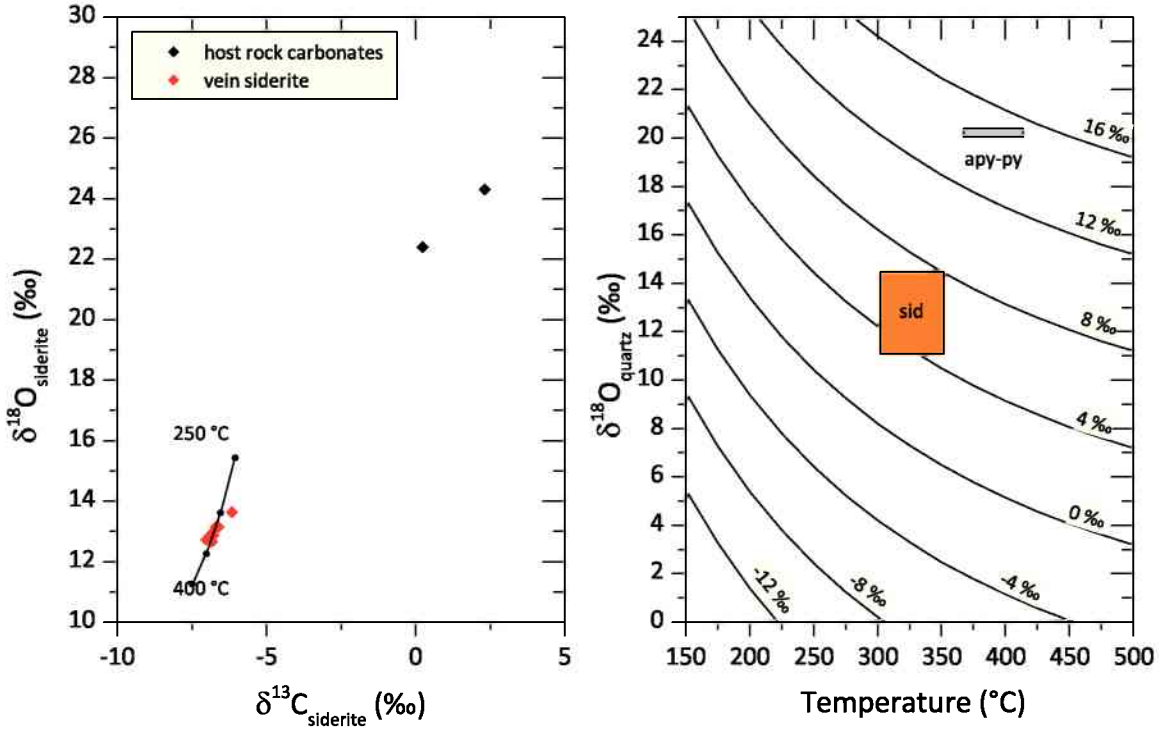

Figure 44: *left: $\delta^{13}C - \delta^{18}O$ plot of Erzwies vein siderites and host rock carbonates. Data fitted by a model for the precipitation of siderite from a CO_2 or H_2CO_3 bearing fluid of constant isotopic composition ($\delta^{13}C = -14.5$ ‰, $\delta^{18}O = 7$ ‰) over a temperature range of 300 - 350 °C. The siderite curve is calculated using the fractionation factors of* Zheng (1999) *for $\Delta_{CO_2-siderite}$ and $\Delta_{siderite-H_2O}$. right: Oxygen isotopic composition of quartz forming fluids at the Erzwies deposit derived from microthermometric data of* Belocky (1992) *and* Feitzinger & Paar (1991) *and oxygen isotope fractionation in the quartz-H_2O system (solid curves:* Sharp & Kirschner, 1994*). The oxygen isotopic composition of the ore forming fluid was $\delta^{18}O = 4 - 8$ ‰for the siderite paragenesis and $\delta^{18}O = 14 - 16$ ‰ for the apy-py paragenesis.*

for the siderite paragenesis. An additional limiting factor of the model is the fact that the chemical composition of the ore veins is very low in CaO and enriched in MnO. The necessary amounts of Mn cannot be explained only by leaching of primary enriched carbonates. The source of the Mn therefore still remains unknown.

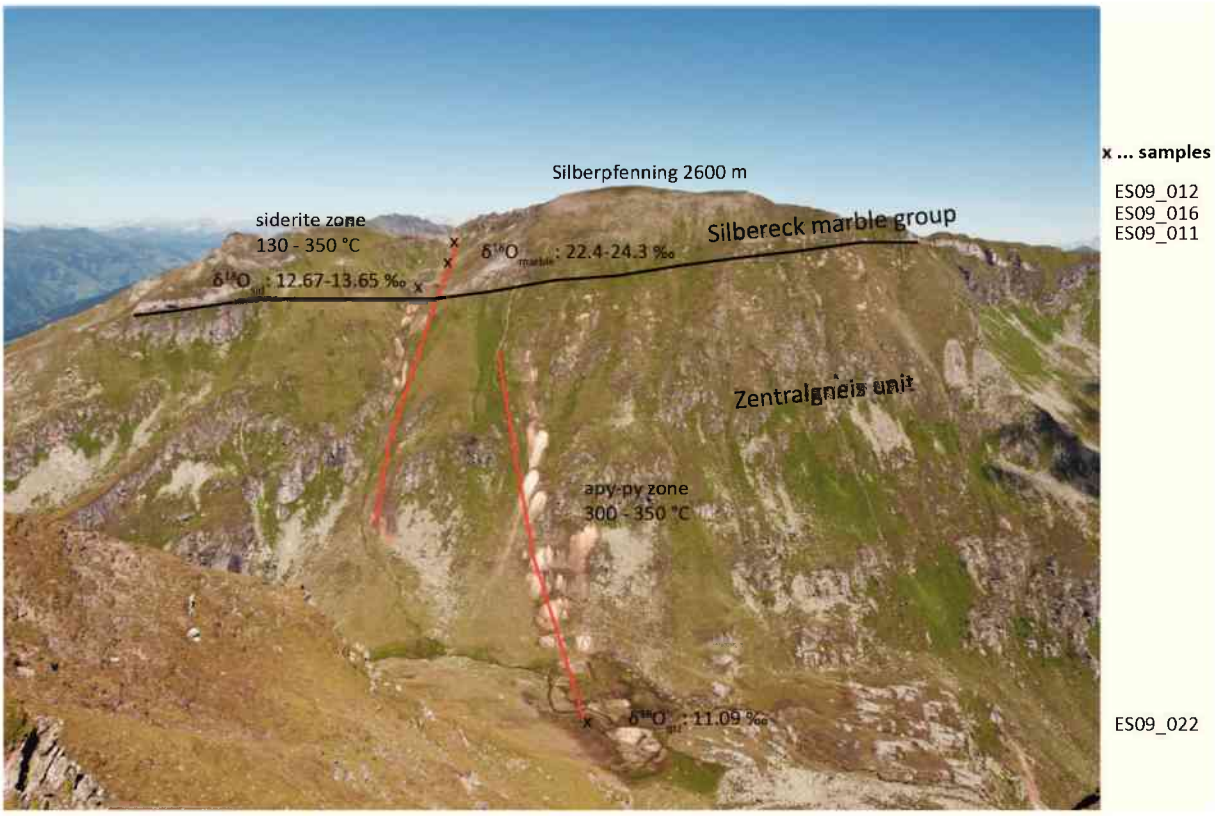

Figure 45: *Southern slope of the Silberpfenning (2600 m) seen from Kolmkarspitz (2529 m). The estimated formation temperatures of the different areas are marked. The red lines mark the two parallel vein systems.*

5. Discussion

5.1. Methodical approach

The main prerequisite using stable isotopes in the mean of a geothermometer is the grade of equilibrium. The determination of isotopic equilibrium between 3 or more phases is relatively simple (JAVOY et al. 1970). But the determination of isotopic equilibrium in the case of two mineral phases is ambivalent. Therefore a different approach is necessary. The first step is to evaluate the textural equilibrium of the mineral assemblage. Textural equilibrium is present when different minerals are crystallized in a granular texture. The grains are of idiomorphic to hypidiomorphic shape and the boundaries form triple junctions. The different mineral phases impede themselves during contemporaneous growth. The mineral phases are evolved from the same fluid and therefore show isotopic equilibrium. This kind of texture is applicable for stable isotope geothermometry. (Figure 46a). When minerals grow independently and temporaneously different they are not in a textural equilibrium. Such minerals cannot demonstrate isotopic equilibrium. Figure 46b shows a mineral phase A where a younger mineral phase B is crosscutting the structure along a joint for example.

Cooling down a precipitate and a possible metamorphic overprint can alter the primary isotopic composition of a mineral assemblage. Calcite and quartz show different exchange rates for oxygen isotopes when they react with a fluid phase. Calcite is therefore affected stronger than quartz. FARVER & YUND (1998) report oxygen grain boundary diffusion rates in calcite aggregates is about 100 times greater than that in feldspar and quartz aggregates. The experimental conditions used (330 to 500 °C, 100 MPa water pressure) approximate natural conditions within hydrothermal systems.

Fluid flow and diffusion (see MANNING, 1974) occur mainly along cleavages (surface diffusion) and grain boundaries (grain boundary diffusion) as well as along mineral cleavage (volume diffusion) (Figure 46c). Atoms in regions of good crystal structure are more restricted and confined in their motion than atoms on free surfaces or grain boundaries (MANNING, 1974). Therefore diffusion along surfaces or boundaries proceeds more readily than volume diffusion.

Vein deposits with quartz-calcite gangue are assumed to be in an ideal equilibrium when the two phases are crystallized alternatingly and the vein does not show any zonation. However exchange reactions with the host rock can influence the isotopic compositions during metamorphic overprint or late alteration caused by fluid flow (Figure 46d). Estimating the grade of isotopic equilibrium or disequilibrium is challenging.

Especially scaling effects due to sampling are crucial. Upscaling from thin-section scale to a vein thickness of several meters in combination with bad outcrop conditions presents a big difficulty. Therefore it is only possible to interpret from a sufficient number of samples. Outliers in stable isotope values and formation may represent younger alteration and contemporaneously isotope exchange effects of vein parts. These values are not showing primary formation conditions.

After selecting appropriate samples with textural equilibrium the choice of analysis method has to be made. SPÖTL & MATTEY (2006) give a practical comparison of microdrill, micromill and laser ablation techniques allied to microsampling of speleothems. Speleothem sampling needs a high spatial resolution. Sampling of gangue mineral inter-

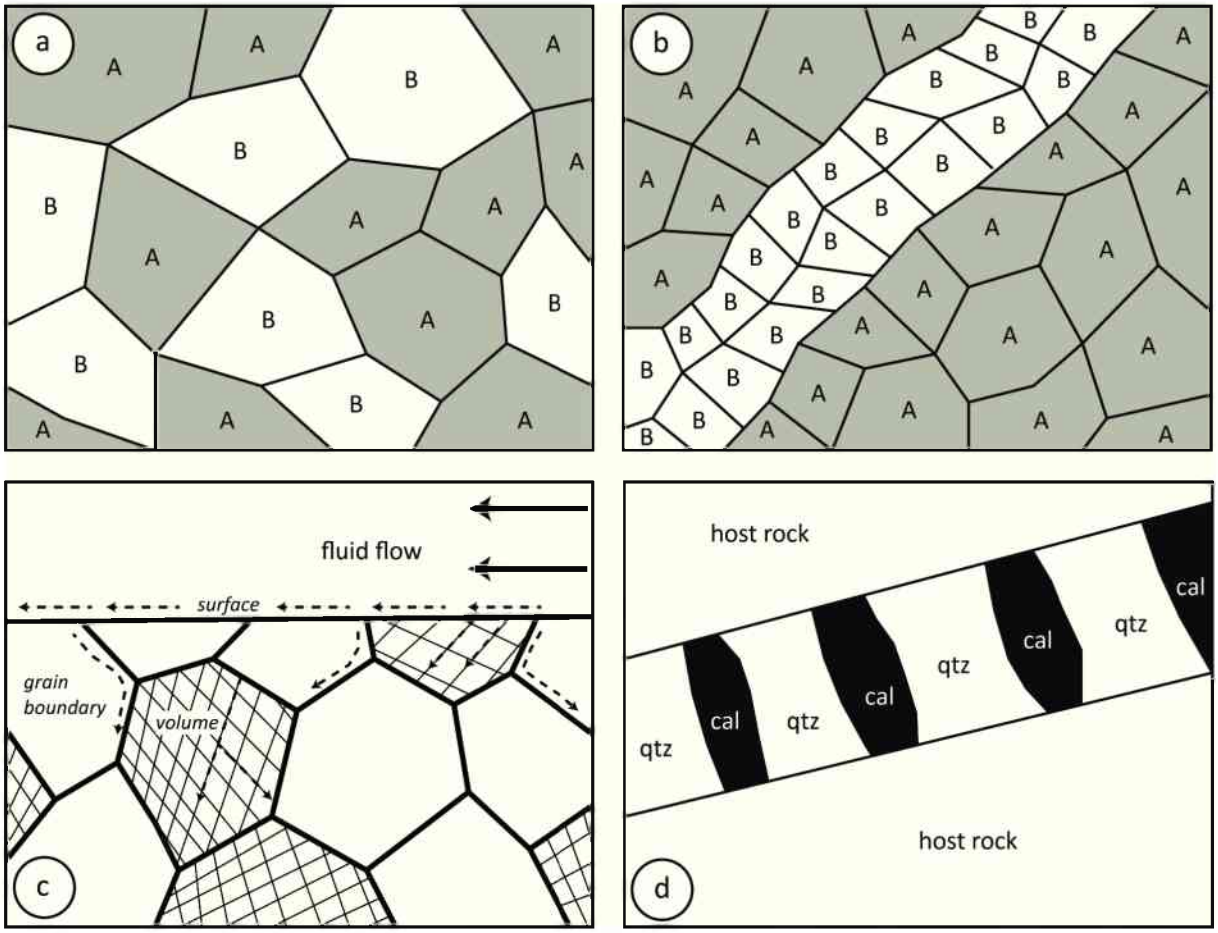

Figure 46: *(a) Interdigitation of two mineral phases A and B in textural equilibrium, (b) Two mineral phases A and B in textural disequilibrium, (c) Schematic diagram illustrating paths of surface diffusion, volume diffusion and grain boundary diffusion (sketch after* MANNING 1974*), (d) Ideal case of vein type mineralisation in textural equilibrium after* SHARP & KIRSCHNER (1994).

growths within ore deposits is similar and can be done in different ways: (1) crushing the sample down to grain size of 1-2 mm with subsequent handpicking and separation of carbonate and quartz grains, (2) manual drilling of carbonate grains - crushing and grinding of the residual sample with subsequent repeated dissolution of carbonate minerals using HCl to receive a quartz concentrate, (3) semi-automated micromilling[12] and (4) laser ablation.

A comparison of different methods suitable for the analysis of carbonates is given in Table 3. Oxygen isotope measurements of quartz can only be done by the laser fluorination method described in Chapter C. Drilling of quartz using tungsten carbide dentist drills is not practicable due to the mineral hardness of quartz. Therefore crushing, hand-picking, grinding and repeated washing with HCl is the most practicable solution to produce a quartz sample for oxygen isotope measurement.

[12]The *MicroMill Sampling Prep Device* of Electro Scientific Industries is the only product on market at the moment.

Method	Measurement precision	Spatial resolution	Time duration
Handpicking	$\delta^{18}O \pm 0.07$ ‰	low	high
	$\delta^{13}C \pm 0.05$ ‰		
Manual microdrilling	$\delta^{18}O \pm 0.07$ ‰	medium	high
	$\delta^{13}C \pm 0.05$ ‰		
Semi-automatic micromilling	$\delta^{18}O \pm 0.07$ ‰	high	high
	$\delta^{13}C \pm 0.05$ ‰		
Laser ablation	$\delta^{18}O \pm 0.3$ ‰	high	low
	$\delta^{13}C \pm 0.2$ ‰		

Table 3: *Summary of different sampling methods in stable isotope analysis applied to carbonate minerals.*

Another crucial point for the application of stable isotopes as geothermometers is the fractionation equation used. Different equations are collected in Table 1. Each equation is only valid for a distinct temperature range. Taking the quartz-calcite mineral pair for example reveals substantial temperature differences. Figure 47 shows formations temperatures in °C versus oxygen isotope fractionation of quartz mineral pairs.

Different equations of various authors are compared: „A" SHARP & KIRSCHNER (1994), „B" ZHENG (1999), „C" Clayton & Keiffer (1991), „D" computed curve with data of SHARP & KIRSCHNER (1994) and ZHENG (1999). Using a fractionation of 2 ‰ between quartz and calcite leads to viable temperature estimations. SHARP & KIRSCHNER (1994) give 390 ±28 °C, ZHENG (1999) shows 190±14 °C and CLAYTON & KEIFFER (1991) show a numerical value of 330 ±18 °C. Computing a fractionation equation for the quartz-calcite pair using the equations of SHARP & KIRSCHNER (1994) for quartz-H_2O and of ZHENG (1999) for calcite-H_2O gives a temperature of 345 ±19 °C. The curves A, C and D are fitting quite well therefore temperature estimations of both seem useful. The equation of ZHENG (1999) gives deviant temperatures due to the enormous temperature range (0 to 1200 °C) it is assumed to be applied. So which calibration should be used at the end? The best thing would be the application of several different calibrations - theoretically based calibrations and empirical ones as well.

Knowledge about the involved carbonate phase is also essential. Figure 48 illustrates the fractionation curves for different quartz-carbonate mineral pairs versus formation temperatures. Calculating formation temperatures with $\triangle_{quartz-carbonate}$ of 2 ‰ gives. Using the equations of SHARP & KIRSCHNER (1994) for quartz-H_2O and of ZHENG (1999) for calcite-H_2O, ankerite-H_2O and siderite-H_2O results in temperature estimations of 344±16 °C for qtz-cal, 302±17 °C for qtz-ank and 251±19 °C for qtz-sid. Fractionation curves of magnesite-H_2O and dolomite -H_2O are parallel and temperatures derived from these equations are similar. Therefore temperature estimations of magnesite and dolomite-magnesite interdigitations are applicable. This fact comes into play when calculating formation temperatures of sedimentary magnesites.

The grade of equilibrium or better the grade of disequilibrium can be used to trace younger hydrothermal alteration of an ore deposit. As discussed before the oxygen composition of carbonates is affected more by migrating younger fluids than quartz (FARVER & YUND, 1998). In this case the covariation for oxygen and carbon isotope ratios is useful to determine the grade of alteration (water/rock ratio). When quartz and carbonates

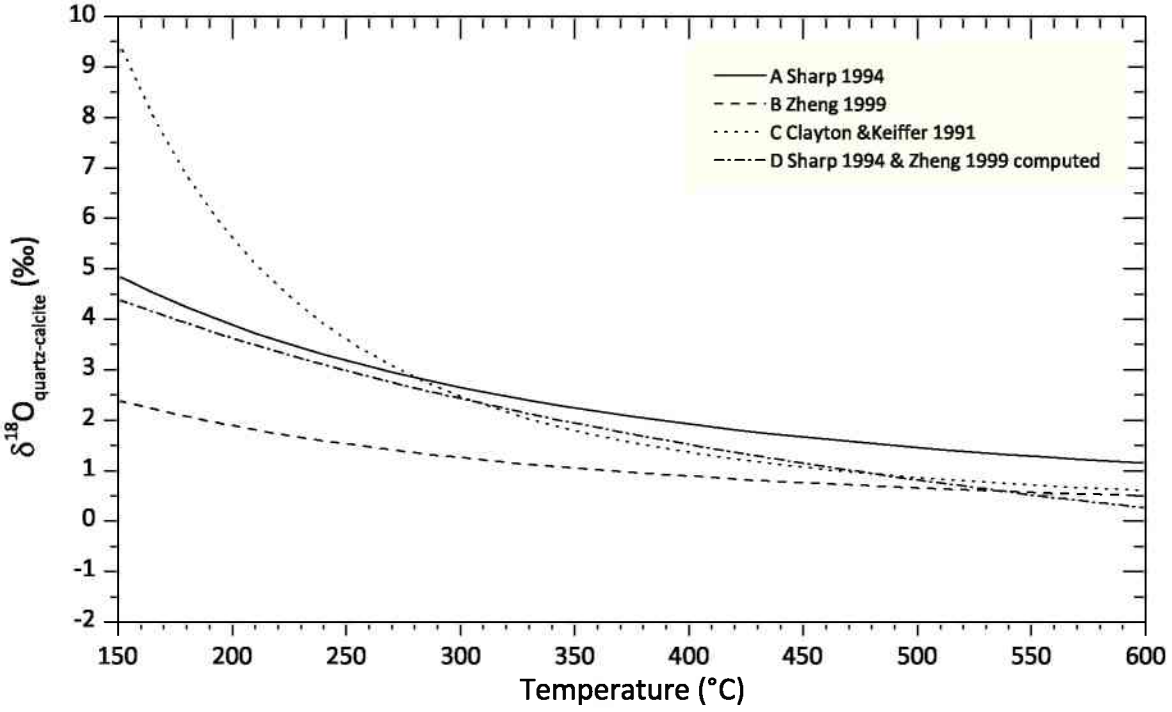

Figure 47: *Formation temperatures [°C] versus oxygen isotope fractionation for the quartz-calcite mineral pairs of different authors: A* Sharp & Kirschner (1994), *B* Zheng (1999), *C* Clayton & Keiffer (1991), *D computed curve with data of* Sharp & Kirschner (1994) *and* Zheng (1999). *For temperatures between 270 and 550 °C curves A, C and D are corresponding quite well. The use of curve B leads to irrealistic temperature estimations when applied to hydrothermal mineralisations.*

are in textural equilibrium measures values of quartz still represent their primary isotopic composition. A similar attempt can be used with sulphides. When the difference between two sulphide phase results in irrealistic temperature estimations a younger fluid alteration is obvious.

5.2. Metallogenetical evolution

Stable isotopic compositions of carbonate and quartz gangue minerals provide more information about ore formation than just temperature. The combination of stable isotope investigations and a profound knowledge of the mineral paragenesis and the regional geological situation allows the interpretation of the metallogenetical evolution of each individual deposit.

The provenance of ore forming fluids of the investigated deposits can be traced back to two distinct groups: The first group shows $\delta^{18}O$ values of obviously hydrothermal deposits like Erzwies-Siglitz, Mitterberg-Buchberg, Radmer, Zinkwand and Tösens with a broad range between 7 and 17.5 ‰. $\delta^{13}C$ is plotting in a more focused range from -8 to -3 ‰. The reconstruction of the involved fluids leads to an oxygen isotopic composition of +7 to +16 ‰ for the carbonate precipitating fluids. The values fall into the field of metamorphogenic waters. Primary magmatic waters, formation waters and volcanic

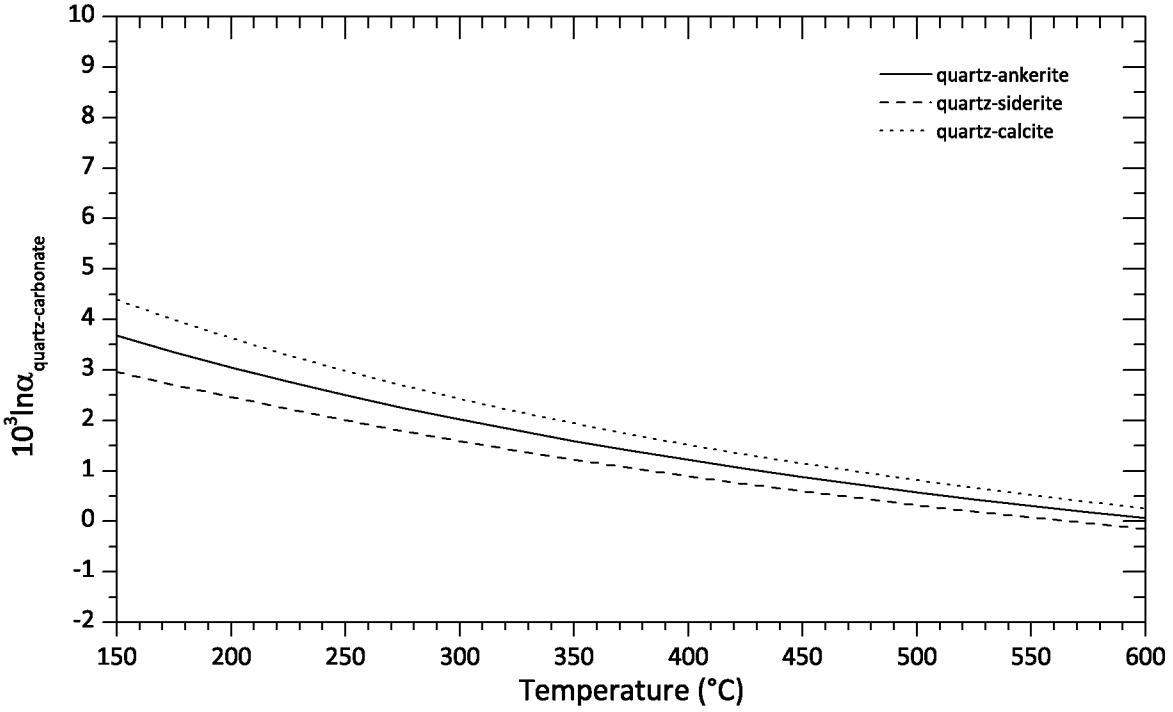

Figure 48: *Oxygen isotope fractionation functions for quartz-calcite , quartz-ankerite and quartz-siderite (based on* Sharp & Kirschner 1994; Zheng 1999*) mineral pairs versus* $\triangle_{quartz-carbonate}$ *. Using a* $\triangle_{quartz-carbonate}$ *of 2 ‰ gives formation temperatures of qtz-cal: 344*$\pm$*16 °C , qtz-ank: 302*$\pm$*17 °C and qtz-sid: 251*$\pm$*19 °C .*

vapour shows $\delta^{18}O$ values between +6 and +10 ‰(Figure 3). A major influence of meteoric water or seawater within the hydrothermal cycle can be excluded using the simple mixing model of Zheng & Hoefs (1993). A mixture of these waters with primary magmatic water, formation water or volcanic vapour would result in isotopically more depleted fluids with $\delta^{18}O$ values well below +10 ‰. Sedimentary rocks show $\delta^{18}O$ values of 11 to 32 ‰ (Hoefs, 2009). During metamorphism waters with $\delta^{18}O$ values of +5 ‰ to +23 ‰ are released (Taylor, 1974). Therefore the only applicable solution are metamorphogenic fluids that precipitate ore deposits with quartz-carbonate gangue. Host rocks for this kind of metamorphogenic waters are formed by metasediments like marbles, organic-rich schists and metasediments. This assumption is reinforced by the carbon isotopic composition of the ore forming fluids. The fluids show negative $\delta^{13}C$ values between -14.5 and -2 ‰. Hydrothermal and thermal decomposition of marine limestones and shales results in fluids depleted in heavy carbon (Zheng & Hoefs, 1993). Mantle derived carbon is also depleted in $\delta^{13}C$ and shows values between -4 and -8 ‰ (Deines, 1980) and can be excluded as source.

The second distinct group is formed by the cryptocrystalline magnesites of the Kraubath deposit. The magnesites show a narrow range between 22.5 and 27.5 ‰ for $\delta^{18}O$ values. $\delta^{13}C$ shows more spreaded values from -22.5 to -10 ‰. In contrast to the hydrothermal deposits an influence of meteoric water is evident. The oxygen isotope composition of the magnesite precipitating solution lies around -2 ‰ and is similar to alkaline, Miocene lake

water of the Lake Pannon (HARZHAUSER et al., 2007) . Mixing depleted, alkaline seawater (-8 ‰) with slightly enriched formation water ($\sim +5$ ‰) provides such conditions.

The evaluation of possible carbon source for the Austroalpine cryptocrystalline magnesite creates some problems. The different possible carbon sources as discussed for Turkish cryptocrystalline magnesite deposits (synopsis in HORKEL 2012) are not applicable at Kraubath. The negative values are assumed to derive either from magmatic carbon (DEINES, 1980) or decarboxylation of biogenic carbonates (GARTZOS et al., 1990; JEDRYSEK & HALAS, 1990). Both possibilities are not possible for Kraubath because surrounding rocks do not show signs of magmatic activity and metacarbonate rocks are not occurring in the surroundings of the deposit. The only possible carbon source is represented by atmospheric CO_2 with a negative $\delta^{13}C$ that is in equilibrium with dissolved CO_2. The absolute values are not computable due to the lack of information about $\delta^{13}C$ of atmospheric CO_2 during Miocene.

The extreme negative values are due to further fractionation along fluid migration pathways. With increasing distance from the main fluid pathways the $\delta^{13}C$ of magnesite decreases. Fluid migration along extensional structures during Miocene is evident.

Stable isotope measurements of the calcite sinter of Maria Buch near Judenburg by SPÖTL in SACHSENHOFER et al. (2000) exhibit $\delta^{13}C$ values of -0.1 to +0.3 ‰ and oxygen values between -13.3 and -11.4 ‰. These values indicate a marine origin of the mineralised waters. SACHSENHOFER et al. (2010) conclude a syn-sedimentary genesis of the calcite sinter. Although an absolute age is not determined a Miocene age seems plausible. In addition the elevated mean temperature of 14 °C as well as B (1650 $\mu g/l$) and Sr (2400 $\mu g/l$) concentrations of mineralised, CO_2- rich spring water near Thalheim speak for deep seated fluid migration paths (ZETINIGG, 1993).

The comparison of the two hydrothermal fluid systems at a regional scale leads to the implication that fluid flow driven by metamorphism is one of the main factors influencing ore genesis within the Eastern Alps. The investigated deposits are different in their tectonostratigraphic position, age and mineralogy. But the mineralising fluids are similar. Eo-Alpine and Neogene metamorphism produced fluids depleted in carbon and enriched in oxygen. POHL & BELOCKY (1994) conclude retrograde leaching as the best model for metamorphogenic metallogenesis, although a possible mantle influx cannot not be neglected. But a major influx of meteoric water can be excluded.

6. Conclusions

6.1. Stable isotope geothermometry - code of best practice

The following section provides informations and rules for the "correct" application of stable isotope geothermometry. These recommendations are only for stable isotope geothermometry and should be crosschecked with classical fluid inclusion techniques like crush-leach analysis and microthermometry to decipher the complexity of hydrothermal ore deposits.

Sampling

The sampling strategy is the first crucial point of all geothermometric applications. It is essential to know the provenance and position of the sample in the deposit. Alteration (silification, argilitic alteration, propylitization, sericitization, greisenization, dolomitization, carbonatization, tourmalinization), weathering and post-depositional fluid flow influences and overprints primary isotopic signatures.When applicable samples have to be taken in form of sections across veins and at different elevation levels to cover a broad range of formation temperatures and possibly influenced vein parts.

Estimation of isotopic equilibrium

A determination of quartz-carbonate interdigitation has to be done macroscopically and microscopically. Granular texture is the main prerequisite of isotopic equilibrium and therefore temperatures estimated are most likely formation temperatures. Younger crosscutting veinlets provide information about remobilisation processes.

Selection of analytical method

The selection of an analytical method is influenced by the factors measurement precision, time and cost. Therefore the a target oriented choice between microdrilling, micromilling and laser ablation has to be made. An outline of oxygen measurements of quartz-carbonate pairs with subsequent refinement done by micromill and/or microdrill methods would return the best results.

Selection of fractionation equation

A realistic temperature estimation done with oxygen isotope mineral pairs stands and falls with the fractionation equation applied. For the quartz-calcite, the quartz-ankerite and the quartz-siderite mineral pairs computed equations with data of SHARP & KIRSCHNER (1994) and ZHENG (1999) provide formation temperatures in good agreement with classical geothermometers. When only one carbonate or silicate phase is present a plausible estimation of the oxygen fractionation of the mineralising fluid has to be done.

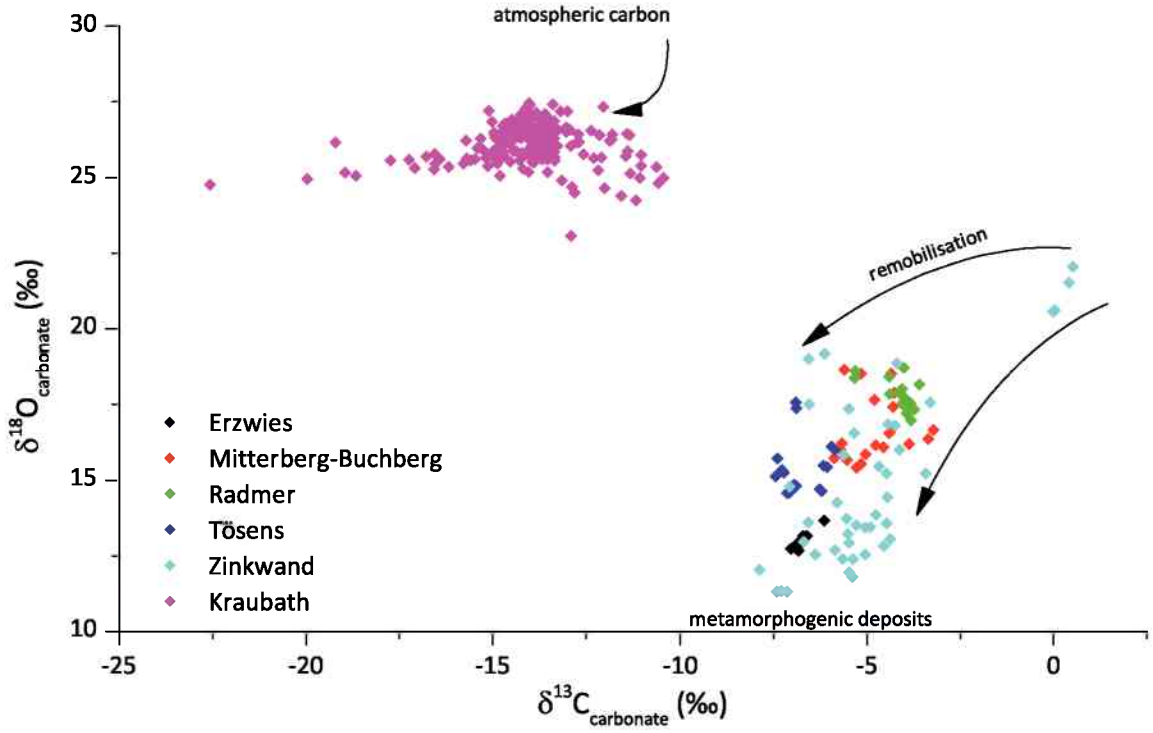

Figure 49: *Oxygen and carbon isotopic compositions of gangue carbonates hosted by metamorphogenic and low-tempered hydrothermal/sedimentary ore deposits. The metamorphogenic deposits are of different formation ages but the mineralising fluids are similar an have equilibrated during migration through the crust. The low-tempered hydrothermal/sedimentary magnesite deposit shows strong fractionation of carbon due to fractionation during migration and strong meteoric influx.*

6.2. Regional geologic implications

Comparing the results of the individual deposits described in Chapter 4 gives insights into ore formation within the Austroalpine and Sub-Penninic units. Isotopic compositions of gangue quartz and carbonates reveal two different groups of ore deposits (Figure 49). Vein type deposits are of metamorphogenous origin and present party remobilised primary enriched or fine dispersed metals. Metamorphism with accompanying temperature, pressure and fluid flow leaches primary deposited metals from metasediments. Transportation happened via acidic fluids and subsequent deposition occurred at temperatures of 300 to 450 °C for sulphides and lower temperatures for carbonates and quartz.

Gold district Rauris-Gastein

Massive fluid flow driven by the E directed movements of the Neogene extrusion tectonics (Frisch et al. 1998) and the updoming of the Tauernwindow with subsequent brittle tectonics formed the main favourable conditions for ore genesis within the Sub-Penninic units. The mineralising fluid was characterised by positive $\delta^{18}O$ values between 7 and 16 ‰. The negative $\delta^{13}C$ values derive from oxidized carbon. The isotopic composition of the mineralising fluids is due to minor mixing of meteoric or formation waters with metamorphogenic waters. The main transport medium for the dissolved carbon species

is formed by metamorphogenic water.

Copper district Mitterberg-Mühlbach-Larzenbach

Fluid flow and ore deposition at the copper district Mitterberg-Mühlbach-Larzenbach are closely linked to Eo-Alpine metamorphism. (KRALIK et al. 1987) report metamorphic conditions between sub-greenschist and greenschist facies from higher structural levels like the Mitterberg area. Nappe stacking provided temperature and pressure for fluid movement. The mineralising fluid was characterised by enrichment in oxygen (15 to 17 ‰) and sparse depletion in heavy carbon (-6 to -4 ‰). The carbon value represents crustal average. During migration the fluids were influenced by sulphate bearing formation waters hosted by hangingwall Permian sediments (Werfen formation). Stratabound mineralisations were remobilised and subsequently deposited in form of ore veins. Migration distances therefore were limited. A similar mineralisation is the Au bearing copper mineralisation at Larzenbach/Hüttau where stratabound as well as discordant veins occur within low grade metasedimentary rocks (KUCHA & RAITH, 2009).

Iron (Copper) district Noric Nappe

Ore genesis is closely linked with Eo-Alpine orogenesis. The mineralising fluid strongly influenced through the migration within the hangingwall Permian evaporites and marine sediments of the Northern Calcareous Alps. The fluid was characterised by enrichment in oxygen (9 to 13 ‰) and sparse depletion in heavy carbon (-2 to -4 ‰).

Chromite-Asbestos-Magnesite district Hochgrössen-Kraubath

Magnesite genesis at Kraubath is linked with extensional movements causing the subsidence of the Fohnsdorf basin during Miocene. Alkaline lake waters and meteoric waters migrating within the ultramafic rocks and leaching Mg^{2+}. Alkaline lake waters with $\delta^{13}C$ values of -2 ‰ caused the precipitation of vein type magnesite. These waters result from the mixing of fresh meteoric water and groundwater with longer retention times. During migration groundwaters are getting enriched in $\delta^{18}O$ due to leaching of serpentine minerals. The more depleted lake waters (up to -8 ‰) are the source of sedimentary magnesite.

Polymetallic ore district Schladming

The Ni-Co-Bi mineralisation was formed after the Eo-Alpine metamorphic peak when extensional tectonics provided pathways for fluid migration. A relatively high tempered, metamorphogenous brine derived from phyllonitic blackschist due to retrograde leaching mixed with low tempered meteoric waters. Fluid migration distance was limited to black schists within the Schladming crystalline.

Polymetallic Cu-Fe-Zn-Pb district Stubai-Ötztal

The ore deposit of Tösens is linked with Alpine nappe stacking. Relatively high tempered metamorphogenic brines remobilised primary enriched metasediments. The mineralising

fluids show enrichment in oxygen between 13 and 15.5 ‰.

6.3. Concluding remarks

Some questions on stable isotope geothermometry have been answered. But stable isotope investigations applied to ore deposits in the Austroalpine remain challenging in the future. The good knowledge of the structure and relatively well known geological history of the Eastern Alps makes it possible to reconstruct fluid flows in time and space as well as at a regional scale. Especially the great number of small and medium ore deposits within the Palaeozoic units (Greywackezone nappe system or Graz Palaeozoic) provides a broad field of study. The understanding of fluid flow and precipitation mechanisms is still a crucial point in the evaluation of ore deposits. Stable isotope investigations provide a fast and relatively inexpensive method for gaining knowledge about these processes when the methods are applied at samples deriving from well known positions within mineral deposits and the results are evaluated carefully.

Direct measurements of stable isotope ratios on primary fluid inclusion of the investigated deposits would provide information about the mineralising fluids directly and would allow an examination of the applied fluid provenance reconstructions. Especially at the Kraubath magnesite deposit direct measurements of the mineralising fluids would provide further insights. But this kind of analysis is still an elaborate one and not practicable as a standard routine in economic geology.

References

Bakker, R.: 2011. The use of quantities, units and symbols in fluid inclusion research. *Berichte der Geologischen Bundesanstalt 87*, 5–11.

Barnes, I. & O'Neil, J.: 1969. The relationship between fluids in some fresh alpine-type ultramafics and possible modern serpentinitization, Western United States. *Geological Society of America Bulletin 80*, 1947–1960.

Bashir, E., Naseem, S., Akthar, T., & Shireen, K.: 2009. Characteristics of ultramafic rocks and associated magnesite deposits, Nal Area, Khuzdar, Baluchistan, Pakistan. *Journal of Geology and Mining Research 1*, 34–41.

Bashir, E., Naseem, S., Sheikh, S., & Kaleem, M.: 2009. Mineralogy of the Kraubath-type magnesite deposits of the Khuzdar area, Balochistan, Pakistan. *Journal of the Earth Sciences Application and Research Centre of Hacettepe University 30*, 169–180.

Belocky, R.: 1992. Regional vergleichende Untersuchung lagerstättenbildender Fluide in den Ostalpen als Hinweis auf eine mögliche metamorphe Ableitung. *Braunschweiger geologisch-paläontologische Dissertationen 14*, 1–103.

Bernhard, J.: 1965. Die Mitterberger Kupferkieslagerstätte Erzführung und Tektonik. *Jahrbuch der Geologischen Bundesanstalt 109*, 3–90.

Bottomley, D., Renaurd, J., Kotzer, T., & Clark, I.: 2002. Iodine-129 constraints on residence times of deep marine brines in the Canadian Shield. *Geology 30*, 587–590.

Bottrell, S., Yardley, B., & Buckley, F.: 1988. A modified crush-leach method for the analysis of fluid inclusion electrolytes. *Bulletin Minéralogie 111*, 279–290.

Braithwaite, C. & Zedef, V.: 1996. Hydromagnesite stromatolites and sediments in an alkaline lake, Salda Gölü, Turkey. *Journal of Sedimentary Research 5*, 991–1002.

Buttmann, H.: 1913. Die Kupferkieslagerstätten von Mitterberg. Ph.D. thesis, Königl. Sächs. Bergakademie zu Freiberg.

Canfield, D., Farquhar, J., & Zerkle, A.: 2010. High isotope fractionations during sulfate reduction in a low-sulfate euxinic ocean analog. *Geology 38*, 5, 415–418.

Canfield, D. & Thamdrup, B.: 1994. The production of 34S-depleted sulfide during bacterial disproportionation of elemental sulfur. *Science 266*, 1973–1975.

Claypool, G., Holser, W., Kaplan, I., Sakai, H., & Zak, I.: 1980. The age curves of sulfur and oxygen isotopes in marine sulfate and their mutual interpretation. *Chemical Geology 28*, 199–260.

Clayton, R. & Keiffer, S.: 1991. Oxygen isotopic thermometer calibrations. In *Stable Isotope Geochemistry: A tribute to Samuel Epstein*, H. Taylor, J. O'Neil, & I. Kaplan, Eds. Number 3 in Special Publication. The Geochemical Society, 3–10.

CLAYTON, R., O'NEIL, J., & MAYEDA, T.: 1972. Oxygen isotope exchange between quartz and water. *Journal of Geophysical Research 77*, 3057–3067.

DABITZIAS, S.: 1980. Petrology and genesis of the Vavdos cryptocrystalline magnesite deposits, Chalkidiki peninsula, Northern Greece. *Economic Geology 75*, 1138–1151.

DÍAZ-GONZÁLEZ, L., SANTOYO, E., & REYES-REYES, J.: 2008. Tres nuevos geotermómetros mejorados de Na/K usando herramientas computacionales y geoquimiométricas: aplicación a la predicción de temperaturas de sistemas geotérmicos. *Revista mexicana de ciencias geológicas 25*, 465–482.

DEINES, P.: 1980. The carbon isotopic composition of diamonds: Relationship to diamond shape, color, occurrence and vapor composition. *Geochimica et Cosmochimica Acta 44*, 943–961.

DIETMAYER-KRÄUTLER, M.: 2013. Untersuchungen an ausgewählten Magnesitlagerstätten Serbiens. B.Sc. thesis, Montanuniversität Leoben.

DOLNICEK, Z., FOJT, B., PROCHASKA, W., KUCERA, J., & SULOVSKY, P.: 2009. Origin of the Zalesi U-Ni-Co-As-Ag/Bi deposit, Bohemian Massif, Czech Republic: fluid inclusion and stable isotope constraints. *Mineralium Deposita 44*, 81–97.

EBNER, F.: 1997. Die geologischen Einheiten Österreichs und ihre Rohstoffe. In *Handbuch der Lagerstätten der Erze, Industrieminerale und Energierohstoffe Österreichs*, L. WEBER, Ed. Archiv für Lagerstättenforschung, 19. 49–229.

EBNER, F.: 1998. Die Entwicklungsgeschichte der Ostalpen und ihre Beziehung zu den Lagerstätten. *Berg- und Hüttenmännische Monatshefte 143*, 209–214.

EBNER, F.: 2002. Alpidische Stoffmobilisation und Lagerstättenbildung in den Ostalpen. *Berg- und Hüttenmännische Monatshefte 147*, 397–402.

EBNER, F., CERNY, I., EICHHORN, R., GÖTZINGER, M., PAAR, W., PROCHASKA, W., & WEBER, L.: 1999. Mineral Resources in the Eastern Alps and Adjoining Areas. *Mitteilungen der Österreichischen Geologischen Gesellschaft 92*, 157–184.

EBNER, F., DIETMAYER, M., KROISSENBRUNNER, P., MALI, H., UNTERWEISSACHER, T., & HORKEL, K.: 2012. Cryptocrystalline magnesite hosted by sediments adjoining ultramafic rock complexes. In *Proceedings 29th Meeting of Sedimentology*, S. MISSONI & H. GAWLICK, Eds. International Association of Sedimentologists, Schladming, 605.

EBNER, F. & WILSON, I.: 2006. Magnesit- globales Potenzial und geologische Lagerstättencharakteristik. *Berg- und Hüttenmännische Monatshefte 151*, 164–174.

ECE, O., MATSUBAYA, O., & ÇOBAN, F.: 2005. Genesis of hydrothermal stockwork-type magnesite deposits associated with ophiolite complexes in the Kütahya-Eskişehir region, Turkey. *Neues Jahrbuch für Mineralogie, Abhandlungen 181,* 2, 191–205.

EXNER, C.: 1962. Geologische Karte der Sonnblickgruppe 1:50 000. Geologische Bundesanstalt, Wien.

FALLICK, A., ILICH, M., & RUSSEL, M.: 1991. A stable isotope study of the magnesite deposits associated with the alpine-type ultramafic rocks of Yugoslavia. *Economic Geology 86*, 847–861.

FANLO, I., SUBIAS, I., GERVILLA, F., PANIAGUA, A., & GARCIA, B.: 2004. The composition of Co-Ni-Fe Sulfarsenides, diarsenides and triarsenides from the San Juan de Plan deposit, Central Pyrenees, Spain. *Canadian Mineralogist 42*, 1221–1240.

FARVER, J. R. & YUND, R.: 1998. Oxygen grain boundary diffusion in natural and hot-pressed calcite aggreates. *Earth and Planetary Science Letters 161*, 189–200.

FEHN, U. & SNYDER, G.: 2005. Residence times and source ages of deep crustal fluids: interpretation of ^{129}I and ^{36}Cl results from the KTB-VB drill site, Germany. *Geofluids 5*, 42–51.

FEITZINGER, G. & PAAR, W.: 1991. Gangförmige Gold-Silber-Vererzungen in der Sonnblickgruppe (Hohe Tauern, Kärnten). *Archiv für Lagerstättenforschung der Geologischen Bundesanstalt 13*, 17–50.

FINGER, F., FRASL, G., HAUNSCHMID, B., LETTNER, H., VON QUADT, A., SCHERMAIER, A., SCHINDLMAYR, A., & STEYRER, H.: 1993. The Zentralgneise of the Tauern Window (Eastern Alps): Insight into an Intra-Alpine Variscan Batholith. In *Pre-Mesozoic Geology in the Alps*, J. RAUMER & F. NEUBAUER, Eds. Springer, Berlin, 515–535.

FOUILLAC, C. & MICHARD, G.: 1981. Sodium/lithium ratio in water applied to geothermometry of geothermal reservoirs. *Geothermics 10*, 55–70.

FRANK, W.: 1987. Evolution of the Austroalpine Elements in the Cretaceous. In *Geodynamics of the Eastern Alps*, H. FLÜGEL & P. FAUPL, Eds. Deuticke, Vienna, 379–406.

FRANK, W. & WEBER, L.: 1997. Lagerstättenbildung in Zusammenhang mit Metamorphosevorgängen. In *Handbuch der Lagerstätten der Erze, Industrieminerale und Energierohstoffe Österreichs*, L. WEBER, Ed. Archiv für Lagerstättenforschung der Geologischen Bundesanstalt, 542–544.

FRIEDMAN, I. & O'NEIL, J.: 1977. Compilation of stable isotope fractionation factors of geochemical interest. *U.S. Geol. Surv. Prof. Pap. 440-KK,*, 49 pp.

FRIEDRICH, O.: 1968. Die Vererzung der Ostalpen, gesehen als Glied des Gebirgsbaues. *Archiv für Lagerstättenforschung in den Ostalpen 8*, 1–136.

FRIEDRICH, O.: 1975. Kurzbericht über die Vererzung der Schladminger Tauern. *Archiv für Lagerstättenforschung in den Ostalpen 15*, 117–127.

FRISCH, W., KUHLEMANN, J., DUNKL, I., & SCHUSTER, R.: 1998. Palinspastic reconstruction and topographic evolution of the Eastern Alps during late Tertiary extrusion. *Tectonophysics 297*, 1–15.

FROITZHEIM, N., PLASIENKA, D., & SCHUSTER, R.: 2008. Alpine tectonics of the Alps and Western Carpathians. In *The geology of central Europe. Volume 2: Mesozoic and Cenozoic*, T. MCCANN, Ed. Geological Society London, 1141–1232.

FUCHS, H.: 1988. Erzmikroskopische und mineralchemische Untersuchungen der Erzvorkommen Zinkwand - Vöttern in den Niederen Tauern bei Schladming. *Archiv für Lagerstättenforschung der Geologischen Bundesanstalt 9*, 33–45.

GARTZOS, E.: 1990. Carbon and oxygen isotope constraints and the origin of magnesite deposits, North Evia (Greece). *Schweizer Mineralogisch Petrographische Mitteilungen 70*, 67–72.

GODOVIKOV, A. & KOLONIN, G.: 1966. Experimentelle Untersuchungsbedingungen von Wismut und die Möglichkeiten deiner Benutzung als geologisches Thermometer. *Zeitschrift für Angewandte Geologie 12*, 128–130.

GOLYSHEV, S., PADALKO, N., & PECHENKIN, S.: 1981. Fractionation of stable oxygen and carbon isotopes in carbonate systems. *Geochemistry International 18*, 85–99.

GREGORY, R. & CRISS, R.: 1986. Isotopic exchange in open and closed systems. In *Stable Isotopes in High Temperature Geological Processes*, J. VALLEY, H. TAYLOR, & J. O'NEIL, Eds. 16. Mineralogical Society of America,, Washington, 91–127.

HAFELLNER, M.: 1995. Chemische Untersuchungen lagerstättenbildender Fluide ausgewählter Lagerstätten in den Ostalopen. M.S. thesis, Montanuniversität Leoben.

HAMMER, W.: 1923. Geologische Spezialkarte der Republik Österreich 1:75 000 - 5245 Nauders. Geologische Bundesanstalt, Wien.

HARZHAUSER, M., LATAL, C., & PILLER, W. E.: 2007. The stable isotope archive of Lake Pannon as a mirror of Late Miocene climate change. *Palaeogeography, Palaeoclimatology, Palaeoecology 249*, 335–350.

HEINRICHS, H. & HERRMANN, A.: 1990. *Praktikum der analytischen Geochemie*, Springer. 669 pp.

HEJL, E.: 1997. "Cold spots" during the Cenozoic evolution of the Eastern Alps: thermochronological interpretation of apatite fission-track data. *Tectonophysics 272*, 159–173.

HEJL, E., ROCKENSCHAUB, M., & SLAPANSKY, P.: 1987. Geochronologische Daten aus den Schladminger Tauern und ihre geologische Interpretation. *Arbeitstagung der Geologischen Bundesanstalt Blatt 127 Schladming*, 94–103.

HEJL, E. & SLAPANSKY, P.: 1984. Neue petrographische und geochemische Daten zur Metamorphose im Bereich der Schladminger Tauern. *Jahresbericht Hochschulschwerpunkt S 15 4*, 17–31.

HIESSLEITNER, G.: 1929. Das Nickelkobalterzvorkommen Zinkwand-Vöttern in den Niederen Tauern bei Schladming. *Berg- und Hüttenmännisches Jahrbuch 79*, 203–240.

HIESSLEITNER, G. & CLAR, E.: 1950. Der Blei-Silberbergbau Tösens. Unpublished report, Klagenfurt.

HÖLL, R.: 1975. Die Scheelitlagerstätte Felbertal und der Vergleich mit anderen Scheelitvorkommen in den Ostalpen. *Bayer. Akad. Wiss., math.-natw. Kl. Abh., N. F. 157 A-B*, 114.

HÖLL, R. & EICHHORN, R.: 2001. Tungsten Mineralization and Metamorphic Remobilization on the Felbertal Scheelite Deposit, Central Alps, Austria. *Reviews in Econmic Geology 11*, 233–264.

HOECK, V. & KOLLER, F.: 1999. Mesozoic metamorphic evolution of the Tauern Window. *Acta Montanistica Slavica 2*, 145–147.

HOEFS, J.: 2009. *Stable Isotope Geochemistry*, Springer. 285 pp.

HORKEL, K.: 2012. Integrated geological and geophysical exploration methods for cryptocrystalline magnesite. Ph.D. thesis, Montanuniversität Leoben.

JAVOY, M., FOURCADE, S., & ALLEGRE, C.: 1970. Graphical method for examination of 18O/16O fractionations in silicate rocks. *Earth and Planetary Science Letters 10*, 12–16.

JEDRYSEK, M. & HALAS, S.: 1990. The origin of magnesite deposits from the Polish Foresudetic Block ophiolites: preliminary δ^{18}O and δ^{13}C investigations. *Terra Research 2*, 154–159.

JURKOVIC, I. & PAMIC, J.: 2003. Carbon and oxygen isotope composition of the Dinaridic ophiolite related magnesites. In *Mineral Exploration and Sustainable Development*, D. ELIOPOULOS et al., Ed. 2. Millpress, 883–886.

KADIR, S., KOLAYLI, H., & EREN, M.: 2012. Genesis of sedimentary- and vein-type magnesite deposits at Kop Mountain, NE Turkey. *Turkish Journal of Earth Sciences 21*, 1–18.

KAMPSCHULTE, A. & STRAUSS, H.: 2004. The sulfur isotopic evolution of Phanerozoic seawater based on the analysis of structurally substituted sulfate in carbonates. *Chemical Geology 204*, 255–286.

KEELING, C.: 1961. The concentration and isotopic abundances of carbon dioxide in rural and marine air. *Geochimica et Cosmochimica Acta 24*, 322–334.

KEELING, C., WHORF, T., WAHLEN, M., & VAN DER PFLICHT, J.: 1995. Interannual extremes in the rate of rise of atmospheric carbon dioxide since 1980. *Nature 375*, 666–670.

KERESTEDJIAN, T.: 1997. Chemical and morphological features of arsenopyrite, concerning its use as a geothermometer. *Mineralogy and Petrology 60*, 231–243.

KHARAKA, Y. & MARINER, R.: 1989. Chemical Geothermometers and their Application to formation waters of sedimenary basins. In *Thermal history of sedimentary basins, Methods and case studies*, N. NAESER & T. MCCULLOH, Eds. 319 pp.

KLEMM, D.: 1965. Synthesen und Analysen in den Dreiecksdiagrammen FeAsS-CoAsS-NiAsS und FeS2-CoS2-NiS2. *Neues Jahrbuch Mineralogische Abhandlungen 103*, 205–255.

KÖPPEL, V.: 1997. Bleisotope. In *Handbuch der Lagerstätten der Erze, Industrieminerale und Energierohstoffe Österreichs*, L. WEBER, Ed. Archiv für Lagerstättenforschung der Geologischen Bundesanstalt, 485–495.

KRALIK, M., KRUMM, H., & SCHRAMM, M.: 1987. Low grade and very low grade metamorphism in the Northern Calcareous Alps and in the Greywacke Zone; illite crystallinity data and isotopic ages. In *Geodynamics of the Eastern Alps*, H. FLÜGEL & P. FAUPL, Eds. 164–178.

KRETSCHMAR, U. & SCOTT, S.: 1976. Phase relations involving arsenopyrite in the system Fe-As-S and their application. *Canadian Mineralogist 14*, 364–386.

KRETZ, R.: 1983. Symbols for rock-forming minerals. *American Mineralogist 68*, 277–279.

KROISSENBRUNNER, P.: 2012. Zu den δ^{18}O und δ^{13}C Isotopenverhältnissen des Kraubather Magnesits (Augraben und Gulsen). B.Sc. thesis, Montanuniversität Leoben.

KUCHA, H. & RAITH, J.: 2009. Gold-oxysulphides in copper deposits of the Greywacke Zone, Austria: A mineral chemical and infrared fluid inclusion study. *Ore Geology Reviews 35*, 87–100.

LI, Y. & LIU, J.: 2006. Calculation of sulfur isotope fractionation in sulfides. *Geochimica et Cosmochimica Acta 70*, 1789–1795.

LIU, Y., GENSER, J., HANDLER, R., FRIEDL, G., & NEUBAUER, F.: 2001. ^{40}Ar/^{39}Ar muscovite ages from the Penninic-Austroalpine plate boundary, Eastern Alps. *Tectonics 20*, 526–547.

MACAULAY, C., FALLICK, A., HASZELDINE, R., & GRAHAM, C.: 2000. Methods of laser-based stable isotope measurements applied to diagenetic cements and hydrocarbon reservoir quality. *Clay Minerals 35*, 313–322.

MANDL, G. & MATURA, A.: 1995. Geologische Karte der Republik Österreich 1.50 000 - 127 Schladming. Geologische Bundesanstalt, Wien.

MANNING, J.: 1974. Diffusion kinetics and mechansism in simple crystals. In *Geochemical Transport and Kinetics*, A. HOFMANN, B. GILETTI, H. YODER, & R. YUND, Eds. 634. Carnegie Institution of Washington Publication, 3–15.

MARTIN, A., BRASIER, A., FALLICK, A., PRAVE, A., CONDON, D., ROMASHKIN, A., RYANCHIK, D., LEPLAND, A., & MELEZHIK, V.: 2012. Oxygen isotope ratios in amygdaloidal silica from 2058 Ma Kuetsjärvi Volcanic Formation, Russia. *Chemical Geology submitted*, –.

MATSUHISA, Y., GOLDSMITH, J., & CLAYTON, R.: 1979. Oxygen isotope fractionation in the system quartz-albite-anorthite-water. *Geochimica et Cosmochimica Acta 43*, 1131–1140.

MATURA, A.: 1980. Die Schladminger und Wölzer Tauern. In *Der geologische Aufbau Österreichs*, R. OBERHAUSER, Ed. Springer, 363–368.

MATURA, A.: 1987. Schladminger Kristallinkomplexe. *Arbeitstagung der Geologischen Bundesanstalt Blatt 127 Schladming*, 13–24.

MCCAFFREY, M., LAZAR, B., & HOLLAND, H.: 1987. The evaporation path of seawater and the coprecipation of Br^- and K^+ with halite. *Journal of Sedimentary Petrology 57*, 928–937.

MELCHER, F. & MEISEL, T.: 2004. A Metamorphosed Early Cambrian Crust-Mantle Transition in the Eastern Alps, Austria. *Journal of Petrology 45*, 1689–1723.

MELCHER, F., MEISEL, T., PUHL, J., & KOLLER, F.: 2002. Petrogenesis and geotectonic setting of ultramafic rocks in the Eastern Alps: constraints from geochemistry. *Lithos 65*, 69–112.

MISRA, K. & FLEET, M.: 1975. Textural and compositional variations in a Ni-Co-As assemblage. *Canadian Mineralogist 13*, 8–14.

NEUBAUER, F.: 1988. Bau und Entwicklungsgeschichte des Rennfeld-Mugel- und des Gleinalm-Kristallins (Ostalpen). *Abhandlungen der Geologischen Bundesanstalt 42*, 1–136.

NEUBAUER, F.: 1994. Kontinentkollision in the Ostalpen. *Die Geowissenschaften 12*, 136–140.

NEUBAUER, F., DALLMEYER, R., DUNKL, I., & SCHIRNIK, D.: 1995. Late Cretaceous exhumation of the metamorphic Gleinalm Dome, Eastern Alps: kinematics, cooling history and sedimentary response in sinistral wrench corridor. *Tectonophysics 242*, 79–98.

NEUBAUER, F. & FRISCH, W.: 1993. The Austro-Alpine Metamorphic Basement E of the Tauern Window. In *Pre-Mesozoic Geology in the Alps*, J. RAUMER & F. NEUBAUER, Eds. Springer, Berlin, 515–535.

NEUBAUER, F., HANDLER, R., HERMANN, S., & PAULUS, G.: 1994. Tectonostratigraphy and structure of the Eastern Greywacke Zone, Eastern Alps. *Mitteilungen der Österreichischen Geologischen Gesellschaft 87*, 61–74.

OFNER, L.: 2002. Charakteristik der Kupfermineralisationen im Raum Eisenerz - Radmer - Johnsbach (Grauwackenzone/Steiermark). M.S. thesis, Montanuniversität Leoben.

OHMOTO, H.: 1972. Systematics of Sulfur and Carbon Isotopes in Hydrothermal Ore Deposits. *Economic Geology 67*, 551–578.

OHMOTO, H. & RYE, R.: 1979. Isotopes of sulfur and carbon. In *Geochemistry of Hydrothermal Ore Deposits*, H. BARNES, Ed. John Wiley & Sons, 509–567.

O'NEIL, J.: 1986. Theoretical and Experimental Aspects of Isotopic Fractionation. In *Stable Isotopes in High Temperature Geological Processes*, J. VALLEY, H. TAYLOR, & J. O'NEIL, Eds. Reviews in Mineralogy, 16. Mineralogical Society of America, 1, 1–40.

PAAR, W.: 1978. Die Uranknollen-Paragenese von Mitterberg (Salzburg, Österreich). *Neues Jahrbuch Mineralogische Abhandlungen 131*, 254–271.

PAAR, W.: 1997. Edelmetalle. In *Handbuch der Lagerstätten der Erze, Industrieminerale und Energierohstoffe Österreichs*, L. WEBER, Ed. Archiv für Lagerstättenforschung der Geologischen Bundesanstalt, 276–287.

PAAR, W. & CHEN, T.: 1979. Gersdorffit (in zwei Strukturvarietäten) und Sb-hältiger Parkerit, $Ni_3(Bi,Sb)_2S_2$, von der Zinkwand, Schladminger Tauern, Österreich. *TMPM Tschermaks Mineralogisch Petrographische Mitteilungen 26*, 59–67.

PESTAL, G., HEJL, E., BRAUNSTINGL, R., & SCHUSTER, R.: 2009. Geologische Karte von Salzburg 1:200.000: Erläuterungen. *Geologische Bundesanstalt, Wien*, 1–162.

PETRASCHECK, W.: 1926. Das Alter alpiner Erze. *Verhandlungen der Geologischen Bundesanstalt* -, 108–109.

PETRASCHECK, W.: 1963. Die alpin-mediterrane Metallogenese. *Geologische Rundschau 53*, 376–389.

PETRASCHECK, W.: 1975. Zur Altersbestimmung einiger ostalpiner Lagerstätten. *Mitteilungen der Österreichischen Geologischen Gesellschaft 68*, 79–87.

PETRASCHECK, W.: 1976. Mineral Zoning and Plate Tectonics in the Alpine - Mediterranean Area. *Geological Association of Canada, Special Paper 14*, 353–359.

PETRASCHECK, W.: 1986. The Metallogeny of the Eastern Alps in Context with the Circum-Mediterranean Metallogeny. *Schriftenreihe der Erdwissenschaftlichen Kommission 8*, 127–134.

POHL, W.: 1990. Genesis of magnesit deposits - models and trends. *Geologische Rundschau 79*, 192–292.

POHL, W.: 2011. *Pohl: Economic Geology: Principles and Practice*, Wiley-Blackwell. 680 pp.

POHL, W. & BELOCKY, R.: 1994. Alpidic Metamorphic Fluids and Metallogenesis in the Eastern Alps. *Mitteilungen der Österreichischen Geologischen Gesellschaft 86*, 141–152.

POHL, W. & BELOCKY, R.: 1999. Metamorphism and metallogeny in the Eastern Alps. *Mineralium Deposita 34*, 614–629.

PROCHASKA, W.: 1993. Untersuchungen stabiler Isotope an alpidischen Ganglagerstätten in den Ostalpen. *Berg- und Hüttenmännische Monatshefte 138*, 138–144.

PROCHASKA, W.: 1999. Die Bedeutung der chemischen Zusammensetzung von Einschlußfluiden und laugbaren Salzen für die Genese von hydrothermalen und sedimentären Karbonatgesteinen der Ostalpen. *Mitteilungen der Österreichischen Geologischen Gesellschaft 90*, 175–183.

REDEN, G.: 1991. Beiträge zur Geologie, Geophysik und Geochemie der Gesteine und Mineralisationen im gebiet der Goldvorkommen in den Hohen Tauern (Bad Gastein - Kolm Saigurn - Heiligenblut) mit besonderer Berücksichtigung der Gangmineralisationen. Ph.D. thesis, Univ. Wien.

REDLICH, K.: 1909. Types of magnesite deposits. *Zeitschrift für praktische Geologie 17*, 300–310.

REDLICH, K. & SELLNER, F.: 1923. Die Radmer. In *Bergbaue Steiermarks*, K. REDLICH, Ed. Deuticke, Wien, 99–144.

ROBINSON, B. & KUSAKABE, M.: 1975. Quantitative preperation of SO2 for 34S/32S analysis from sulphides by combusion with cuprous oxide. *Analytical Chemistry 47*, 1147–1181.

ROBL, K. & PAAR, W.: 1994. Fluid Inclusion - Untersuchungen an Golderzen der Goldzeche, Sonnblickgruppe, (Hohe Tauern, Kärnten). *Mitteilungen der Österreichischen Mineralogischen Gesellschaft 139*, 151–158.

SACHSENHOFER, R., GRUBER, W., & DUNKL, I.: 2010. Das Miozän der Becken von Leoben und Fohnsdorf. *Journal of Alpine Geology 53*, 9–38.

SACHSENHOFER, R., KOGLER, A., POLESNY, H., STRAUSS, P., & WAGREICH, M.: 2000. The Neogen Fohnsdorf Basin: basin formation and basin inversion during lateral extrusion in the Eastern Alps (Austria). *International Journal of Earth Science 89*, 415–430.

SACHSENHOFER, R., STRAUSS, P., WAGREICH, M., ABART, R., DECKER, K., GOLDBRUNNER, J., GRUBER, W., KRIEGL, C., & SPÖTL, C.: 2000. Das miozäne Fohnsdorfer Becken - Eine Übersicht. *Mitteilungen der Gesellschaft der Geologie- und Bergbaustudenten in Österreich 44*, 173–190.

SCHAUBERGER, O.: 1986. Bau und Bildung der Salzlagerstätten des ostalpinen Salinars. *Archiv für Lagerstättenforschung der Geologischen Bundesanstalt 7*, 217–254.

SCHEDL, A.: 1981. Geologische, geochemische und lagerstättenkundliche Untersuchungen im ostalpinen Altkristallin der Schladminger Tauern. Ph.D. thesis, Universität Wien.

SCHMID, S., FÜGENSCHUH, B., KISSLING, E., & SCHUSTER, R.: 2004. Tectonic map and overall architecture of the Alpine orogen. *Eclogae Geologicae Helvetiae 97*, 93–117.

SCHRAMM, M.: 1977. Über die Verbreitung epi- und anchimetamorpher Sedimentgesteine in der Grauwackenzone und in den Nördlichen Kalkalpen (Österreich). *Geologisch-Paläontologische Mitteilungen Innsbruck 7*, 3–20.

SCHROLL, E. & PROCHASKA, W.: 1997. Wasserstoff- und Sauerstoffisotopie. In *Handbuch der Lagerstätten der Erze, Industrieminerale und Energierohstoffe Österreichs*, L. Weber, Ed. Archiv für Lagerstättenforschung der Geologischen Bundesanstalt, 449–485.

SCHULZ, O.: 1979a. Beiträge zur Metallogenese in den Ostalpen. *Verhandlungen der Geologischen Bundesanstalt* -, 237–264.

SCHULZ, O.: 1979b. Metallogenese in den österreichischen Ostalpen - Proceedings 3rd ISMIDA Leoben. *Verhandlungen der Geologischen Bundesanstalt* -, 471–478.

SCHUSTER, R., KOLLER, F., HÖCK, V., HOINKES, G., & BOUSQUET, R.: 2004. Explanatory notes to the map: Metamorphic strucuture of the alps - Metamorphic evolution of the Eastern Alps. *Mitteilungen der Österreichischen Mineralogischen Gesellschaft 149*, 175–199.

SCHUSTER, R. & STÜWE, K.: 2008. Permian metamorphic event in the Alps. *Geology 36*, 603–606.

SCOTT, V. & LOVE, G.: 1983. *Quantitative Electron-Probe Microanalysis*, John Wiley & Sons. 345 pp.

SELVERSTONE, J.: 1985. Petrologic constraints on imbrication, metamorphism and uplift in the SW Tauern window, eastern Alps. *Tectonics 4*, 7, 687–704.

SHARP, Z.: 1990. A laser-based microanalytical method for the in-situ determination of oxygen isotope ratios in silicates and oxides. *Geochimica et Cosmochimica Acta 54*, 1353–1357.

SHARP, Z.: 2007. *Principles of Stable Isotope Geochemistry*, Prentice Hall. 344 pp.

SHARP, Z., ESSENE, E., & KELLY, W.: 1985. A re-examination of the arsenopyrite geothermometer: pressure considerations and applications to natural assemblages. *The Canadian Mineralogist 23*, 517–534.

SHARP, Z. D. & KIRSCHNER, D. L.: 1994. Quartz-calcite oxygen isotope themometry: a calibration based on natural isotopic variations. *Geochimica et Cosmochimica Acta 58*, 4491–4501.

SHEPPARD, S. & SCHWARCZ, H.: 1970. Fractionation of carbon and oxygen isotopes and magnesium between coexisting metamorphic calcite and dolomite. *Contributions to Mineralogy and Petrology 26*, 161–198.

SHIRO, Y. & SAKAI, H.: 1972. Calculation of the reduced partition function ratios of alpha-beta quartz and calcite. *Japan Chemical Society Bulletin 45*, 2355–2359.

SKINNER, B.: 1997. Hydrothermal Mineral Deposits: What We Do and Don't Know. In *Geochemistry of Hydrothermal Ore Deposits*, H. BARNES, Ed. John Wiley & Sons, 1–26.

SLAPANSKY, P. & FRANK, W.: 1987. Structural Evolution and Geochronolgy of the Northern Margin of the Austroalpine in the Northwestern Schladming Crystalline (NE Radstädter Tauern). In *Geodynamics of the Easter Alps*, H. FLÜGEL & P. FAUPL, Eds. Deuticke, 244–262.

SPERL, G., UNTERWEISSACHER, T., EBNER, F., MALI, H., & OFNER, L.: 2010. Steirische Eisenstraße - Montanhistorische Exkursion. *Journal of Alpine Geology 53*, 1–8.

SPÖTL, C. & MATTEY, D.: 2006. Stable isotope microsampling of speleothems for paleoenvironmental studies: A comparison of microdrill, micromill and laser ablation techniques. *Chemical Geology 235*, 48–58.

SPÖTL, C. & PAK, E.: 1996. A strontium and sulfur isotopic study of Permo-Triassic evaporites in the Northern Calcareous Alps, Austria. *Chemical Geology 131*, 219–234.

SPÖTL, C. & VENNEMANN, T.: 2003. Continuous-flow isotope ratio mass spectrometric analysis of carbonate minerals. *Rapid Communications in Mass Spectrometry 17*, 1004–1006.

TAYLOR, B.: 1974. The application of oxygen and hydrogen isotope studies to problems of hydrothermal alteration and ore deposition. *Economic Geology 69*, 843–883.

TAYLOR, H.: 1979. Oxygen and hydrogen isotope relationships in hydrothermal mineral deposits. In *Geochemistry of Hydrothermal Ore Deposits*, H. BARNES, Ed. J. Wiley and Sons, New York, 236–277.

THALHAMMER, O., EBNER, F., HORKEL, K., & MALI, H.: 2010. The Kraubath Ultramafic Massif. *Journal of Alpine Geology 53*, 137–158.

THALHAMMER, O., STUMPFL, E., & JAHODA, R.: 1989. The Mittersill Scheelite Deposit, Austria. *Economic Geology 84*, 1153–1171.

THÖNI, M.: 1999. A review of geochronological data from the Eastern Alps. *Schweizer Mineralogisch Petrographische Mitteilungen 79*, 209–230.

TOLLMANN, A.: 1977. *Geologie von Österreich, Band 1: Die Zentralalpen*, Wien. 766 pp.

TUFAR, W.: 1969. Das Problem der ostalpinen Metallogenese, beleuchtet am Beispiel einiger Erzparagenesen vom Alpenostrand. *Sitzungsberichte der Österreichischen Akademie der Wissenschaften mathematisch-naturwissenschaftliche Klasse Abteilung I 177*, 1–20.

TUFAR, W.: 1974. Zur Altersgliederung der ostalpinen Vererzung. *Geologische Rundschau 65*, 105–124.

UCIK, F.: 2006. Der Verfall der Gebäude beim Silberbergbau Tösens im Oberinntal. *Jahrbuch der Geologischen Bundesanstalt 146*, 65–67.

UNTERWEISSACHER, T., HORKEL, K., MALI, H., & EBNER, F.: 2009. Geologie der Magnesitlagerstätten im Raum Tavşanli (Türkei). *Mitteilungen des naturwissenschaftlichen Vereines für Steiermark 139*, 149 – 160.

VAVTAR, F.: 1982. Topomineralische Gold-Quarz-Gänge des Siglitz-Pochart-Erzwies-Revieres (Gastein, Hohe Tauern). *Archiv für Lagerstättenforschung der Geologischen Bundesanstalt 2*, 143–148.

VAVTAR, F.: 1988. Die Erzanreicherungen im Nordtiroler Stubai-, Ötztal- und Silvrettakristallin. *Archiv für Lagerstättenforschung der Geologischen Bundesanstalt 9*, 103–153.

VERMA, S., PANDARINATH, K., & SANTOYO, E.: 2008. SolGeo: A new computer program for solute geothermometers and its application to Mexican geothermal fields. *Geothermics 37*, 597–621.

VERMA, S. & SANTOYO, E.: 1997. New improved equations for Na/K, Na/Li and SiO_2 geothermometers by outlier detection and rejection. *Journal of Volcanology and Geothermal Research 79*, 9–23.

VOHRYZKA, K.: 1968. Die Erzlagerstätten von Nordtirol und ihr Verhältnis zur alpinen Tektonik. *Jahrbuch der Geologischen Bundesanstalt 111*, 3–88.

WAGNER, T. & LORENZ, J.: 2002. Mineralogy of complex Co-Ni-Bi vein mineralization, Bieber deposit, Spessart, Germany. *Mineralogical Magazine 66*, 385–407.

WEBER, L.: 1990. Die Blei-Zinkerzlagerstätten des Grazer Paläozoikums und ihr geologischer Rahmen. *Archiv für Lagerstättenforschung der Geologischen Bundesanstalt 12*, 1–289.

WEBER, L., Ed.: 1997a. *Handbuch der Lagerstätten der Erze, Industrieminerale und Energierohstoffe Österreichs.* Archiv für Lagerstättenforschung, 19, 1-607. Geologische Bundesanstalt, Wien.

WEBER, L.: 1997b. Metallogenetical Map of Austria 1:500 000 including Industrial Minerals and Mineral Fuels. Geologische Bundesanstalt, Wien.

WEBER, L.: 1999. Interaktives Rohstoff Informationsystem - Metallogenetische Karte von Österreich IRIS 2.4.

WEBER, L. & PAAR, W.: 1997. Penninische Fenster. In *Handbuch der Lagerstätten der Erze, Industrieminerale und Energierohstoffe Österreichs*, L. WEBER, Ed. Archiv für Lagerstättenforschung der Geologischen Bundesanstalt 19, 266–287.

WENINGER, H.: 1981. Kraubath/Steiermark: Der Ultramafit von Kraubath und seine Mineralien. *Lapis 6*, 27–33.

WHITICAR, M.: 1996. Stable isotope geochemistry of coals, humic kerogens and related natural gases. *International Journal of Coal Geology 32*, 191–215.

YUND, R.: 1962. The system Ni-As-S: phase relations and mineralogical significance. *American Journal of Science 260*, 761–782.

ZEDEF, V., RUSSEL, M., FALLICK, A., & HALL, A.: 2000. Genesis of Vein Stockwork and Sedimentary Magnesite and hydromagnesite Deposits in the Ultramafic Terranes of Southwestern Turkey: A Stable Isotope Study. *Economic Geology 95*, 429–446.

ZETINIGG, H.: 1993. Der Thalheimer Schloßbrunnen. In *Die Mineral- und Heilwässer Österreichs - Geologische Grundlagen und Spurenelemente*, J. ZÖTL & J. GOLDBRUNNER, Eds. Springer Verlag Wien New York, 223–224.

ZHANG, L.-G., LIU, J.-X., ZHOU, H., & CHEN, Z.-S.: 1989. Oxygen isotope fractionation in the quartz-water-salt system. *Economic Geology 89*, 1643–1650.

ZHENG.: 1999. Oxygen isotope fractionation in carbonate and sulfate minerals. *Geochemical Journal 33*, 109–126.

ZHENG, Y.-F. & HOEFS, J.: 1993. Carbon and oxygen isotopic covariations in hydrothermal calcites. *Mineralium Deposita 28*, 79–89.

Appendix

A. Localities

Sample	Zone	Easting	Northing	Elevation	Description
Mitterberg					
MB 09_01	33 T	358183	5251616	1370	mine dump 250m NE Mitterberghaus
MB 09_03	33 T	358183	5251616	1370	mine dump 250m NE Mitterberghaus
MB 09_05	33 T	358183	5251616	1370	mine dump 250m NE Mitterberghaus
MB 09_06	33 T	358183	5251616	1370	mine dump 250m NE Mitterberghaus
MB 09_08	33 T	358183	5251616	1370	mine dump 250m NE Mitterberghaus
MB 09_09	33 T	358183	5251616	1370	mine dump 250m NE Mitterberghaus
MB 09_10	33 T	358183	5251616	1370	mine dump 250m NE Mitterberghaus
MB 09_12	33 T	365063	5251601	685	"Roter Palfen"
MB 09_13	33 T	357851	5251391	1330	mine dump "Emil" adit
MB 09_14	33 T	357851	5251391	1330	mine dump "Emil" adit
MB 09_15	33 T	357851	5251391	1330	mine dump "Emil" adit
MB 09_17	33 T	357851	5251391	1330	mine dump "Emil" adit
Buchberg					
all samples					"Buchberg" adit near Bischofshofen
Radmer					
all samples					stope backfill "Paradeis" adit
Tösens					
TS 09_01 D	32T	624939	5203574	2124	mine dump
TS 09_01 E	32T	624939	5203574	2124	mine dump
TS 09_01 G	32T	624939	5203574	2124	mine dump
TS 09_01 I	32T	624939	5203574	2124	mine dump
TS 09_10	32T	626506	5201178	2595	mine dump
TS 09_11	32T	626506	5201178	2595	mine dump
TS 09_11 A	32T	626506	5201178	2595	mine dump
TS 09_13	32T	626879	5201305	2816	vein outcrop
TS 09_15	32T	627039	5201327	2757	exploration pit
TS 09_16	32T	627041	5201364	2850	mine dump "Berglerkar"
Zinkwand					
ZW 09_01	33 T	400416	5295966	2300	mine dump "Himmelkönigin" adit
ZW 09_02	33 T	400416	5295966	2300	mine dump "Himmelkönigin" adit
ZW 09_03	33 T	400416	5295966	2300	mine dump "Himmelkönigin" adit
ZW 09_04	33 T	400416	5295966	2300	mine dump "Himmelkönigin" adit
ZW 09_05	33 T	400441	5236025	2250	mine dump "Mutterkirchenthal" adit
ZW 09_06	33 T	400441	5236025	2250	mine dump "Mutterkirchenthal" adit
ZW 09_07	33 T	400441	5236025	2250	mine dump "Mutterkirchenthal" adit
ZW 09_08	33 T	400441	5236025	2250	mine dump "Mutterkirchenthal" adit
ZW 09_09	33 T	400441	5236025	2250	mine dump "Mutterkirchenthal" adit
ZW 09_10	33 T	400441	5236025	2250	mine dump "Mutterkirchenthal" adit
ZW 09_11	33 T	400441	5236025	2250	mine dump "Mutterkirchenthal" adit
ZW 09_12	33 T				mine dump "Mutterkirchenthal" adit
ZW 09_13	33 T				mine dump "Mutterkirchenthal" adit
ZW 09_14	33 T				"Fürst Lobkowitzzeche" underground
ZW 09_15	33 T				"Fürst Lobkowitzzeche" underground
ZW 09_16	33 T				"Fürst Lobkowitzzeche" underground
ZW 09_17	33 T			2240	"Himmelkönigin" underground

Sample	Zone	Easting	Northing	Elevation	Description
ZW 09_18	33 T			2240	"Himmelkönigin" underground
ZW 09_19	33 T			2190	"Mutterkirchenthal" underground backfill
ZW 09_20	33 T			2190	"Mutterkirchenthal" underground solid
ZW 09_21	33 T			2190	"Mutterkirchenthal" underground solid
ZW 09_22	33 T			2185	"Mutterkirchenthal" underground solid
ZW 09_23	33 T			2185	"Mutterkirchenthal" underground solid
ZW 09_24	33 T			2195	"Mutterkirchenthal" underground solid
ZW 09_26	33 T				"Schmiedenstollen" underground backfill
ZW 09_27	33 T			2210	"Schmiedenstollen" underground solid
ZW 09_28	33 T	400441	5236025	2250	Collection J.Grill
ZW 09_29	33 T	400441	5236025	2250	Collection J.Grill
ZW 10_01	33 T				"Fürst Lobkowitzzeche" underground
ZW 10_03	33 T				"Mutterkirchenthal" underground solid vein
ZW 10_04	33 T				"Mutterkirchenthal" underground solid vein
ZW 10_06	33 T				mine dump "Mutterkirchenthal" adit
ZW 10_07	33 T				mine dump "Mutterkirchenthal" adit
IG 01	33 T				"Ignazibaue" underground
IG 02 A	33 T				"Ignazibaue" underground
IG 02 B	33 T				"Ignazibaue" underground
RB 10_01 A	33 T				"Roßblei" underground
RB 10_01 B	33 T				"Roßblei" underground
RB 10_05	33 T				"Roßblei" underground
Kraubath					
Augraben	33 T	496350	5237145	720	
Gulsen	33 T	494970	5236565	615	

Coordinates are given UTM system using WGS 84 reference ellipsoid. Elevation data is given in meters above sea level. Coordinates for underground samples represent the location of the mine portal.

B. Bulk fluid inclusion leachates

Sample	Min	F	Cl	Br	NO_3	SO_4	I	Li	Na	K	Mg	Ca	Br/Cl x 10^3	I/Cl x 10^6	I/Br	K/Na	Ca/Na	Li/Na	I/Na	Br/Na	Q+/Q-
		µg/l	µg/l	µg/l	µg/l	µg/l	µg/l	µg/l	µg/l	µg/l	µg/l	µg/l	mol/mol	mol/mol	mol/mol	mol/mol	mol/mol	mol/mol	mol/mol	mol/mol	
Erzwies																					
ES 09_12	qtz	40	434	2	41	22	1	0	659	674	242	271	2.43	399.90	0.164	0.601	0.236	0.000	1.967	0.001	5.122
ES 09_13	qtz	58	334	2	66	28	0	0	842	707	121	256	2.78	383.75	0.138	0.494	0.174	0.000	0.838	0.001	5.469
ES 09_16	qtz	7	850	1	57	272	1	0	442	276	888	8958	0.78	265.26	0.342	0.367	11.615	0.000	4.731	0.001	17.676
ES 09_22 A	qtz	2	1803	9	55	366	1	0	1745	180	112	1681	2.13	112.11	0.053	0.061	0.553	0.001	0.334	0.001	2.915
Mitterberg																					
MB 09_01	ank	91	21988	122		1586	6	71	12179	971	5129	6797	2.46	75.41	0.031	0.047	0.320	0.019	0.104	0.003	2.010
MB 09_01	qtz	3	7280	29	26	186	1	0	4158	319	169	920	1.78	32.41	0.018	0.045	0.127	0.000	0.045	0.002	1.184
MB 09_013	ank	25	25779	249	0	3593	2	77	11275	777	16187	24918	4.28	18.58	0.004	0.041	1.268	0.023	0.022	0.006	3.840
MB 09_017	ank	55	45889	464		259	19	391	17735	1224	14034	12516	4.49	114.49	0.026	0.041	0.405	0.073	0.149	0.008	2.016
MB 09_017	qtz	15	33113	210	137	592	3	5	17236	1606	717	4830	2.81	22.21	0.008	0.055	0.161	0.001	0.013	0.004	1.147
Mb 09_03	ank	2	63186	699		487	31	674	24444	1395	27634	20221	4.91	139.11	0.028	0.034	0.475	0.091	0.131	0.008	2.486
MB 09_03	qtz	7	25694	210	58	486	3	3	12979	811	434	2558	3.63	33.51	0.009	0.037	0.113	0.001	0.027	0.005	1.014
MB 09_06	ank	9	42143	383		2610	21	379	17688	1121	19498	26125	4.04	136.58	0.034	0.037	0.847	0.071	0.178	0.006	3.012
MB 09_06	qtz	306	6417	36	478	185	1	0	3330	395	93	892	2.47	29.30	0.012	0.070	0.154	0.000	0.020	0.003	0.990
MB 09_08	ank	37	61917	0		635	10	665	26440	1867	25721	22361	0.00	45.85	0.000	0.042	0.485	0.083	0.040	0.000	2.569
MB 09_08	qtz	4	14858	92	83	265	1	0	8107	780	494	2295	2.73	18.00	0.007	0.057	0.162	0.000	0.021	0.003	1.235
MB 09_13	qtz	20	11790	117	43	621	1	1	6049	886	176	1317	4.41	17.18	0.004	0.086	0.125	0.000	0.018	0.006	1.050
Buchberg																					
BU 10_01 A	ank	291	11768	110		224	2	44	6586	486	7148	12167	4.16	41.60	0.010	0.043	1.060	0.022	0.029	0.005	4.247
BU 10_01 A	qtz	1	9113	67	0	240	1	18	5438	255	5713	10982	3.27	44.98	0.014	0.028	1.158	0.011	0.037	0.004	4.807
BU 10_01 B	ank	185	45670	407		2669	8	209	24442	1576	14299	18649	3.96	48.35	0.012	0.038	0.438	0.028	0.034	0.005	2.385
BU 10_01 B	qtz	1	13353	69	479	83560	0	2	7707	447	2648	8097	2.28	9.93	0.004	0.034	0.603	0.001	0.011	0.003	0.456
BU 10_01 C	ank	28	42917	554		382	7	231	21960	1142	11982	15787	5.73	45.98	0.008	0.031	0.412	0.035	0.040	0.007	2.275
BU 10_01 C	qtz	8	25959	216	53	1055	0	4	14423	886	247	1321	3.70	3.82	0.001	0.036	0.053	0.001	0.003	0.004	0.972
BU 10_01 D	ank	591	40121	519		582	8	185	20308	1361	13417	18699	5.74	53.36	0.009	0.039	0.528	0.030	0.052	0.007	2.524
BU 10_01 D	qtz	6	13376	116	780	138	0	1	7856	775	275	4007	3.84	9.20	0.002	0.058	0.293	0.000	0.011	0.004	1.481
BU 10_02 B	ank	25	47729	582		457	8	267	25308	1348	14369	17771	5.41	44.32	0.008	0.031	0.403	0.035	0.040	0.007	2.377
BU 10_02 B	qtz	2	8880	57	106	126	1	1	5697	460	1550	5952	2.85	20.11	0.007	0.047	0.599	0.001	0.034	0.003	2.677
BU 10_03	ank	55	52539	408		1130	9	234	29566	1427	15704	18540	3.45	46.74	0.014	0.028	0.360	0.026	0.036	0.004	2.361
BU 10_03	qtz	16	14938	73	734	2157	1	16	9121	671	4639	11762	2.18	20.89	0.010	0.043	0.740	0.006	0.024	0.002	2.886
Radmer																					
RA 10_08	ank	1	45523	565	0	3152	6	315	19033	1686	35746	14881	5.51	36.23	0.007	0.052	0.448	0.055	0.044	0.009	3.391
RA 11_01	ank	39	61768	0		2284	15	279	27098	3295	22046	27413	0.00	66.73	0.000	0.071	0.580	0.034	0.057	0.000	2.503
RA 11_01	qtz	3	17741	114	55	212	1	11	4674	5018	235	3362	2.86	17.86	0.006	0.631	0.413	0.007	0.023	0.007	1.025
RA 11_03	ank	44	42409	0		1511	10	171	17800	4081	17082	27908	0.00	66.88	0.000	0.135	0.899	0.032	0.086	0.000	3.009
RA 11_03	qtz	1305	12068	83	55	143	1	2	2901	3951	174	3425	3.04	17.62	0.006	0.801	0.677	0.003	0.035	0.008	0.997
RA 11_04	ank	70	25999	315		526	8	221	12261	1452	17800	19013	5.37	87.40	0.016	0.070	0.890	0.060	0.165	0.007	4.011
RA 11_04	qtz	4	1654	15	135	77	1	0	883	465	11	500	4.10	88.54	0.022	0.309	0.325	0.000	0.917	0.005	1.499
RA 11_05	ank	51	51904	553		938	15	320	23227	2374	18457	27479	4.73	80.90	0.017	0.060	0.679	0.046	0.080	0.007	2.684
RA 11_05	qtz	2	3633	30	313	73	0	0	1754	911	527	3525	3.65	24.10	0.007	0.305	1.153	0.000	0.032	0.005	2.910
RA 11_06	ank	49	38924	429		274	11	213	17527	1822	21988	20637	4.89	78.13	0.016	0.061	0.675	0.040	0.072	0.007	3.309
RA 11_06	qtz	1706	6850	52	93	60	0	0	1875	2602	568	3988	3.38	19.82	0.006	0.816	1.220	0.001	0.159	0.008	1.375
RA 11_07	ank	67	46165	488		331	12	262	20946	2393	25556	21774	4.69	73.34	0.016	0.067	0.596	0.041	0.081	0.007	3.185
RA 11_07	qtz	3	2352	20	56	52	0	0	1426	845	1290	4668	3.86	28.99	0.008	0.348	1.878	0.000	0.241	0.004	6.150
RA 11_08	ank	9	10475	100	0	223	2	34	4785	404	16865	19283	4.23	48.68	0.012	0.050	2.312	0.024	0.035	0.006	8.526
RA 11_08	qtz	9	24834	182	21	614	4	18	7035	6158	2062	13311	3.24	47.77	0.015	0.515	1.085	0.009	0.096	0.007	1.815
RA_SLG_01	ank	184	34975	0		749	10	158	18256	2223	24769	22105	0.00	81.93	0.000	0.072	0.695	0.029	0.103	0.000	3.968
RA_SLG_01	qtz	4	5637	40	1194	116	1	0	1806	1734	159	1513	3.15	34.89	0.011	0.565	0.481	0.001	0.074	0.006	1.166
Zinkwand																					
ZW 09_01	qtz	1	3561	132	51	28	1	0	2275	542	175	2013	16.50	73.93	0.004	0.140	0.508	0.000	0.082	0.017	2.198
ZW 09_07	cal	3	66243	3077		66	25	404	27242	5555	17686	18290	20.61	106.87	0.005	0.120	0.385	0.049	0.091	0.033	1.966
ZW 09_15	cal	18	4509	51		14	5	14	3009	393	8055	13075	5.04	314.18	0.062	0.077	2.493	0.016	0.282	0.005	11.294
ZW 09_16	cal	154	2495	16		30	4	8	2107	591	1927	8652	2.83	405.16	0.143	0.165	2.355	0.012	0.703	0.002	8.800
ZW 09_16	qtz	1	2006	13	44	24	2	0	1539	144	47	863	2.85	237.23	0.083	0.055	0.322	0.000	0.379	0.002	2.026
ZW 09_18	qtz	3	2405	63	30	35	1	2	2093	332	2155	6008	11.57	69.51	0.006	0.093	1.647	0.003	0.092	0.009	8.239
ZW 09_20	qtz	18	7152	310	41	15	2	1	3697	419	230	1196	19.22	65.10	0.003	0.067	0.186	0.001	0.038	0.024	1.206
ZW 09_22	qtz	1	5594	246	2	41	2	5	3061	402	6530	13494	19.55	75.52	0.004	0.077	2.529	0.005	0.043	0.023	8.373
ZW 09_24	qtz	3	6107	161	52	29	0	0	3379	589	1134	3028	11.67	16.49	0.001	0.103	0.514	0.000	0.025	0.014	2.311
ZW 10_01	cal	0	3288	72	1	58	2	2	1894	186	7322	11259	9.77	148.08	0.015	0.058	3.409	0.003	0.061	0.011	13.189
ZW 10_01	qtz	9	843	8	1	25	1	0	962	200	1981	7587	4.06	198.11	0.049	0.122	4.524	0.000	0.161	0.002	23.610
ZW 10_07	qtz	1	3262	88	36	78	1	0	1968	251	219	1423	11.94	56.41	0.005	0.075	0.415	0.000	0.075	0.013	1.899
ZW 10_15	qtz	2	10356	109	38	27	5	7	5417	657	613	4848	4.66	123.31	0.026	0.071	0.513	0.004	0.083	0.006	1.852
Tösens																					
TS 09_010	qtz	23	5991	26	172	66	0	0	1863	741	90	865	1.92	16.20	0.008	0.234	0.266	0.000	0.013	0.004	0.862
TS 09_011	cal	11	1875	25	0	59	1	2	1230	112	12591	15746	5.89	160.12	0.027	0.054	7.342	0.004	0.018	0.006	34.122
TS 09_011	qtz	22	2173	25	45	730	0	0	1401	497	12	257	5.05	0.00	0.000	0.208	0.105	0.000	0.000	0.005	1.111
TS 09_011 A	qtz	8	3049	50	0	69	1	0	2047	301	92	2033	7.31	109.22	0.015	0.086	0.570	0.000	0.112	0.007	2.325
TS 09_013	qtz	15	2630	31	37	20	1	0	1760	319	10	482	5.22	123.06	0.024	0.106	0.157	0.000	0.101	0.005	1.434

C. Stable isotopes

Sample	Min	$\delta^{13}C_{VPDB}$	$\delta^{18}O_{VSMOW}$	Min	$\delta^{18}O_{VSMOW}$	Remarks
Mitterberg						
MB09_01	ank	-4.30	17.41	qtz	17.2	
MB09_03	ank	-3.87	16.20	qtz	17.9	
MB09_05	ank	-5.15	18.52			
MB09_06	ank	-4.80	17.66	qtz	14.3	
MB09_08	ank	-5.03	15.86	qtz	17.0	
MB09_09	ank	-4.55	16.08			
MB09_10	ank	-4.35	18.52			
MB09_12	ank	-3.36	16.36			
MB09_13	ank	-4.39	16.55	qtz	17.4	
MB09_14	ank	-3.21	16.65			
MB09_15	ank	-4.37	16.57			
MB09_17	ank	-5.59	18.65	qtz	17.7	
Buchberg						
BU 10_01 A	ank	-5.53	15.66	qtz	17.4	
BU 10_01 B	ank	-5.87	15.72	qtz	16.6	
BU10_01 C	ank	-5.16	15.72	qtz	18.5	
BU10_01 D	ank	-5.27	15.66	qtz	16.7	
BU10_02 B	ank	-5.66	15.54	qtz	17.0	
BU 10_03	ank	-5.70	15.45	qtz	17.0	
Radmer						
RA 10_01	ank	-3.73	17.34			
RA 10_02	ank	-3.59	18.16			
RA 10_03 A	ank	-4.01	18.72			
RA 10_03 B	ank	-3.81	16.97			
RA 10_04	ank	-4.21	17.92			
RA 10_06	ank	-3.91	17.49			
RA 10_08	ank	-4.06	17.53			
RA 10_09	ank	-4.04	17.81			
RA 10_10	ank	-3.94	17.51			
RA 11_01	ank	-5.52	17.35	qtz	2.3	
RA 11_02	ank	-3.82	17.61			
RA 11_03	ank	-5.32	18.38	qtz	2.2	
RA 11_04	ank	-3.85	18.26	qtz	2.9	
RA 11_05	ank	-4.34	18.48	qtz	19.8	
RA 11_06	ank	-3.90	17.60	qtz	2.3	
RA 11_07	ank	-4.15	17.84	qtz	19.6	
RA 11_08	ank	-5.27	18.50	qtz	21.2	
RA 11_10	ank	-3.91	17.06			
RA 11_11	ank	-3.91	17.18			
RA 11_12	ank	-4.42	18.44			
RA11_SLG_01	ank	-3.73	17.58	qtz	21.6	
Tösens						
TS09_01 D	cal	-6.91	14.82			
TS09_01 E	cal	-6.88	17.47			
TS09_01 G	cal	-7.43	15.11			
TS09_01 I	cal	-7.10	14.57			
TS09_10	cal	-7.25	15.30	qtz	13.5	
TS09_11	cal	-7.39	15.71	qtz	15.2	
TS09_11 A	cal	-6.23	14.66	qtz	13.4	
TS09_13				qtz	12.8	
TS09_15	cal	-6.11	15.45			
TS09_16	cal	-5.89	16.05			
Zinkwand						
IG01	cal	-4.34	17.36			
IG02 A	cal	-3.83	21.33			

Sample	Min	$\delta^{13}C_{VPDB}$	$\delta^{18}O_{VSMOW}$	Min	$\delta^{18}O_{VSMOW}$	Remarks
IG02 B	cal	-4.57	14.60			
ZW_RE 01	cal	-6.57	13.59			
ZW_RE 02	cal	-5.61	15.84			
ZW_RE 03	cal	-4.12	16.00			
ZW_RE 04	cal	-4.25	16.81			
ZW 09_01	cal	-4.47	15.22	qtz	14.0	
ZW 09_02	cal	0.28	21.33			
ZW 09_03	cal	-0.01	20.56			
ZW 09_04	cal	-5.34	16.55			
ZW 09_05	cal	-6.12	19.18			
ZW 09_06	cal	-7.27	11.32			
ZW 09_07	cal	-4.46	13.58			
ZW 09_08	cal	-5.39	13.36			
ZW 09_09	cal	-7.07	14.78			
ZW 09_10	cal	0.41	21.52			
ZW 09_11	cal	-4.38	13.04			
ZW 09_12	cal	-4.43	16.85			
ZW 09_13	cal					
ZW 09_14	cal	-3.41	15.23			
ZW 09_15	cal	-5.47	12.92	qtz	14.9	
ZW 09_15 B	cal	-4.68	15.46			
ZW 09_16	cal	-5.55	13.73	qtz	16.4	
ZW 09_17	cal	-5.84	12.68			
ZW 09_17 A	cal	-6.38	12.55			
ZW 09_17 B	cal	-4.75	13.85			
ZW 09_17 C	cal	-5.04	13.42			
ZW 09_18	cal	-5.81	14.24	qtz	13.2	
ZW 09_19	cal	-5.38	12.39			
ZW 09_20	cal	-4.92	13.45	qtz	18.4	
ZW 09_21	cal	-5.04	12.55			
ZW 09_22	cal	-4.54	12.80	qtz	14.8	
ZW 09_23	cal	-7.59	11.68			
ZW 09_24	cal			qtz	13.5	
ZW 09_26	cal	-5.47	17.36			
ZW 10_01	cal	-3.29	17.57	qtz	15.6	
ZW 10_03	cal	-6.54	19.00			
ZW 10_04	cal	-6.54	17.50			
ZW 10_06	cal	-5.64	12.40			
ZW 10_07 A	cal	-6.69	12.95	qtz	13.5	
ZW 10_07 B	cal	-4.20	17.92			
RB 10_01 A	cal	-0.48	21.99			
RB 10_01 B	cal	0.70	24.02			
RB 10_05	cal	-1.00	20.95			
Erzwies						
ES 09_06	sid	-6.71	5.70			
ES 09_08	cal	0.23	22.40			
ES 09_09 B	sid	-6.89	12.86			
ES 09_11-1	cal	2.32	24.30			
ES 09_11-2	sid	-6.60	13.15			
ES 09_12	sid	-6.15	13.65	qtz	14.5	
ES 09_13	sid	-7.02	12.73	qtz	14.5	
ES 09_14	sid	-6.85	12.93			
ES 09_15	sid	-6.82	12.67			
ES 09_16	sid	-6.79	12.89	qtz	2.3	
ES 09_17 A	sid	-6.70	13.15			
ES 09_18	sid	-6.90	12.74			
ES 09_22 E				qtz	11.1	
Kraubath						
Gu 1	mag	-11.27	22.91			cement

Sample	Min	$\delta^{13}C_{VPDB}$	$\delta^{18}O_{VSMOW}$	Min	$\delta^{18}O_{VSMOW}$	Remarks
Gu 2	mag	-12.77	23.84			cement
Gu 3	mag	-11.20	22.07			cement
Gu 4	mag	-7.86	21.93			cement
Gu 5	mag	-6.92	17.75			cement
Gu 6	mag	-10.70	25.19			cement
Gu 7	mag	-11.25	25.52			cement
Gu 8	mag	-12.45	24.91			cement
Gu 9	mag	-11.18	24.22			cement
Gu 10	mag	-11.05	20.83			cement
Gu 11	mag	-12.14	23.28			cement
Gu 12	mag	-14.65	24.59			cement
Gu 13	mag	-11.29	24.86			cement
Gu 13-2	mag	-12.92	23.07			breccia component
Gu 14	mag	-11.18	24.24			breccia component
Gu 15	mag	-11.32	25.14			breccia component
Gu 16	mag	-11.07	25.00			breccia component
Gu 17	mag	-10.63	25.35			breccia component
Gu 18	mag	-11.44	25.71			breccia component
Gu 19	mag	-11.03	25.76			breccia component
Gu 20	mag	-12.09	25.66			breccia component
Gu 21-2	mag	-11.56	24.40			breccia component
Gu 21	mag	-10.44	24.99			breccia component
Gu 22	mag	-12.82	24.51			breccia component
Gu 22-2	mag	-10.58	24.83			breccia component
Gu 23	mag	-12.02	24.66			breccia component
Gu 24	mag	-13.53	25.18			breccia component
Gu 25	mag	-11.04	25.40			breccia component
Gu 26	mag	-12.88	24.69			breccia component
Gu 26-2	mag	-12.30	25.64			breccia component
Au1	mag	-14.54	26.39			breccia
Au2	mag	-14.56	26.62			breccia
Au3	mag	-14.65	26.78			breccia
Au4	mag	-14.28	26.77			breccia
Au5	mag	-14.93	26.29			breccia
Au6	mag	-14.36	26.85			network
Au6-2	mag	-14.95	26.38			network
Au7	mag	-14.21	26.51			vein
Au8	mag	-15.02	26.84			vein
Au9	mag	-14.12	27.29			breccia
Au10	mag	-14.97	26.49			network
Au11	mag	-14.25	27.08			breccia
Au12	mag	-14.36	26.89			breccia
Au13	mag	-14.34	26.85			network
Au13-2	mag	-14.65	26.61			network
Au14	mag	-14.69	26.77			vein
Au14-2	mag	-14.50	26.91			vein
Au15	mag	-14.34	26.91			vein
Au15-2	mag	-14.50	26.47			vein
Au16	mag	-14.68	26.50			vein
Au16-2	mag	-14.57	26.46			vein
Au17	mag	-13.67	26.90			vein
Au17-2	mag	-13.67	26.66			vein
Au18	mag	-14.10	25.84			vein
Au18-2	mag	-14.84	26.03			vein
Au19	mag	-13.61	27.10			vein
Au19-2	mag	-13.79	26.69			vein
Au20	mag	-13.54	26.98			vein
Au21	mag	-14.00	27.10			vein
Au21-2	mag	-13.84	27.15			vein

Sample	Min	$\delta^{13}C_{VPDB}$	$\delta^{18}O_{VSMOW}$	Min	$\delta^{18}O_{VSMOW}$	Remarks
Au22	mag	-14.37	26.80			network
Au23	mag	-14.50	26.76			breccia
Au23-2	mag	-14.25	26.66			breccia
Au24	mag	-14.53	26.21			network
Au25	mag	-14.57	26.14			network
Au25-2	mag	-13.15	24.91			network
Au26	mag	-14.82	26.31			network
Au27	mag	-14.06	26.97			network
Au27-2	mag	-14.14	26.57			network
Au27-3	mag	-14.41	26.73			network
Au28	mag	-14.40	26.63			network
Au29	mag	-14.02	26.80			vein
Au29-2	mag	-13.78	26.99			vein
Au30	mag	-14.61	26.54			vein
Au30-2	mag	-13.92	26.11			vein
Au31	mag	-14.22	26.65			breccia
Au31-2	mag	-14.32	26.66			breccia
Au32	mag	-13.70	26.76			breccia
Au33	mag	-15.33	26.28			network
Au 33-2	mag	-14.57	26.17			network
Au34	mag	-14.12	26.48			breccia
Au34-2	mag	-14.73	26.71			network
Au35	mag	-13.53	25.77			vein
Au35-2	mag	-13.82	26.18			vein
Au36	mag	-14.26	26.30			vein
Au36-2	mag	-14.48	26.56			vein
Au37	mag	-14.43	26.51			vein
Au37-2	mag	-14.65	26.63			vein
Au38	mag	-14.93	26.38			breccia
Au39	mag	-13.98	26.35			breccia
Au39-2	mag	-14.20	26.76			breccia
Au40	mag	-14.22	25.82			network
Au41	mag	-14.08	26.32			vein
Au42	mag	-14.21	25.29			network
Au42-2	mag	-14.29	25.55			network
Au42-3	mag	-14.59	26.40			network
Au43	mag	-13.98	26.91			vein
Au43-2	mag	-13.40	27.42			vein
Au44	mag	-14.74	25.76			network
Au44-2	mag	-14.71	26.15			network
Au45	mag	-13.51	25.62			network
Au46	mag	-14.42	26.61			breccia
Au47	mag	-13.20	27.19			vein
Au48	mag	-13.76	25.89			network
Au49	mag	-13.41	26.39			network
Au50	mag	-14.93	26.39			network
Au51	mag	-14.49	26.20			network
Au51-2	mag	-14.37	25.87			network
Au52	mag	-15.73	26.22			network
Au53	mag	-13.82	26.04			network
Au54	mag	-13.01	27.19			network
Au55	mag	-13.89	26.48			vein
Au56	mag	-14.74	26.54			network
Au57	mag	-16.56	25.77			network
Au59	mag	-15.15	25.38			vein
Au60	mag	-14.41	26.62			vein
Au61	mag	-15.70	25.62			network
Au62	mag	-14.82	25.05			network
1-1	mag	-13.84	26.42			vein

Sample	Min	$\delta^{13}C_{VPDB}$	$\delta^{18}O_{VSMOW}$	Min	$\delta^{18}O_{VSMOW}$	Remarks
1-2	mag	-13.73	26.21			vein
1-3	mag	-13.04	26.66			vein
1-4	mag	-13.60	26.33			vein
1-5	mag	-13.97	26.00			vein
2-1	mag	-13.48	26.71			vein
2-2	mag	-13.47	26.71			vein
2-3	mag	-13.65	26.42			vein
2-4	mag	-13.35	26.46			vein
2-5	mag	-13.51	26.66			vein
2-6	mag	-13.36	26.29			vein
3-1	mag	-13.47	26.65			vein
3-2	mag	-13.28	26.59			vein
3-3	mag	-13.36	26.87			vein
3-4	mag	-13.04	26.52			vein
4-1	mag	-12.58	25.77			vein
5-1	mag	-13.40	26.29			vein
5-2	mag	-13.91	26.64			vein
5-3	mag	-13.82	26.56			vein
5-4	mag	-13.72	26.63			vein
7-1	mag	-13.34	25.56			vein
6-1	mag	-13.62	26.09			vein
6-2	mag	-13.56	26.32			vein
6-3	mag	-13.57	26.61			vein
6-4	mag	-13.68	26.33			vein
6-5	mag	-12.94	26.58			vein

D. Sulphur Isotopes

Sample	Mineral	$\delta^{34}S$	Remarks	Reference
Mitterberg-Buchberg				
MB09_003	cpy	2.5		1
MB09_006	cpy	2.2		1
MB09_013	cpy	2.5		1
MB09_017	cpy	2.5		1
BU 10_01 A	py	9.1		1
BU 10_01 B	cpy	3.9		1
BU10_01 D	py	5.6		1
BU10_02 B	py	3.7		1
BU10_02 B	cpy	5.7		1
Radmer				
RA10_04	cpy	2.2		1
RA10_08	cpy	2.9		1
RA11_03	cpy	4.8		1
RA11_04	cpy	3.0		1
RA11_08	cpy	3.9		1
RA11_09	cpy	2.1		1
Tösens				
TS09_10	gal	−1.2		1
TS09_11 A	cpy	6.1		1
TS09_013	gal	−0.1		1
Tösens	py	0.8		2
Tösens	py	1.2		2
Tösens	gal	−1.4		2
Tösens	gal	−1.5		2
Tösens	gal	−1.3		2
Tösens	gal	−1.3		2
Tösens	sph	2.4		2
Tösens	sph	2.5		2
Tösens	sph	2.6		2
Zinkwand				
ZW 09_01	gdf	−1.3		1
ZW 09_12	gdf	−10.0		1
ZW 09_24	gdf	−3.6		1
Erzwies				
ES 09_012	py	4.6		1
ES 09_16	py	2.1		1
ES 09_22 A	py	2.7		1
ES 09_22 E	py	0.9		1
ES 09_22 A	apy	2.9		1
Au district Rauris-Gastein	gal	−1.3	average (n = 13)	3
Au district Rauris-Gastein	sph	−5.9		3
Au district Rauris-Gastein	sph	1.4		3
Au district Rauris-Gastein	apy	1.4		3
Au district Rauris-Gastein	apy	2.0		3
Au district Rauris-Gastein	py	0.9	average (n = 6)	3

1 ... this study, 2 ... Vavtar (1988), 3 ... data of Reden (1991) & Schroll published in Weber (1997)

E. Electron Microprobe Results

The results of electron microprobe measurements are given in g/100 g.

Mitterberg

Sample	Min	As	Sb	Cu	Hg	Co	Pb	Fe	Ni	S	Zn	Sum
MB09_004_py01	cpy			34.8		0.0650	0.0880	30.8		34.8		101
MB09_004_cupy01	cpy		0.0390	34.9		0.0400	0.125	30.5		34.6		100
MB09_004_cupy03	cpy			34.8		0.0290	0.174	30.1		33.8		98.9
MB09_004_cupy06	cpy		0.0360	34.8		0.0370	0.0830	30.3		34.7		99.9
MB09_004_py02	py			0.0750		0.0960	0.145	46.9	0.0730	54.0		101
MB09_004_cupy08	cpy			34.9		0.0540	0.169	30.7		34.8		101
MB09_004_cupy09	cpy			34.2		0.0320	0.147	30.4		34.3		99.1
MB09_004_cupy12	cpy			34.8		0.0510	0.104	30.5		34.8		100
MB09_006_cupy01	cpy			35.2		0.0560	0.0830	30.3		34.7		100
MB09_006_cupy02	cpy			34.7		0.0470	0.0880	30.4		34.8		100
MB09_006_cupy03	cpy			34.5		0.0800	0.0420	30.5		34.7		99.8
MB09_006_cupy04	cpy			34.6		0.0550	0.120	30.6		34.6		100
MB09_004_cupy04	cpy			34.5		0.0390	0.177	30.2		34.6		99.6
MB09_004_cupy11	cpy			34.5		0.0650	0.111	30.8		34.6		100
MB09_004_cupy10	cpy			34.6		0.0360	0.198	30.7		34.7		100
MB09_004_cupy02	cpy			35.1		0.0440	0.0800	30.5		34.3		100
MB09_004_cupy05	cpy			35.1		0.0540	0.145	30.2		35.2		101
MB09_004_cupy07	cpy		0.0280	34.8		0.0370	0.233	29.8		34.7		99.5
MB09_004_py03	py	0.0530		0.0840		0.121	0.227	46.4		53.3		100
MB09_004_fahl03	tet	1.85	27.7	38.5	0.986		0.112	3.35		25.0	3.85	102
MB09_004_fahl02	tet	2.90	26.5	39.6	0.936		0.0630	3.77		25.5	3.50	103
MB09_004_fahl01	tet	10.5	14.4	40.5	0.619		0.0670	4.46		27.1	3.14	101
MB09_006_py01	gdf	42.9		0.111		6.72	0.0790	11.4	17.5	20.5		99.3
MB09_006_py03	gdf	43.1				3.48	0.0720	13.0	19.5	20.3		99.6
MB09_006_py02	gdf	43.6		0.0590		0.740	0.0950	16.2	19.0	20.1		99.9

Radmer

Sample	Min	As	S	Cu	Hg	Co	Sb	Fe	Ni	Pb	Zn	Sum
Ra10_04fahldkl01	ten	10.6	27.1	41.6	1.06	0.0226	12.1	2.11		0.0537	5.50	100
Ra10_04fahldkl02	ten	10.7	27.3	41.6	1.14		11.8	2.38		0.116	5.07	100
Ra10_04fahldkl03	ten	8.02	26.3	39.9	1.91		16.2	2.30		0.136	4.80	99.6
Ra10_04fahldkl04	ten	7.52	26.0	38.4	2.73	0.0480	17.0	3.78		0.121	2.61	98.3
Ra10_04fahldkl05	ten	10.7	27.1	41.4	1.71	0.0296	11.9	3.82		0.120	3.13	100
Ra10_04fahldkl06	ten	9.92	27.1	40.5	1.13	0.0230	13.4	1.92		0.0764	6.93	101
Ra10_04fahldkl07	ten	5.62	26.0	39.5	2.71	0.0417	19.9	3.84		0.136	2.68	100
Ra10_04fahldkl08	ten	5.97	26.2	39.3	1.43	0.0240	20.1	2.14		0.0985	5.08	100
Ra10_04fahldkl09	ten	7.22	26.5	39.8	2.03	0.0424	17.8	3.39		0.0979	3.54	100
Ra10_04fahldkl10	ten	7.20	26.4	40.0	2.50	0.0408	17.5	3.34		0.0234	3.44	100
Ra10_04fahldkl11	ten	8.17	26.6	40.6	2.00	0.0338	16.3	2.92		0.0686	4.03	101
Ra10_04fahldkl12	ten	7.79	26.4	40.0	1.91	0.0444	16.4	3.37		0.0824	3.73	99.7
Ra10_04fahldkl13	ten	8.31	26.6	40.2	2.06	0.0470	15.9	3.70		0.124	3.25	100
Ra10_04fahldkl14	ten	8.15	26.6	40.2	2.45	0.0510	16.3	4.42		0.0695	2.25	101
Ra10_04fahldkl15	ten	8.14	26.4	40.6	2.61	0.0407	16.1	3.13		0.0785	3.71	101
Ra10_04fahldkl16	ten	7.46	26.4	40.0	2.39	0.0474	16.8	3.30		0.0784	3.33	100.0
Ra10_04fahldkl17	ten	10.3	27.1	40.8	1.22		12.8	2.34		0.0783	5.41	100
Ra10_04fahldkl18	ten	8.55	26.6	40.6	1.93	0.0369	15.6	3.98		0.0742	3.10	101
Ra10_04fahldkl19	ten	7.69	26.3	40.2	2.14	0.0268	16.9	2.54		0.0883	4.63	101
Ra10_04fahldkl20	ten	6.08	25.9	39.4	2.44	0.0498	18.9	3.12		0.137	3.98	100
Ra10_04_FE1d	ten	6.25	25.4	40.3	1.81	0.0238	18.6	2.54		0.139	4.74	99.8
Ra10_04_FE2d	ten	11.4	26.4	41.2	1.12		11.0	2.42		0.196	5.35	99.1
Ra10_04_FEd3	ten	10.8	26.8	41.3	1.21		12.0	2.59		0.0547	5.23	100
Ra10_04_FE4d	ten	8.80	26.0	40.2	2.58	0.0227	14.6	3.19		0.172	3.71	99.3
Ra10_04_FE5d	ten	9.73	26.5	40.7	1.74	0.0392	13.5	2.58		0.0622	5.01	99.8
Ra10_04_fahlhell01	tet	7.88	26.7	40.3	2.41	0.0420	16.8	3.35			3.29	101
Ra10_04_fahlhell02	tet	5.71	26.0	39.5	2.73	0.0390	19.4	3.67			2.79	99.9
Ra10_04_fahlhell05	tet	7.99	26.4	40.2	2.61	0.0420	16.6	3.38		0.0531	3.37	101
Ra10_04_fahlhell06	tet	10.8	27.3	41.1	1.89	0.0288	11.9	3.08		0.127	4.30	101
Ra10_04_fahlhell07	tet	1.49	25.1	37.3	0.579		26.3	0.835		0.121	6.93	98.8
Ra10_04_fahlhell08	tet	7.77	26.5	40.1	2.61	0.0277	16.9	3.36		0.0940	3.69	101
Ra10_04_fahlhell09	tet	5.52	26.0	39.7	2.86	0.0425	20.2	2.94		0.0721	3.81	101
Ra10_04_fahlhell10	tet	6.63	26.4	39.8	1.14		19.1	2.05		0.0543	5.65	101
Ra10_04_fahlhell11	tet	0.537	25.4	38.3	1.31		28.4	0.619		0.0772	7.02	102
Ra10_04_fahlhell12	tet	2.26	25.3	38.2	2.18		25.6	1.03		0.0703	6.11	101
Ra10_04_fahlhell13	tet	2.24	25.3	38.5	1.13	0.0253	25.8	1.25		0.0698	6.25	101
Ra10_04_fahlhell14	tet	3.48	25.1	38.9	4.36	0.0847	23.1	3.50		0.0357	2.23	101
Ra10_04_fahlhell15	tet	3.40	25.4	38.6	3.99	0.0574	23.5	3.42		0.0224	2.35	101
Ra10_04_fahlhell16	tet	1.49	25.1	38.0	2.69		27.0	1.44		0.0600	5.54	101
Ra10_04_fahlhell17	tet	1.90	25.3	38.7	1.02		26.3	1.000		0.0794	6.88	101
Ra10_04_fahlhell18	tet	3.48	25.3	38.9	2.50	0.0412	23.2	1.59		0.103	5.47	101
Ra10_04_fahlhell19	tet	2.18	25.0	37.8	1.82	0.0227	25.5	1.10		0.100	6.22	99.8
Ra10_04_FEh1	tet	1.94	24.2	38.7	3.46		25.6	1.32		0.108	5.45	101
Ra10_04_FE2h	tet	1.39	24.6	39.0	1.76		27.1	1.19			6.24	101
Ra10_04_FE3h	tet	0.696	24.9	38.6	0.615		28.2	0.849			8.05	102
Ra10_04_FE4h	tet	2.24	25.0	38.5	2.47		25.9	1.30			5.75	101
Ra10_04_FE5h	tet	1.51	24.8	38.4	2.75		26.3	1.35			5.66	101
Ra10_04_FE1m	ten	6.36	25.4	40.5	3.10	0.0445	18.6	4.07		0.178	2.50	101
Ra10_04_FE2m	ten	7.21	25.6	40.4	2.87	0.0286	17.1	4.21		0.191	2.35	99.9

Sample	Min	As	S	Cu	Hg	Co	Sb	Fe	Ni	Pb	Zn	Sum
Ra10_04_FE3m	ten	7.02	25.4	39.4	2.94	0.0297	17.1	3.72		0.274	3.21	99.0
Ra10_04_FE4m	ten	8.30	26.4	40.7	1.88	0.0325	15.5	2.57		0.0646	4.81	100
Ra10_06_Py2	py	0.0652	52.7	0.0303		0.166	0.0263	46.7		0.238		100.0
Ra10_06_Py3	py	2.02	50.9	0.0330		0.0639		45.0	0.298	0.192		98.5
Ra10_06_Py4	py	0.456	53.1	0.0289		0.0689		46.2	0.0407	0.161		100
Ra10_06_Py5	py	0.266	53.3	0.0859		0.0820		47.1	0.0590	0.214		101
Ra10_06_Pycore01	py		53.6	0.0449		0.0806		47.0	0.0852	0.195	0.0236	101
Ra10_06_Pycore01	py		53.7	0.0536		0.0759		46.7	0.0914	0.180		101
Ra10_06_Pyrim01	py	0.122	53.7	0.331		0.0869		46.9	0.0457	0.179		101
Ra10_06_Pycore02	py	0.0518	52.8	0.0487		0.185		46.7	0.0399	0.202	0.0241	100
Ra10_06_Pycore03	py		53.4			0.0797		47.4		0.188		101
Ra10_05_Py1	py		53.3	0.248		0.0707		46.8		0.238		101
Ra10_05_Py2	py		53.9	0.0685		0.0966	0.0494	43.9	1.87	0.213		100
Ra10_05_Py3	py		54.2	0.0301		0.0700		47.0		0.125		101
Ra10_05_Py4	py		53.1	0.0460		0.0596		44.0	2.15	0.207		99.5
Ra10_05_Py5	py	0.0234	53.6	0.0352		0.0741		46.8		0.196	0.0241	101
Ra10_05_Py6	py		53.5	0.162		0.0760		46.9		0.191		101
Ra10_05_Py7	py		53.8	0.0646		0.0649		47.0		0.159		101
Ra10_05_Py8	py		53.7	0.0484		0.0733		47.8		0.206	0.0492	102
Ra10_04_py1	py		52.0			0.149		46.9		0.200	0.145	99.4
Ra10_06_Py1	py	0.0799	53.7	0.0403		0.102		47.0	0.0260	0.173	0.0430	101
Ra10_04_CP1	cpy		34.8	34.2		0.0560		28.9		0.108	1.69	99.8
Ra10_06_CP	cpy		35.0	35.0		0.0444		29.4		0.121		99.6
Ra10_06_CP2	cpy	0.0208	35.0	33.9		0.0513		29.9		0.107		99.0
Ra10_06_PyinclusCP01	cpy		35.0	34.4		0.0475		30.1		0.129		99.7
Ra10_06_PyincCP02	cpy		35.7	33.8		0.0487		31.0		0.147		101
Ra10_05_CP01	cpy		35.0	35.1		0.0437		29.5		0.118		99.8
Ra10_05_CP02	cpy		34.8	34.7		0.0412		29.7		0.169		99.4
Ra10_05_CP03	cpy		35.7	35.0		0.0389		29.7		0.159		101
Ra10_05_CP04	cpy		35.3	34.9		0.0484		29.6		0.111		100.0
Ra10_05_CP05	cpy	0.0229	34.9	34.8		0.0356		30.0		0.116		99.8
Ra10_05_CP06	cpy		35.0	34.8		0.0383	0.0283	29.8		0.167		99.8

Zinkwand

Sample	Min	Bi	Cu	Fe	Ni	Co	As	Sb	S	Zn	Pb	Sum
ZW09_001_apy01	apy			33.7	0.0880		46.3		18.3		0.140	100
ZW09_001_apy02	apy			34.9	0.0280	0.412	44.1	0.129	19.5	0.0360	0.0440	99.1
ZW09_001_apy03	saf			20.7	2.49	5.34	69.7	0.0710	0.860			99.2
ZW09_001_apy04	saf			18.1	2.63	6.95	69.2		0.599	0.0360		97.6
ZW09_001_apy05	saf			20.0	3.18	5.25	68.2	1.01	1.22	0.0390	0.139	99.0
ZW09_001_apy06	saf			21.1	2.63	4.90	70.5		0.587	0.0210		99.7
ZW09_001_apy07	saf			20.1	3.29	4.82	70.1	0.565	0.597			99.5
ZW09_001_apy08	saf			19.7	3.16	5.73	69.9	0.315	0.516			99.4
ZW09_001_apy09	saf			19.4	3.25	5.73	70.3	0.207	0.295		0.0570	99.3
ZW09_001_apy10	saf			17.9	3.51	7.00	70.3	0.146	0.572		0.0540	99.6
ZW09_001_apy11	apy			31.7	0.108	3.08	47.3	0.0510	17.4		0.0920	99.7
ZW09_001_apy12	apy			27.6	0.410	6.55	47.5	0.0740	17.2		0.134	99.4
ZW09_001_apy13	apy			29.1	0.315	5.39	48.2	0.185	16.5		0.126	99.8
ZW09_001_apy14	apy			28.3	0.567	5.77	48.2	0.191	16.7			99.8
ZW09_001_apy15	apy			32.5	0.0770	2.70	47.0	0.104	17.6	0.0310	0.127	100
ZW09_001_apy16	apy			27.3	0.481	6.70	48.7	0.106	16.5		0.0870	99.9
ZW09_001_apy17	apy			31.8	0.0880	2.85	47.1	0.0740	17.5		0.192	99.6
ZW09_001_apy18	saf			17.7	3.49	7.20	69.9	0.345	0.664			99.3
ZW09_001_apy19	saf			18.8	3.50	6.14	70.0	0.594	0.490			99.6
ZW09_001_apy20	saf			18.0	3.36	7.04	69.9	0.443	0.452			99.3
ZW09_001_apy21	saf			17.9	3.35	6.95	70.0	0.343	0.584		0.0220	99.1
ZW09_001_apy22	saf			19.2	3.22	6.01	69.9	0.351	0.423		0.0560	99.2
ZW09_001_apy23	saf			18.2	3.36	7.13	68.8	0.329	1.13			99.0
ZW09_001_apy24	apy		0.0220	26.6	0.575	7.20	48.3	0.149	16.5	0.0490	0.113	99.6
ZW09_001_apy25	apy			27.6	0.627	5.95	48.4	0.194	16.5		0.0490	99.4
ZW09_001_apy26	apy			31.6	0.0760	3.04	46.9	0.0570	17.6		0.0340	99.4
ZW09_001_apy27	saf			17.6	3.35	7.35	70.0	0.298	0.609			99.2
ZW09_001_apy28	saf			20.9	2.48	5.46	70.5	0.420	0.370			100
ZW09_001_apy29	saf			18.8	3.44	6.60	69.3	0.512	0.817	0.0210		99.5
ZW09_001_apy30	apy			28.0	0.449	6.40	48.4	0.129	16.7			100
ZW09_001_apy31	apy			33.0	0.0500	2.32	46.6	0.0870	18.2		0.0500	100
ZW09_001_apy32	apy		0.0290	26.8	0.471	6.93	48.5	0.154	16.4		0.0980	99.4
ZW09_001_apy33	saf			23.6	1.66	2.98	70.6	0.258	0.272			99.4
ZW09_001_apy34	apy			32.1	0.0790	2.59	47.3	0.0540	17.6		0.0710	99.8
ZW09_001_apy34	saf		0.0200	17.3	3.99	6.97	69.9	0.183	0.348			98.7
ZW09_001_apy35	apy			28.2	0.589	5.70	48.2	0.0880	16.5		0.132	99.3
ZW09_001_apy35	apy			27.8	0.446	6.24	48.6	0.173	16.1		0.0240	99.5
ZW09_001_apy36	apy			27.2	0.395	7.40	47.8	0.170	16.7		0.0230	99.7
ZW09_001_apy36	sku			2.25	1.17	17.2	78.5	0.0580	0.0750			99.3
ZW09_001_apy37	sku			2.11	1.20	17.5	78.4		0.0870		0.0770	99.4
ZW09_001_apy38	saf			17.8	3.85	6.71	70.4	0.233	0.310			99.4
ZW09_001_apy39	saf			17.7	3.84	6.73	69.9	0.302	0.298			98.8
ZW09_001_apy40	apy			31.2	0.256	3.98	47.9	0.0380	17.0		0.0690	101
ZW09_001_apy41	apy			27.7	0.723	6.19	48.9	0.141	15.8	0.0320		99.6
ZW09_001_apy42	sku			2.32	1.18	17.1	78.5	0.0680	0.124	0.0480		99.4
ZW09_001_apy43	sku			2.41	1.17	17.2	78.2	0.0540	0.131			99.3
ZW09_001_apy44	saf			17.5	4.02	6.71	70.2	0.291	0.330			99.2
ZW09_001_apy45	apy			32.0	0.153	2.74	47.2	0.0340	17.5			99.6
ZW09_05 an10	apy			30.8	0.180	2.18	48.5		18.3			100
ZW09_05 an11	apy			33.6	0.180	0.177	46.1		20.2			100
ZW09_05 an12	loe			22.3	1.60	3.12	72.4		0.866			100
ZW09_05 an13	apy			31.8	0.148	1.42	48.0		18.6			99.9
ZW09_05 an14	loe			22.5	1.53	2.92	71.9		1.22			100
ZW09_05 an15	apy			31.9	0.113	1.60	47.5		18.8			100

Sample	Min	Bi	Cu	Fe	Ni	Co	As	Sb	S	Zn	Pb	Sum
ZW09_05 an16	loe			22.9	1.64	2.96	71.2		1.47			100
ZW09_05 an17	apy			31.4	0.213	1.65	48.4		18.3			99.9
ZW09_05 an18	loe			23.5	1.41	2.45	70.1		2.71			100
ZW09_05 an2	apy			34.0		0.0403	45.1		20.1			99.3
ZW09_05 an3	apy			33.9	0.0626		45.6		19.8			99.4
ZW09_05 an4	apy			31.2	0.512	0.847	49.0		17.6			99.1
ZW09_05 an5	apy			33.2	0.0870	0.0610	47.2		18.5			99.0
ZW09_05 an6	loe			22.0	1.41	3.92	72.5		0.941			101
ZW09_05 an7	loe			22.7	1.58	2.89	72.3		1.13			101
ZW09_05 an8	loe			22.9	1.51	3.12	71.8		1.52			101
ZW09_05 an9	loe			22.4	1.59	2.95	72.2		1.53			101
ZW09_012-grA202	gdf			1.58	29.1	2.66	56.8	1.23	9.80			101
ZW09_012-grA203	gdf			1.56	27.9	2.39	56.7	1.25	10.3			100
ZW09_012-grA204	gdf			1.53	29.7	2.04	57.1	1.44	10.1			102
ZW09_012-grA205	gdf			1.63	28.4	2.54	56.7	1.10	10.5			101
ZW09_012-an02	gdf			1.63	29.7	2.39	56.5	1.20	10.3			102
ZW09_012-an03	nic			0.0880	43.8	0.0260	45.7	2.07	0.0800			91.8
ZW09_012-an04	gdf			1.70	29.4	2.62	55.4	1.20	10.4			101
ZW09_012-an09	gdf			1.33	27.8	3.63	57.2	1.18	9.37			101
ZW09_012-an10	nic			0.143	45.1	0.204	53.0	1.56	0.0560			100
ZW09_012-an11	nic			0.0530	42.6	0.0780	53.3	2.03				98.3
ZW09_012-grA1	gdf			1.60	28.7	2.49	60.9	1.42	10.8			106
ZW09_012-grA2	gdf			1.49	28.8	2.40	57.3	1.64	10.2			102
ZW09_012-grA3	gdf			1.48	29.6	2.42	57.1	1.25	10.3			102
ZW09_012-grA4	gdf			1.40	29.7	2.03	56.7	1.32	9.64			101
ZW09_012-grA5	gdf			1.67	28.6	2.48	57.4	1.33	10.4			102
ZW09_012-grA6	gdf			1.04	28.9	2.70	59.0	1.50	9.32			103
ZW09_012-grA201	gdf			1.50	29.3	2.37	57.4	1.51	9.87			102
ZW09_012-grB1	gdf			1.14	30.1	2.21	58.2	1.72	9.70			103
ZW09_012-grB2	gdf			1.40	28.5	2.40	56.7	1.43	10.3			101
ZW09_012-grB3	gdf			1.52	30.0	2.19	56.7	1.35	10.5			102
ZW09_012-grB4	gdf			0.996	29.2	2.62	57.7	1.52	9.89			102
ZW09_012-grB5	gdf			0.669	31.3	1.21	54.4	2.56	11.9			102
ZW09_012-grC1	gdf			1.56	28.9	2.63	57.2	1.29	10.5			102
ZW09_012-grC2	gdf			1.12	28.4	3.16	58.7	1.33	9.41			102
ZW09_012-grC3	gdf			1.17	29.3	2.81	58.7	0.884	9.60			103
ZW09_012-grC4	gdf			1.27	29.6	2.33	57.7	1.29	9.68			102
ZW09_012-grC5	gdf			1.31	28.5	2.64	57.7	1.10	9.63			101
ZW09_012-kon01	gdf			2.38	21.6	9.76	54.6	0.292	12.2			101
ZW09_012-kon02	saf*			9.66	9.52	9.47	71.5	0.0550	0.373			101
ZW09_012-kon03	saf*			9.28	9.92	9.36	71.4	0.262	0.306			101
ZW09_012-kon04	gdf			2.23	22.3	8.66	55.4	0.248	11.7			101
ZW09_012-kon05	saf*			9.99	9.69	8.61	72.4	0.396	0.283			101
ZW09_012-kon06	saf*			10.1	10.3	8.71	71.0	0.0820	0.487			101
ZW09_012-kon07	gdf			2.38	21.4	9.10	54.9	0.363	11.9			100
ZW09_14 1	apy			31.7	0.476	0.300	47.2		19.1			98.8
ZW09_14 10	apy			34.1	0.0270		44.5		20.6			99.2
ZW09_14 11	apy			34.1	0.0237	0.0363	44.7		21.0			99.9
ZW09_14 12	apy			33.4	0.146	0.381	45.2		20.5			99.6
ZW09_14 13	apy			33.8			45.7		20.4			99.9
ZW09_14 14	apy			33.8	0.0512	0.0265	44.4		20.2			98.5
ZW09_14 15	apy			33.6			45.0		20.5			99.1
ZW09_14 16	apy			33.2	0.0273	0.0347	49.1		18.8			101
ZW09_14 17	apy			33.4	0.107	0.283	44.7		20.7			99.2
ZW09_14 18	apy			27.8	0.803	4.35	48.7		17.9			99.6
ZW09_14 19	apy			26.3	1.30	4.89	50.8		16.0			99.3
ZW09_14 2	apy			27.3	0.814	4.31	50.6		16.5			99.6
ZW09_14 20	apy			27.7	1.04	4.04	48.5		17.4			98.6
ZW09_14 21	apy			32.6	0.412	0.398	46.1		19.4			99.0
ZW09_14 22	apy			26.8	0.981	5.18	50.3		17.4			101
ZW09_14 23	apy			30.7	0.465	2.01	47.1		19.3			99.6
ZW09_14 24	apy			28.9	0.811	3.58	48.4		18.0			99.6
ZW09_14 25	apy			30.2	0.641	2.36	46.8		19.4			99.3
ZW09_14 26	apy			34.2	0.106	0.120	44.3		21.2			99.9
ZW09_14 27	apy			33.8	0.0413		45.0		20.4			99.3
ZW09_14 29	apy			34.1		0.0517	44.4		20.9			99.4
ZW09_14 3	apy			31.6	0.300	1.19	46.9		19.0			99.0
ZW09_14 30	apy			33.5	0.0962	0.0469	44.8		20.2			98.7
ZW09_14 4	apy			33.6	0.135		46.1		20.3			100
ZW09_14 5	apy			33.4	0.0446		45.6		20.6			99.7
ZW09_14 6	apy			33.3	0.0441		44.4		21.0			98.7
ZW09_14 7	apy			33.6	0.0836	0.171	45.5		20.5			99.8
ZW09_14 8	apy			27.5	0.851	4.92	48.7		17.7			99.6
ZW09_14 9	apy			32.5	0.286	0.743	45.8		20.1			99.4
ZW09_017-an01	apy		0.0340	35.0	0.176	0.112	45.2	0.158	20.0			101
ZW09_017-an010	brn	0.687	13.5			0.0250		24.8	18.4		42.9	100
ZW09_017-an011	brn	0.422	13.6	0.196				24.8	20.8		43.2	103
ZW09_017-an012	apy			35.2	0.0240	0.0740	45.1	0.266	19.0	0.0660	0.0660	99.8
ZW09_017-an013	brn	0.292	13.6					24.6	19.8		42.9	101
ZW09_017-an014	brn	0.745	13.8	0.0390		0.0200		24.8	20.4		42.1	102
ZW09_017-an015	gal	0.591	0.339	0.0260				0.0280	13.4		86.8	101
ZW09_017-an016	bou	1.89		0.0270	0.0460			24.1	17.5		56.5	100
ZW09_017-an017	bou	1.75		0.0530				24.3	19.1		55.8	101
ZW09_017-an018	bou	1.08				0.0290		24.1	18.0		56.5	99.8
ZW09_017-an019	brn	0.414	13.4		0.0200			24.8	17.9		42.8	99.3
ZW09_017-an02	apy	0.0460		35.7	0.0520	0.0840	44.4	0.234	20.4		0.0820	101
ZW09_017-an020	bou	1.72	0.0880					24.8	18.4		55.8	101
ZW09_017-an022	brn	0.425	13.4					24.3	18.3		42.8	99.2
ZW09_017-an023	sph			4.70					31.4	63.1	0.0220	99.2
ZW09_017-an024	bou	1.49						24.5	16.8	0.0220	55.7	98.5
ZW09_017-an025	brn	0.416	13.7	0.0340				24.6	20.3		42.6	102
ZW09_017-an026	brn	0.328	13.6					24.6	19.2		43.1	101

Sample	Min	Bi	Cu	Fe	Ni	Co	As	Sb	S	Zn	Pb	Sum
ZW09_017-an027	gal	0.549		0.0200				0.126	12.1		86.7	99.5
ZW09_017-an028	gal	0.435	0.0620	0.0780				0.0290	12.5		85.9	99.0
ZW09_017-an029	cpy		34.2	29.9		0.0400		0.0280	33.7	0.0570	0.0860	98.1
ZW09_017-an03	apy	0.0370	0.0310	35.3	0.0860	0.0550	45.5	0.0810	19.6			101
ZW09_017-an03	apy	0.0370	0.0310	35.3	0.0860	0.0550	45.5	0.0810	19.6			101
ZW09_017-an030	po		0.171	59.3	0.0230	0.0760		0.0730	37.9			97.5
ZW09_017-an031	tet	0.0240	37.9	5.35			1.10	28.8	26.4	2.29		102
ZW09_017-an032	po	0.186	0.0740	58.6	0.0270	0.102	0.0650	0.0330	39.7			98.7
ZW09_017-an033	tet	0.141	38.2	5.26			1.90	27.8	26.4	2.23		102
ZW09_017-an034	py		0.0660	46.1	0.297	0.0890			49.9			96.5
ZW09_017-an035	cpy	0.0500	34.1	30.6		0.0440		0.0280	34.4	0.0690		99.3
ZW09_017-an036	po	0.120	0.341	59.3		0.0710	0.0680	0.0370	38.2		0.0390	98.2
ZW09_017-an037	tet	0.128	38.2	5.38			1.88	27.3	25.2	2.03	0.0280	100
ZW09_017-an04	apy			35.5	0.0400	0.0660	44.5	0.0580	20.0	0.0590	0.0300	100
ZW09_017-an05	apy	0.0570		35.3	0.0200	0.0770	45.5	0.0290	18.7			99.7
ZW09_017-an06	apy			35.3	0.137	0.0880	45.7		18.1	0.0340	0.105	99.4
ZW09_017-an07	sph			5.46			0.0330	0.0350	34.4	63.2		103
ZW09_017-an09	cpy		34.5	30.7		0.0270			37.0	0.0530	0.0510	102
ZW09_020	apy			34.0		0.0403	45.1		20.1			99.3
ZW09_020	apy			33.9	0.0626		45.6		19.8			99.4
ZW09_020	apy			33.6	0.180	0.177	46.1		20.2			100
ZW09_020	apy			33.2	0.0870	0.0610	47.2		18.5			99.0
ZW09_020	apy			31.9	0.113	1.60	47.5		18.8			100
ZW09_020	apy			31.8	0.148	1.42	48.0		18.6			99.9
ZW09_020	apy			31.4	0.213	1.65	48.4		18.3			99.9
ZW09_020	apy			30.8	0.180	2.18	48.5		18.3			100
ZW09_020	apy			31.2	0.512	0.847	49.0		17.6			99.1
ZW09_020	loe			23.5	1.41	2.45	70.1		2.71			100
ZW09_020	loe			22.9	1.64	2.96	71.2		1.47			100
ZW09_020	loe			22.9	1.51	3.12	71.8		1.52			101
ZW09_020	loe			22.5	1.53	2.92	71.9		1.22			100
ZW09_020	loe			22.4	1.59	2.95	72.2		1.53			101
ZW09_020	loe			22.7	1.58	2.89	72.3		1.13			101
ZW09_020	loe			22.3	1.60	3.12	72.4		0.866			100
ZW09_020	loe			22.0	1.41	3.92	72.5		0.941			101
ZW09_021-an10	apy			34.6		0.0580	47.1	0.126	17.1		0.0590	99.0
ZW09_021-an11	loe			29.0		0.0530	72.4	0.456	1.09	0.0460	0.0370	103
ZW09_021-an12	loe	0.0350		28.6		0.102	72.4	0.905				102
ZW09_021-an13	apy			35.1		0.0840	47.0	0.0880	17.5	0.0220		99.8
ZW09_021-an14	apy	0.111		35.2	0.0230	0.0440	47.1	0.0520	18.8			101
ZW09_021-an15	apy	0.320	0.0260	34.9		0.0720	47.0		16.7			99.1
ZW09_021-an16	apy			34.9	0.0230	0.0560	46.2	0.0810	18.2		0.0210	99.5
ZW09_021-an17	apy	0.0250	0.0220	35.0	0.0210	0.0680	46.8	0.0990	16.5		0.0280	98.6
ZW09_021-an18	loe			29.2		0.0370	72.0		0.981	0.0240		102
ZW09_021-an2	apy			34.5	0.429	0.121	48.0	0.0200	16.1			99.2
ZW09_021-an3	apy			34.8	0.191	0.202	47.5	0.0480	18.5			101
ZW09_021-an4	apy			35.1	0.0460	0.114	45.9		19.2			100
ZW09_021-an5	apy	0.108		34.7	0.193	0.133	47.2	0.100	18.9			101
ZW09_021-an6	apy		0.0460	35.8	0.0440	0.0590	45.7		21.8			103
ZW09_021-an7	apy			35.0	0.149	0.225	46.7		19.9	0.0390	0.0230	102
ZW09_021-an8	apy	0.0240		34.9	0.132	0.124	46.4	0.0770	18.8	0.0330		100
ZW09_021-an9	loe			28.5	0.0330	0.0490	72.4	0.768	0.507		0.0530	102
ZW09_024-an01	gdf			2.26	30.0	1.97	54.1	1.39	12.1			102
ZW09_024-an02	gdf			2.06	29.3	2.12	53.4	1.43	12.7			101
ZW09_024-an03	gdf			2.12	29.8	2.11	54.5	1.46	12.3			102
ZW09_024-an04	gdf			2.14	29.8	2.14	54.7	1.58	12.0			102
ZW09_024-an05	gdf			2.05	29.0	2.04	54.0	1.23	12.2			100
ZW09_024-an07	gdf			1.42	29.5	1.80	56.1	1.57	10.8			101
ZW09_024an08	nic			0.154	45.1	0.107	53.1	2.55	0.0800			101
ZW09_024an09	nic			0.0620	46.3	0.0330	53.7	2.50	0.181			103
ZW09_024an10	nic			0.0950	45.1	0.0360	53.5	2.51	0.106			101
ZW09_024an11	gdf			1.52	30.5	1.56	54.6	1.58	11.6			101
ZW09_024an12	gdf			1.64	30.8	1.59	55.0	1.51	11.9			102
ZW09_024an13	nic			0.0260	45.1	0.0470	53.2	2.70	0.103			101
ZW09_024an14	nic			0.0810	45.4	0.0420	53.5	2.53	0.0990			102
ZW09_024an15	gdf			1.45	30.6	1.54	55.4	1.80	11.2			102
ZW09_024an16	nic			0.142	45.1	0.0960	53.8	2.71	0.0570			102
ZW09_024an17	gdf			1.42	30.1	1.81	56.0	1.92	11.3			103
ZW09_024an19	nic			0.0840	46.2	0.118	53.7	2.40	0.0870			103
ZW09_024an20	gdf			1.86	28.6	2.43	53.5	1.45	12.3			100
ZW09_024an21	nic			0.128	45.8	0.108	53.6	2.56	0.122			102
ZW09_024an22	gdf			1.81	29.7	2.27	54.2	1.38	12.5			102
ZW09_024an23	nic			0.146	44.7	0.109	53.4	2.43	0.102			101
ZW09_024an24	gdf			1.52	30.3	2.20	55.6	1.73	11.6			103
ZW09_024-an27	nic			0.142	45.6	0.0730	53.5	2.48	0.0870			102
ZW09_024-an28	nic			1.57	30.6	1.72	56.2	1.55	11.5			103
ZW09_024-an28	nic			0.0940	44.5	0.0860	53.5	2.71	0.111			101
ZW09_025-an30	apy			35.3		0.0560	45.5	0.148	20.0			101
ZW09_025-an31	loe			29.0	0.0410	0.0410	71.5		1.67			102
ZW09_025-an32	apy			35.0		0.0500	45.1	0.0760	19.8			100
ZW09_025-an33	loe			28.6	0.0250	0.0580	72.8	0.475	0.447			102
ZW09_025-an34	loe			28.4	0.0380	0.0330	72.9	0.411	0.199			102
ZW09_025-an35	apy			34.9		0.0620	46.6	0.459	19.0			101
ZW09_025-an36	loe			28.6	0.0200	0.0730	73.0	0.303	0.135			102
ZW09_025-an37	apy			34.6		0.0710	46.2	0.0970	19.0			99.9
ZW09_025-an38	loe			28.5		0.0620	72.2	0.728	0.418			102
ZW09_025-an40	loe			28.5	0.0370	0.0280	72.6	0.759	0.113			102
ZW09_025-an41	loe			28.6	0.0620	0.0560	70.5	0.971	0.880			101
ZW09_025-an42	loe			28.6	0.0390	0.0720	70.6	1.46	1.16			102
ZW09_025-an43	loe			28.7		0.0580	71.1	0.113	1.02			101
ZW09_025-an44	loe			28.6		0.0600	71.0	0.130	0.902			101
ZW09_025-an45	loe			28.3	0.0460	0.0330	72.3	0.815	0.0990			102

Sample	Min	Bi	Cu	Fe	Ni	Co	As	Sb	S	Zn	Pb	Sum
ZW09_025-an50	loe			28.4		0.0420	71.4	1.60	0.844			102
ZW09_025-an51	loe			28.7		0.0640	70.4	1.52	1.25			102
ZW09_025-an52	loe			28.7		0.0380	70.6	0.0780	0.894			100
ZW09_025-an53	loe			28.6	0.0340	0.0450	71.0	2.06	0.527			102
ZW09_026-an03	apy	0.0800		35.2	0.174	0.0500	42.0	1.65	18.7	0.0270		97.9
ZW09_026-an08	apy			35.1	0.0800	0.248	43.7	0.744	18.8	0.0300		98.6
ZW09_026-an12	jam	5.41	0.0470	3.42	0.114		0.144	32.0	19.2	0.0230	39.9	100
ZW09_026-an15	apy			35.2	0.743	0.194	43.0	0.0990	19.3			98.5
ZW09_026-an16	saf			14.0	18.0	4.10	43.6	0.0810	18.8			98.5
ZW09_026-an17	apy	0.0600		33.4	1.08	1.23	43.1	0.0980	18.5		0.0380	97.6
ZW09_026-an18	apy			35.5	0.0460	0.0720	43.4	0.549	19.8			99.3
ZW09_026-an19	apy	0.141		35.1	0.129	0.0730	41.6	2.34	19.4			98.8
ZW09_026-an20	apy	0.0380		34.0	0.538	0.693	43.0	0.834	17.9		0.129	97.2
ZW09_028	apy			34.0			44.0		20.5			98.6
ZW09_028	apy			33.8			44.7		20.1			98.6
ZW09_028	apy			33.9			44.9		20.1			98.9
ZW09_028	apy			33.9			45.0		20.4			99.4
ZW09_028	apy			33.9			45.1		20.2			99.2
ZW09_028	apy			33.6	0.0277	0.0442	45.2		19.4			98.3
ZW09_028	apy			33.8			45.2		20.4			99.4
ZW09_028	apy			33.9			45.4		20.3			99.7
ZW09_028	apy			33.8			45.4		20.3			99.5
ZW09_028	apy			33.5		0.0618	45.8		19.8			99.1
ZW09_028	apy			33.9		0.0979	45.8		19.9			99.7
ZW09_028	apy			33.7			45.8		20.2			99.8
ZW09_028	apy			33.7		0.0503	45.9		19.8			99.3
ZW09_028	apy			33.8	0.0454		46.4		19.3			99.5
ZW09_028	apy			33.6		0.0343	46.5		19.1			99.2
ZW09_028	loe			27.5	0.0623	0.0415	69.1		2.26			99.0
ZW09_028	loe			27.9	0.104	0.0379	69.8		2.26			100
ZW09_028	loe			27.1	0.146		72.0		0.142			99.4
ZW09_028	loe			27.1	0.0623	0.0461	72.5		0.152			99.9
ZW09_028	loe			27.3	0.170	0.0901	73.1		0.130			101

Tösens

Sample	Min	As	Sb	Cu	Co	Pb	Fe	Ag	S	Zn	Sum
Tösens											
TS09_011_sulf01	bou	0.0450	20.7	1.24		61.5	0.0650	0.0520	17.8		101
TS09_011_sulf07	bou	0.0510	20.8	1.28		61.5			17.7		101
TS09_011_sulf04	bou	0.0200	21.0	1.26		62.0			17.6		102
TS09_011_sulf05	bou		20.0	1.14		62.5	0.0310		16.7		100
TS09_01F_zns02	bou		20.1	1.38		62.2			17.5		101
TS09_01F_pbs03	bou	0.0450	20.5	1.45		61.6			17.3		101
TS09_011_sulf03	bou		20.9	1.28		62.3			17.8	0.0240	102
TS09_011_sulf02	bou		20.7	1.24		63.5		0.0410	17.9	0.0390	103
TS09_011Ä_pbs01	bou		25.8			56.7	0.205		18.4	2.24	103
TS09_011_sulf09	gud	0.102	61.1		0.0470	0.128	27.7		15.4		105
TS09_011_sulf08	gud	0.102	61.4		0.0390	0.131	27.7	0.0420	15.5		105
TS09_011_sulf10	gud	0.144	60.6		0.0470	0.0710	28.4		15.7	0.0410	105
TS09_011_pbs05	gal		0.0560			86.0			13.6		99.7
TS09_011_pbs04	gal		0.126			86.2		0.0300	13.5		99.8
TS09_01F_pbs02	gal		0.444			86.3		0.290	13.5		101
TS09_011_pbs02	gal		0.156			86.5		0.0240	13.5		100
TS09_011_pbs07	gal		0.0460	0.0470		86.9			13.4		100
TS09_011_pbs08	gal		0.0540			87.0	0.0350	0.0350	13.4		101
TS09_01J_pbs05	gal		0.145	0.0210		87.1			13.5		101
TS09_01F_pbs04	gal		0.194			87.3	0.0200	0.135	13.5		101
TS09_01F_pbs01	gal		0.155			86.7	0.0320	0.0260	13.4		100
TS09_011_pbs06	gal		0.112			86.4		0.0280	13.6		100
TS09_01F_pbs05	gal		0.256			85.5		0.125	13.2	0.0200	99.2
TS09_011_pbs09	gal					86.2	0.0280		13.3	0.0220	99.6
TS09_01J_pbs07	gal		0.0930			87.0	0.0490		13.5	0.0920	101
TS09_011_pbs01	gal		0.126			86.7	0.0280		13.4	0.116	100
TS09_01F_pbs06	gal		0.198			86.6	0.0410		13.3	0.120	100
TS09_01D_PbS04	gal		0.123			86.0	0.0450		13.3	0.128	99.7
TS09_01D_PbS03	gal		0.0960			87.2	0.0260		13.6	0.136	101
TS09_01F_pbs07	gal		0.275			86.3	0.0360	0.0320	13.4	0.157	100
TS09_01_Pbs01	gal		0.0850			86.2	0.0430		13.4	0.159	99.9
TS09_01D_PbS05	gal		0.0460			86.5			13.5	0.203	100
TS09_01F_pbs09	gal		0.165			86.8			13.5	0.268	101
TS09_011_pbs03	gal		0.0680			87.5			13.3	0.320	101
TS09_01D_Pbs02	gal		0.184			86.8			13.4	0.347	101
TS09_01F_pbs08	gal		0.146			86.1		0.0240	13.3	0.425	100
TS09_01J_pbs08	gal		0.153			85.2	0.0440		13.4	0.483	99.3
TS09_01J_pbs06	gal		0.0840			86.2			13.4	0.505	100
TS09_01F_pbs10	gal		0.101	0.0240		85.8	0.0350	0.0420	13.6	0.599	100
TS09_01F_apy01	py	1.39			0.262	0.288	46.0		52.0		100
TS09_011Ä_py05	py				0.0690	0.277	47.8		53.4	0.0210	102
TS09_011A_py04	py	0.0210			0.0820	0.291	47.4		53.8	0.0820	102
TS09_011A_py02	py	0.111			2.59	0.263	45.2		53.3	0.127	102
TS09_011A_py01	py	0.0920			3.53	0.170	43.7		53.2	0.183	101
TS09_011A_py03	py	0.0200			1.23	0.0880	46.6		53.3	0.729	102
TS09_011A_zns01	sph				0.0460	0.126	4.91		33.0	59.7	98.0
TS09_011A_zns04	sph				0.0580		5.88		33.2	59.8	99.3
TS09_01Dzns01	sph			0.0850		0.196	5.25		33.5	60.7	100
TS09_011A_zns03	sph				0.0630	0.0800	5.82		33.4	60.8	100
TS09_011_zns02	sph				0.0390	0.155	5.82		33.4	60.8	100
TS09_011_zns01	sph			0.0320	0.0290	0.0890	6.07		33.3	60.9	101
TS09_01J_sph08	sph			0.0330		0.110	4.82		32.9	61.0	99.2

Sample	Min	As	Sb	Cu	Co	Pb	Fe	Ag	S	Zn	Sum
TS09_01D_ZnS05	sph			0.0390		0.184	4.67		33.3	61.2	99.7
TS09_011A_zns02	sph			0.0280	0.0640	0.103	5.75		33.5	61.2	101
TS09_011_zns03	sph			0.0810		0.210	5.83	0.0230	33.2	61.2	101
TS09_01J_sph09	sph				0.0470	0.172	5.55		32.9	61.4	100
TS09_011A_zns05	sph		0.0280	0.0280	0.0680	0.210	5.47	0.0210	33.3	61.5	101
TS09_01D_ZnS02	sph	0.0200				0.191	5.33		33.9	61.8	102
TS09_01D_ZnS03	sph			0.0990		0.106	5.44		33.9	61.9	102
TS09_01J_sph10	sph			0.0320		0.218	5.58		33.3	61.9	101
TS09_011A_zns06	sph			0.0310	0.0380	0.0530	5.37		33.2	62.0	101
TS09_011A_zns07	sph	0.0470	0.0200		0.0310	0.231	5.21		33.3	62.0	101
TS09_01F_zns03	sph				0.0280	0.0900	4.86		33.0	62.1	100
TS09_01F_zns01	sph					0.0270	4.55		33.3	62.6	101
TS09_01F_zns05	sph					0.209	4.63		33.3	62.7	101
TS09_01F_zns04	sph				0.0340	0.146	5.21		33.5	62.8	102
TS09_01D_ZnS04	sph					0.0800	4.48		33.4	63.0	101
TS09_01F_zns06	sph				0.0230	0.125	4.47		33.3	63.0	101

Erzwies

Sample	Min	Ag	Cu	Fe	Co	As	Sb	S	Zn	Pb	Sum
ES09_018an01	gal	0.0280	0.0250					14.0	0.0680	88.5	103
ES09_018an05	gal		0.0310					13.8		89.1	103
ES09_018an01	gal			0.0390				13.7		88.5	102
ES09_018an06	gal	0.0470	0.0390	0.0410				13.5		88.8	103
ES09_018an04	gal			0.0530				13.8		88.4	103
ES09_018an01	gal	0.0740		0.0620	0.0480			13.4		87.3	101
ES09_009an4	gal	0.117		0.0710	0.0330		0.0240	13.6	0.110	88.4	102
ES09_009an3	gal			0.0780			0.0820	13.7	0.0250	88.3	102
ES09_009an10	gal		0.0480	0.110				13.6	0.0330	89.2	104
ES09_009an09	gal			0.152				13.7		89.1	103
ES09_018an09	gal		0.324	0.169			0.194	13.8		88.6	103
ES09_009an8	gal		0.0400	0.203			0.175	13.4		88.9	103
ES09_018an11	cc		69.0	1.08			0.0270	18.7	0.0260	9.52	98.6
ES09_018an10	cc	0.0890	72.1	1.22				19.2	0.0440	7.16	100.0
ES09_009an5	sph		0.0350	2.04		0.0380	0.0520	33.6	63.2		99.5
ES09_009	sph		0.0360	2.18			0.295	33.9	62.2		99.1
ES09-002_PbS02	gal	1.41	0.0250	0.0490				13.5		83.7	98.7
ES09_022C_pbs01	gal	0.947		0.0540		0.0540		13.5	0.0470	83.2	97.9
ES09_018an07	gal		0.267	0.0750			0.0940	13.4	0.0790	88.8	103
ES09_22D_pbs01	gal	1.96		0.355				14.0		81.6	98.0
ES09_022A_pbs02	gal	0.563		0.401		0.0380	0.0350	13.6		85.5	100
ES09-002_sulf01	apy			36.2	0.0670	40.8		22.3		0.160	99.6
ES09_022A_apy11	apy			36.3	0.0610	41.7	0.0220	21.9		0.0990	100
ES09_022A_apy01	apy			36.3	0.0520	42.5		21.6		0.0230	101
ES09_022C_apy16	apy			36.4	0.0400	42.4		21.5		0.0240	100
ES09_022A_apy06	apy			36.5	0.0690	41.9	0.0280	22.0		0.108	101
ES09_022C_apy04	apy		0.0240	36.5	0.0400	42.4		21.7			101
ES09_022C_apy15	apy			36.6	0.0650	41.8	0.0260	22.2		0.0800	101
ES09_22D_apy08	apy			36.7	0.0550	41.7	0.0310	22.1			101
ES09_022C_apy20	apy		0.0260	36.7	0.0640	41.6	0.0380	22.0		0.108	101
ES09_022C_apy17	apy			36.7	0.0470	42.2		22.1		0.108	101
ES09_022A_apy04	apy		0.0200	36.7	0.0700	42.5		21.7		0.0700	101
ES09_22D_apy04	apy			36.7	0.0660	41.5		22.0		0.105	100
ES09_022C_apy05	apy			36.8	0.0690	40.8		22.7		0.154	101
ES09_022A_apy12	apy			36.8	0.0600	42.7		21.9		0.0460	102
ES09_22D_apy01	apy			36.8	0.0750	41.9	0.0360	21.7		0.105	101
ES09-002_apy10	apy			36.9	0.0510	41.6		22.0		0.0320	101
ES09_022A_apy09	apy			36.9	0.0650	41.6		22.2	0.0310	0.128	101
ES09_22D_apy03	apy			36.9	0.0590	41.9	0.0450	22.1		0.126	101
ES09-002_apy03	apy			36.9	0.0660	40.4	0.0340	22.6			100
ES09-002_apy06	apy			36.9	0.0560	40.9	0.0460	22.5	0.0250	0.126	101
ES09_022C_py05	apy			36.9	0.0830	42.3		21.8		0.0920	101
ES09_22D_apy06	apy			37.0	0.0450	42.4		21.7		0.0470	101
ES09_022A_apy13	apy			37.0	0.0510	42.4		21.8		0.0410	101
ES09_022A_apy05	apy			37.0	0.0570	40.7	0.0430	22.9		0.0470	101
ES09-002_apy08	apy			37.0	0.0480	42.4	0.0290	21.6		0.0390	101
ES09_022A_apy15	apy			37.0	0.0720	42.2		22.1		0.0850	101
ES09_022C_apy10	apy			37.0	0.0440	42.0		21.8		0.107	101
ES09_022C_apy09	apy			37.1	0.0500	41.6		22.4		0.0980	101
ES09_022A_apy10	apy		0.0270	37.1	0.0630	42.0		22.1		0.195	101
ES09_022A_apy07	apy			37.1	0.0630	41.6		22.5	0.0430	0.131	102
ES09_022A_apy08	apy			37.1	0.0730	42.0		21.8		0.0770	101
ES09_022A_apy03	apy			37.1	0.0610	42.7		21.5		0.0890	102
ES09-002_apy04	apy			37.1	0.0620	40.7		22.6		0.0860	101
ES09-002_apy05	apy	0.0250		37.2	0.0670	41.0		22.5	0.0250	0.0620	101
ES09_022A_apy14	apy			37.2	0.0590	42.3	0.0290	21.7			101
ES09_22D_apy05	apy			37.2	0.0660	41.2		22.7		0.127	101
ES09-002_apy02	apy			37.2	0.0630	41.1	0.0570	22.5			101
ES09_22D_apy02	apy			37.2	0.0650	41.5		22.3			101
ES09-002_apy07	apy			37.2	0.0580	42.2	0.0270	22.1		0.0630	102
ES09_022C_apy01	apy			37.3	0.0470	41.0		22.5			101
ES09_022C_apy11	apy			37.3	0.0650	42.0	0.0470	22.0			101
ES09_22D_apy10	apy			37.3	0.0740	40.9	0.0280	22.7		0.0330	101
ES09_022C_apy18	apy			37.3	0.0670	41.2		22.8	0.0210	0.0640	102
ES09_022C_apy19	apy		0.0200	37.3	0.0500	42.0	0.0640	22.3		0.0520	102
ES09_22D_apy09	apy			37.4	0.0850	40.8		22.6		0.0960	101
ES09-002_apy01	apy			37.4	0.0530	41.8		21.9		0.171	101
ES09_022C_apy06	apy			37.4	0.0460	41.8		22.3		0.0730	102
ES09_022C_apy02	apy			37.4	0.0520	42.2		22.1	0.0260	0.0400	102
ES09_022C_apy14	apy			37.4	0.0600	42.1		22.1	0.0490	0.0580	102